UNIVERSITY OF CALIFORNIA
Santa Barbara

A Microfluidic Temperature Gradient Device and Its Application to Uncovering Temporal Systems of Robustness in the Developing Embryo of the Nematode *C. elegans*

A Dissertation submitted in partial satisfaction of the requirements for the degree

Doctor of Philosophy in Biochemistry and Molecular Biology.

by

Eric S. Terry

Committee in charge:

Professor Joel H. Rothman, Co-Chair

Professor Carl D. Meinhart, Co-Chair

Professor William C. Smith

Professor Otger Campàs

December 2017

The dissertation of Eric S. Terry is approved.

_____

William C. Smith

_____

Otger Campàs

_____

Joel H. Rothman, Committee Co-Chair

_____

Carl D. Meinhart, Committee Co-Chair

September 2017

A Microfluidic Temperature Gradient Device and Its Application to Uncovering Temporal Systems of Robustness in the Developing Embryo of the Nematode *C. elegans*

Acknowledgements

I would like to first and foremost thank my wife and daughter, Gwen and Natalie, for their love and support. I would also like to thank my advisors, Drs. Joel Rothman and Carl Meinhart. Without their guidance this work wouldn't have been possible. I also thank my committee members Drs. William Smith and Otger Campas. I would also like to thank my parents for their love and support over the years. A special thanks to my friends and colleagues in the Rothman and Meinhart labs, and in particular to Dr. Pradeep Joshi.

Vita of Eric S. Terry
September 2017

Publications, Awards, and Conference Presentations

"Uncovering Evidence of Intercellular Coordination of Division Timing in the early *C. elegans* Embryo With a Novel Microfluidic Temperature Gradient Device": 2017 Manuscript in preparation.

Poster Presentation 2015 International Worm Conference, UCLA

Nominated for 2014 Outstanding Teaching Assistant Award

Nominated for 2016 Graduate Division Mentoring Awards

Student Leadership Award 2004, Cabrillo Student Senate

Research Experience

Carl Meinhart Lab, Mechanical Engineering UCSB
Micro Electrical Mechanical Systems (MEMS) device design and construction.

Joel Rothman Lab, Biology UCSB
Developmental biology research utilizing C. *elegans* as a model organism.

Cynthia Kenyon Lab, Biology, UCSF
Biology of Ageing research utilizing C. *elegans* as a model organism.

Education

University of California at Santa Barbara 2009 - 2017 (Defending Smr. '17)
PhD Candidate Biomolecular Science and Engineering Program
Join appointment in Joel Rothman Laboratory, Department of Molecular, Cellular, and Developmental Biology and Carl Meinhart Laboratory, Department of Mechanical Engineering

University of California at Berkeley 2004 - 2008
BA in Biology/Biochemistry

Cabrillo College, Aptos CA 2003-2005
Associate Degree in Biology

Laboratory Teaching Experience

Cell Biology Laboratory MCDB 103L, UCSB
Winter 2017

Genetics Laboratory MCDB 101L, UCSB
Fall 2016, 2015, 2014, Spring 2014

Mechanical Engineering Machine Shop Laboratory ME 12S, UCSB
Winter 2013, Fall 2012

Biochemistry Laboratory MCDB 109L, UCSB
Spring 2013, 2012, 2011

Introduction to Biology Laboratory First Quarter MCDB 1AL, UCSB
Summer 2011, 2010, Fall 2009

Introduction to Biology Laboratory Second Quarter MCDB 1BL, UCSB
Summer 2010

Guest Lecture

Cell Biology MCDB 103, UCSB
Winter 2013

Biochemistry for Biology Majors MCDB, UCSB
Winter 2014, 2012

Lecture Teaching Assistant Experience

General Biochemistry MCDB 108C
Spring 2017

Plant Biodiversity EEMB 127
Summer 2016

Biochemistry for Biology Majors MCDB 110, UCSB
Winter 2014, 2012, 2011

General Biochemistry MCDB 108A (Online and in-person format), UCSB
Summer 2013, 2012

Introduction to Biology MCDB 1A, UCSB
Summer 2013

Cell Biology MCDB 103, UCSB
Winter 2013

Thermodynamics ME 151A, UCSB
Fall 2010

Mentoring Experience

Mentored in several summer internship programs at UCSB including: CSEP, INSET, Eureka

Professional Experience

PENSCO Trust 2007 - 2009

Conducted asset administration and procedure development duties. Identified, developed, and implemented technical requirements for the management of asset documentation and customer communication.

Crest Corporation/Prasic.com 2006 - 2007

Designed and developed geospatial marketing software for advertising sales force.

Register Tapes Unlimited 2004 - 2006

Outside direct business to business sales.

EMC/Storability 2000 - 2002

Project management for large-scale mission critical IT implementations. Identified key business requirements with client management and management representatives. Identified key technical requirements with technical personnel. Coordinated implementations of multi-vendor, multi-site, IT solutions.

Micro Dynamics/Mazik Inc. 1995 - 2000

IT Consultant. Handled sales, installation, maintenance and management of 100-200 seat networks.

ABSTRACT

Microfluidic Temperature Gradient Device and Its Application to Uncovering Temporal Systems of Robustness in the Developing Embryo of the Nematode *C. elegans*

Eric S. Terry

Animal development is a complex process, shepherded by systems of robustness to ensure its success. To date, such systems that have been experimentally identified, largely have been found to ensure specific and correct cell identities in terms of gene and protein expression and spatial position. Little is known about systems that supervise, guide, and compensate for variability in the timing of events within development. The developing embryo of the nematode *C. elegans* follows a highly-stereotyped sequence of events starting at the two-cell stage where an asymmetric first division results in two cells differing in size, genetic and proteomic

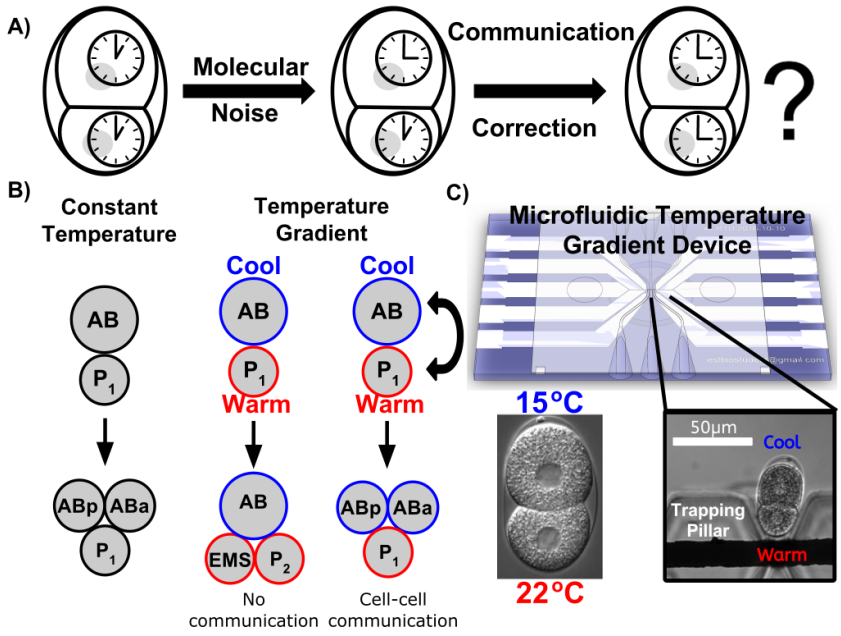

Figure i: Graphical abstract of main experiment described in this dissertation. A) Main question: the cells of a developing embryo have "clocks". Does the developing embryo detect and compensate if the clocks go out of sync. B) Experimental method: two-cell embryo of the nematode C. elegans *is subjected to a temperature gradient to test for compensation in discordant division timings. C) Microfluidic temperature gradient device to change the division rates of the two cells away from their stereotyped division sequence.*

identity, and lineage dependent rates of division. These first two cells stereotypically divide at different times, with the larger dividing before the smaller. This sequence will later result in a number of key cell-cell interactions necessary for successful development. The rigid stereotype of this sequence and the critical nature of the dependent later events, suggests that the sequence itself may be under the influence of a system of robustness. At this stage such a system would necessarily include communication between the two cells to ensure their coordination in time. The work presented here establishes a method of challenging this system, by placing the *C. elegans* embryo in a temperature gradient sufficient to push the temperature dependent rate of division of the two cells away from their stereotyped temporal relationship. To achieve this we built and characterized a novel microfluidic temperature gradient device that can establish a 7.5 ^{O}C temperature gradient across the ~ 50 μm long developing embryo within biologically permissive temperatures. This temperature gradient establishes a condition that would be considered aberrant by the embryo at this stage, if and only if the two cells are monitoring each other's behavior. We have found that within a temperature gradient, the two cells of the embryo identify the existence of an aberrant condition and compensate for it by slowing their division rates. We find that the fold change in division timing of the two cells is dependent on their orientation in the temperature gradient, and that embryos that survive this condition to hatching generally slow down more than those that do not. We are able to reverse the sequence of divisions between the two cells and although they do not hatch, a surprising percentage undergo morphogenesis and result in a product that looks “wormlike” suggesting even later checkpoints and compensation. We also found

that in a fraction of the embryos loaded into the gradient after the first division, the cleavage between the two cells reverses and the two nuclei of the two cells migrate back toward each other.

The behavior of the two-cell embryos in the temperature gradient: 1) surviving a high percentage of time in lower gradients, and even a fraction of the time in higher gradients, 2) the slowing down of each cell relative to its expected behavior at the temperature it is experiencing with greater slowing resulting in a greater likelihood of survival, and 3) the entry of embryos into morphogenesis even after violation of the stereotypical sequence of division at the two-cell stage, constitutes evidence for one and possibly two previously unidentified compensation and coordination mechanisms that act to ensure robustness against variation in the timing of events in the development of the early *C. elegans* embryo.

Table of Contents

List of Tables and Figures

Chapter 1: Introduction and Background - Systems of robustness for "when".

In this first chapter we will seek to meet the following goals: 1) justify the statement that animal development is remarkably successful and complex; 2) that success in the face of this complexity argues for the existence of systems operating at the intercellular level to ensure events happen when they are supposed to, and; 3) lay the groundwork for our investigation into this hypothesized system using the model organism *C. elegans*, and microfluidics.

Development succeeds a high percentage of the time

Across the animal kingdom, development generally succeeds in creating a viable offspring a high percentage of the time. Experimental data exists for a wide variety of species with much of the available data coming from model organisms. The nematode *C. elegans* has an observed hatching rate of approximately 95-99% (Wood, W. B et al. 1980; Ward and Miwa 1978; Ben-David, E. et al. 2017), the fly *Drosophila melanogaster* a 97% hatching rate (Packard, C. 1926), and the frog *Xenopus tropicalis* with an approximate 98% successful development rate (Kosubek, A et al. 2010). Mammalian estimates are a bit more challenging to obtain as the eggs are not observed outside of the animal; however published estimates for lab strains of *Mus musculus* can be found in the range of 84-90% (Sthoeger, Z. M et al. 1993; Flores, L. E et al. 2014). Further examples are afforded as a result of agricultural concerns. Cattle have been reported as having a total level of embryonic

success rate of 62% (Sreenan and Diskin, 1986), while pigs, sheep and goats have embryonic success rates of approximately 70% (Bolet, G. 1986). Finally human development has an estimated success rate of 47%, reviewed by Macklon et al.(2002).

Success of development should be surprising

The success rate for animal development is particularly striking given its complexity and the estimated number of “discrete parts” in the animal. To give us a sense of the complexity involved in development we can construct a toy model, with some of our broad strokes coming from human development. We can begin by estimating the number of “discrete parts” as cells forming a human, which is roughly 40 trillion (Bianconi, E. et al. 2013). To grow from this single cell to the fully formed animal, even the most simple of developmental models would indicate no less than 45 rounds of cell doubling. It would seem reasonable that our total picture of “discrete parts” must also include the stages required to proceed from the starting point of the single cell to the final product.

Given that

$$\sum_{i=1}^{n} 2^i = 2^{n+1} - 2 \ ,$$

we find the total number of unique discrete parts throughout human development is on the order of

$$\sum_{i=1}^{45} 2^i = 2^{n+1} - 2 \approx 7 \times 10^{13}$$

However, our estimate does not fully capture the essence of animal development. To be sure, we have a rough estimate of the potential number of discrete parts throughout development that may be subject to failure, but this estimate is only a little better than if we had been evaluating the growth of a population of single celled organism such as the bacteria *E. coli*. To move us closer to understanding animal development our estimate must also include the concept of cellular context, as for an animal which is at least past the size at which diffusion is dominant, the identity of each cell must at least be correct in the context of its immediate neighbors, which is to say for an animal with a gut, it is not sufficient for there to be the correct number of gut cells in the animal, but rather those gut cells must exist together. By assuming the simplest spatial arrangement of a cell surrounded by its neighbors, and assuming the most compact and simplest spatial form of this arrangement, we can construct a rudimentary model of each cell during development as a center cube in a Rubik's cube. By doing so we find that under the most simple of cases, each cell in the developing embryo exists in the context of its immediate 26 neighbors (a Rubik's cube is three levels of nine cubes for a total of 27 cubes, or 26 surrounding a center cube). To simplify our estimate we will only count potential cell to cell context when there are enough cells for each cell to have 26 neighbors (when there are approximately ~ 2^5 cells) , and further assume that these interactions only happen in binary fashion, ie one cell to another cell without the necessity that three cells talk to each other simultaneously,. To sum this all up, our new estimate of discrete parts throughout development would be the sum of all direct physical interactions between

a cell and its immediate 26 neighbors after each round of division, divided by two to prevent counting each interaction twice.

$$\sum_{i=5}^{45} \frac{2^i \times 26}{2} = 13 \sum_{i=5}^{45} 2^i$$

$$13 \sum_{i=5}^{45} 2^i = 13 \left(\sum_{i=0}^{45} 2^i - \sum_{i=0}^{4} 2^i \right).$$

We calculate

$$\sum_{i=0}^{4} 2^i = 2^{n+1} - 2 = 31,$$

$$\sum_{i=0}^{45} 2^i = 2^{n+1} - 2 \approx 7 \times 10^{13},$$

And find the number of “discrete parts” throughout development to be on the order of:

$$13 \sum_{i=5}^{45} 2^i \approx 9 \times 10^{14}$$

This leads us to the rough conclusion that the number of “discrete parts” that must be defined for successful human development to be on the order of 1 quadrillion.

Of course it is not enough for a system to have a large number of discrete parts to be complex. For example a typical lottery has ~175,000,000 potential winning combinations, but it is not complex by any reasonable definition. Complexity therefore comes from not only the number of “discrete” parts, but rather the realization that these discrete parts must satisfy specific non trivial requirements

both individually, in relation to each other, and as a whole. Each cell along the way must also have the correct identity to move correctly to the next round. A starting point for an estimate of the number of potential identities can be made by estimating the number of identities in the final product, but this is not sufficient, as every trajectory toward that product, and every intermediate step along the way toward that product will have its own requirements of identity. Let us for a moment assume that these intermediate identities are defined by the time we have reached the first half of the divisions. We find that throughout the first 25 rounds of division we have cells totalling

$$\sum_{i=0}^{27} 2^i = 2^{n+1} - 2 \approx 3 \times 10^8 ,$$

with each cell necessarily taking on a unique identity, giving us a total number of cell to identity requirements equaling

$$\left(3 \times 10^8\right)^2 = 9 \times 10^{16} ;$$

a number which renders our earlier estimate merely a rounding error. And yet even this estimate accounts, not for one half of the total number of cells, but one half of the rounds of divisions of cells, leaving out 99.99999% of the total cells that will eventually make up our final animal unaccounted for.

Not only will each “identity” have any of a number of potential discrete values that can be taken on, but each cell will also need to meet requirements in four continuous dimensions of space and time. This is to say that along each step, each cell, within a

certain range of potential values, will have to be the correct type of cell in the correct context of its neighbors, and it will also need to exist in the correct place at the correct time.

This is of course merely a toy model that fails to take into consideration many factors. For example, successful completion of human development due to a single mistake will decrease dramatically as development moves towards conclusion. On the other hand even minor unchecked deviations in satisfying requirements early on will likely have catastrophic consequences.

To translate this level of complexity back to a sense of how remarkable it is that development succeeds at all, we must have some estimate of the likelihood of failure of each “discrete part”, or put another way, a sense of the fragility of the system as a whole. To start us off, we can pick some arbitrarily low frequency of only one in one million of these “discrete parts” as critical, and further estimate that each of these components only has a one in one million chance of failing to satisfy requirements to the point of systemic failure. This would lead us to the conclusion that approximately only one in every 100,000 human embryos that started development should conclude development successfully.

Variation, robustness, and complexity

To more fully understand successful animal development we must have some grasp for the nature of the challenges that development faces, which is to say we must understand the ways in which each of the critical discrete parts within development may be subject to influences that prevent them from satisfying their requirements resulting in systemic failure. Generally speaking, biologists place the challenges which have the ability to move each discrete part away from satisfying its requirements into three broad categories of imposed variation: genetic variation, environmental variation, and molecular noise (Félix and Wagner, 2008). Each of these sources of variation has the ability to cause each discrete part within development to fall outside of its allowable values of identity, location, and schedule, or its what, where, and when. The ability of biology to withstand these forces of variation during development and arrive at a single phenotype despite their influence, has been defined as the quality of "robustness". This idea of robustness encapsulates the notion that along the trajectory of development, the developing organism itself must have ways of counteracting the sources of variation it may experience in order to ensure that development moves forward to successful completion. This statement has two corollaries which may not be immediately evident: 1) robustness, and systems of robustness must be under evolutionary control and be selected for (Félix and Wagner, 2008), and 2) the selection for this robustness must necessarily increase our scope of the total complexity of development, as the very systems themselves that ensure success in the face of

complexity necessarily increase the total complexity of the system (Csete, M. E. 2002).

Systems for robustness

Several systems for developmental robustness have been identified experimentally. Examples of such have largely been associated with systems that help to ensure the coherence of development in the context of component identity and spatial coordination. An example of the former is Hsp90. A review of its action as an agent of robustness along with a handful of additional systems of robustness is reviewed by Gursky et al. (2012). Hsp90 is essential in yeast (Borkovich et al. 1989), *Drosophila melanogaster* (Cutforth and Rubin 1994), and *C. elegans* (Birnby et al. 2000). Fly experiments in which Hsp90 was impaired through mutation or pharmacological means, resulted in phenotypic variation affecting many of the adult structures. The specific phenotypic variation was found to depend on the genetic background of the strain of fly used. The variations themselves, when subjected to selection, became independent of the action of Hsp90 (Rutherford and Lindquist 1998). These results led the authors and others to conclude that Hsp90 acts as a buffer against cryptic variation, preventing divergence from a stereotyped end product in the face of genetic heterogeneity. The ability of Hsp90 to buffer phenotypic variability was also demonstrated in vertebrate development. Pharmacological inhibition of Hsp90 in the semidominant *you-too (yot)* zebrafish strain resulted in a set of novel structural eye malformations for that strain (Yeyati et

al. 2007). *yot* mutant zebrafish canonically lack an optic chiasma and a horizontal myoseptum in the somites. Canonical *yot* phenotypes are fully penetrant but present with varying severity (Karlstrom et al. 1999). In addition to the novel eye malformations, Yeyati et al. (2007) found that the mild inhibition of Hsp90 in this strain did not significantly worsen the canonical phenotype of *yot* embryos, suggesting that the impairment of Hsp90 in the already impaired *yot* background revealed new phenotypes as a result of previously unknown cryptic variation.

As an instructive example of a system that works to ensure robustness in spatial coordination during development, we can turn our attention back to *Drosophila melanogaster*. During early embryonic development, *Drosophila* is a multinucleated syncytium. The single nucleus of the earliest embryo goes through 13 cycles of nuclear division, with the division cycles of each subsequent nuclei occurring nearly simultaneously, and the distribution of nuclei relatively spatially uniform. Only during the 14th division cycle are the nuclei fully cellularized (Foe et al. 2009). Patterns of gene expression assign each cell in the embryo its particular fate. A concentration gradient of maternal product Bicoid along the antero-posterior axis is established before the full cellularization of the embryo. The different levels of Bicoid proceeding from the anterior to posterior of the embryo in part establishes the gene expression pattern that will assign each cell within the gradient to its specific fate after the 14th round of division (Driever and Nüsslein-Volhard 1998). However, the expression profile of Bicoid is variable from wild-type embryo to embryo and the variability is

increased with increased temperature (Houchmandzadeh et al. 2002). The evidence for a system of robustness comes from the finding that expression of one of Bicoid's targets, Hunchback, is not altered by the high level of variability in the Bicoid protein gradient (Houchmandzadeh et al. 2002). Indeed, a study by Lucchetta et al. (2005) sought to test the limits of the system that compensates for variability in Bicoid input and the invariability of Hunchback output. To test the compensatory capacity of the system, the authors subjected the developing *Drosophila* embryo to a temperature gradient of ~ 10^{O}C along its antero-posterior axis for up to one and one half hours. The temperature gradient was sufficiently high to observe that the nuclei in the warmer half of the embryo underwent up to two rounds of division more than those in the cooler end. The shape of the Bicoid gradient has been shown to be a combination of the temperature dependent rates of production, diffusion, and degradation of Bicoid. Despite the adverse conditions, the larvae developed normally, with Hunchback boundaries remaining spatially precise (Lucchetta et al. 2005)

The last example of systems of robustness we will present is perhaps the most striking and profound in its broad implications. This example does not demonstrate a specific component or mechanism for a system of robustness, but provides circumstantial evidence for the possible extremes of system level coordination and phenotypic guidance that are possible with such systems. A pair of recent studies sought to identify whether it would be possible to rescue pancreas development by

introducing rat pluripotent stem cells (PSCs) into the blastocysts of mice compromised for pancreas development, and mouse PSCs into the blastocysts of rats compromised for pancreas development (Kobayashi et al. 2010, Yamaguchi et al. 2017). The authors of the two studies found that such a rescue was possible. They further found that the new pancreata were almost entirely made up of descendents of the donor cells, and that the structures, despite being almost entirely comprised of donor cells from a different species, were morphologically characteristic in size and structure to that of the host organism, as was the size of the whole animal. This finding is significant in view of the fact that wild type rat gestation is 10-15% longer than wild type mouse gestation and that wild type newborn rats are three times the size of wild type newborn mice (Kobayashi et al. 2010). Moreover, the authors found that rat host derived chimeras lacked gallbladders as do wild type rats in general, and that mouse host derived chimeras had gallbladders as do wild type mice in general (Kobayashi et al. 2010).

These findings are remarkable for a number of reasons, but for our purposes here we will focus on the following: the success of these experiments speaks to a system of robustness that can act at the level of gross morphological structures and it can do so in the face of genetic variation found at the level of 12-24 million years of evolutionary divergence (Gibbs et al. 2004, Springer et al. 2003, Adkins et al. 2001). This system is sufficiently malleable to correct for genetic differences that would otherwise result in differences in size and even the presence or lack of presence of

entire genetically predefined structures up to and including at the level of organs and in the context of entire the organism.

Robustness for “When”

The aim of the work presented here is to identify systems for robustness for what surely must be one of the more intractable dimensions in which variation may impose its influence, namely that of time.

Identifying and understanding systems that dictate when things occur in biological development is an active area of research. Perhaps the most fundamental of these is the cell cycle itself. Within the developing organism, inside each cell is a network of genes that controls the progression of the cell through division. This network is largely comprised of cyclin kinases and antagonizing protein phosphatases (PPs) that control entry and exit into and out of interphase and mitotic phases. A review that covers the various components that dictate the timing and levels of control for various species and stages during development is presented by Heim et. al (2017). The action of this network works to establish a molecular clock for each cell that is internal and intrinsic to each cell (Morgan 1997, Begasse and Hyman 2011, Murray and Kirschner 1989, Goldbeter et al. 2012).

The influence of cellular clocks can also be found in the development of the somites that give rise to the vertebrae in vertebrates. A segmented pattern is formed in the

somitic precursors of the skeletal muscles and the vertebrae, that will later result in the segments of the vertebrae, as reviewed by Pourquié (2001,2007). Early mathematical models of this process were dependent on an assumption of a temporal oscillator or clock to help establish the segmentation (Cooke and Zeeman 1976), with genetic evidence found as periodic expression of *c-hairy1* mRNA in these precursor cells in the chick embryo (Palmeirim et al. 1997). This timing mechanism has cell-autonomous components as the oscillatory transcription of *c-hairy1* in the precursor cells continue to persist when parts of this developing tissue are separated from each other (Palmeirim et al. 1997), and cell-non-autonomous components as Jiang et al. (2000) found that mutations in the Notch signalling pathway resulted in the oscillations of these cells in zebrafish moving out of synchrony.

The Notch signalling pathway described above is an interesting example of how developmental clocks may compensate for deviations across cellular components; however, the ubiquity of such compensation systems is still unknown. We have distilled the focus of our work to testing for evidence of a putative system that would act to ensure the successful meeting of two or more discrete components of a system in time; a meeting that is both spatially and temporally defined and necessary for successful development. To give us a framework for why such a system should exist, let us go back for a moment to the toy model we constructed earlier. Let us assume that along the developmental trajectory of our model, there is

a step in which two cells will need to meet and exchange information in order for each to move along their own trajectory correctly. We will further assume that while they have a common antecedent cell at some point, that point is in the past, removed by some number of divisions. This means that the successful exchange of the information between these two cells is dependent on the length of time of division for each of the antecedent cells. What happens as a result of variation in the system, if one of the cells and its antecedents is slightly slower in developing than the other? The result of this timing mismatch would be that the information was not shared and one or both of the cells or one or more of their descendents would encounter a critical error. The length of time each of the antecedent cells takes will be dependent on a number of factors, including all three sources of variation: genetic variation, environmental variation, and molecular noise. From a genetic viewpoint, the length of time taken for each round of division for the antecedents will be dependent on 1) the cellular machinery of the cell cycle along with the required genetic expression profile, and 2) all anabolic and catabolic activity necessary for each antecedent to satisfy its own requirements. For example, the existence of lineage specific cell cycle duration has been demonstrated in *Drosophila* and *Xenopus* embryos (Edgar and O'Farrell 1990, Murakami et al., 2004). In *Drosophila*, the expression pattern of Cdc25 phosphatase *string* (*stg*) controls the timing of the transition from G2 to mitosis in different mitotic domains during the 14th cell cycle. In Xenopus, the Wee1 kinase and Cdc25C phosphatases are necessary for the cell to enter mitosis. Overexpression or disabling of these molecular systems in the

development of either organism leads to embryonic arrest or morphogenic defects (Edgar and O'Farrell 1990, Murakami et al., 2004). Variation in these systems brought on by genetic heterogeneity or even minor mutations, would dictate at least minor fluctuations in cell cycle duration in a lineage-specific, and therefore cell-identity specific, way, opening a possible avenue for evolution to establish systems to minimize effects of perturbations of these systems.

Identifying such a system is not trivial as can be demonstrated by asking and answering the question: how would the failure of such a system present itself experimentally? The answer would depend on the specific case. As a motivating example, let us again turn to our earlier model. We have under consideration a situation in which two cells will come in contact during development and share information that will allow one or both of them to successfully continue onward in development. We know that if one of them is late in relation to the other, either one or both of them will fail to proceed appropriately and development will fail. We hypothesize that this pre-ordained meeting is under the control of a system that ensures that both will meet at the correct time. Now let us assume that, through the generally used laboratory method of imposing random genetic mutations, we have somehow disabled this system, and this system alone. How will such a mutation present itself phenotypically? Three possibilities are: 1) development of that animal will fail and the phenotype will be lethality, 2) if the animal did not experience conditions that required the system to act, the result will be a living animal with no

discernible deviation from wild type, or 3) a probabilistic range of outcomes in which animals will fall into one or the other category at some frequency.

We can, however, look for evidence of the putative system. The lineage-specific cell cycle described above for *Drosophila* could produce a situation where such a system could help to insure successful development in the face temporal developmental fluctuations as a result of genetic variation. For evidence of the putative system working to counter environmental variation we can look to poikilotherms, animals whose internal temperature is generally in equilibrium with the environment. These animals will, at a minimum, experience variation in temperature during the course of development. As all of known life is biochemically based and chemical reaction rates change non-linearly with temperature, each of the processes in each cell will experience at least some **non-linear** time effect when changing from one temperature to another. In the model organism we have been developing above, were it a poikilotherm, the line of antecedents of the two cells will experience a given set of rates of chemical reactions at a particular temperature. If we choose one particular temperature as the baseline such that at that particular temperature everything happens just right, we can ask the question of what happens when the temperature move away from that baseline. As the identities and activities of the two lines of cells diverge from their original common antecedent, so will the list of the differences in their cellular machinery, genetic expression profile, and anabolic and catabolic activity. As these chemical processes and constituents diverge, so will their

response in time in a non-linear fashion, as a result of this new temperature. This non-linear response will result in differences in cell division timing even if the organism is genetically homogeneous. The sensitivity of the organism to this baseline can be seen in a comparison between the temperature-dependent development of *C. elegans* and a closely related sister species *C. briggsae*. *C. briggsae* and *C. elegans* diverged approximately 100 million years ago yet are morphologically very similar, share many genomic characteristic, both gross and molecular, occupy the same ecological niche and share remarkable similarity in developmental pattern and trajectory (Stein et al. 2003 ,Zhao et al. 2008). However they have slightly different temperatures at which development is permissible, with *C. briggsae* able to withstand slightly higher temperatures (Gupta. 2007). A recent study has shown that the activity of the early embryo of both species shares similar temperature-dependent kinetics, but that *C. briggsae* develops slightly slower at a given temperature, and the lower bound of permissive temperature is higher than that of *C. elegans* (Begasse et al. 2015). In fact they found that the range as a whole was shifted between the two species. This is consistent with findings that the developmental timing at a given temperature across divergent *Drosophila* species are different, but that the different developmental stages of all species scales uniformly in time with temperature (Kuntz et al. 2014). With respect to the putative system we are discussing here, the salient point of these studies is not that different organisms have adapted to different temperatures but rather that along the evolutionary course of these diverging species a system of robustness could have

acted to buffer the phenotypic variability during the transition from one optimal temperature to another.

In terms of random noise, we once again realize that all of life is biochemical and necessarily comprised of molecular components and machinery. During the process of division of one cell, these components and machines, including those responsible for the cell cycle and subsequent cell cycle rates are divided and segregated into the two new daughter cells that have arisen from the parent cell. Studies have shown that endosomes, lysosomes, mitochondria, and Golgi vesicles have demonstrated a wide range of partitioning errors during mitosis (Bergeland et al. 2001, Wilson 1916, Wilson 1931, das Neves et al. 2010, Shima et al. 1997). Strong evidence has recently been demonstrated that mitochondrial variability results in variability in transcription (das Neves et al. 2010) and is a source of extrinsic cellular noise (Johnston et al. 2012). A system for ensuring the robustness of “when” developmental events occur, could certainly be a reasonable evolutionary strategy to buffer this type of variation.

We might even see the possible action of such a system in our previously presented example of chimeric mice and rats. The mismatch in gestation timing, along with the differences in size and subsequent likely number of cells at birth and the corresponding mismatch in total number of cellular divisions between rats and mice, hints at the likelihood that at some point in the development of the foreign

cell-derived pancreas within the chimera, a “settling of temporal accounts” amongst the cells of differing backgrounds was necessary for successful development. Such a system might act in two ways: 1) it could identify deviations in acceptable rates and timing of events and act to correct the deviations immediately after or during their occurrence, or 2) have pre-established checkpoints along development that allow for identifying the results of problems that have occurred in the past, and attempt to compensate for them in the present or at some point further in development.

Now that we have established why a system of robustness might exist to ensure “when” should be selected for, we can move our focus to attempting to identify the components of such a system experimentally. If we use traditional genetic means by attempting to disable the system through imposed genetic mutation and evaluating only the end point, we may be unable to discern this mutation from other types of mutations. For example, turning back to our model of two cells meeting in space and time to share information that allows both cells to move forward successfully in development, a mutation that completely disrupted the molecular basis for the communication between the two cells would result in failure of development and lethality, independent of our postulated system. Likewise, a mutation that only partially disabled the communication method would likely fail part of the time, and succeed part of the time, resulting once again in a dead animal some of the time, and an animal that had developed properly the remainder of the time. The same

argument can be applied to mutations that affected the identity of either of the cells, or any of the antecedents of the cells. To identify a system for robustness that ensures the proper meeting of the two cells in time, we would need to know that those two cells have to meet at the correct time, and that changing the timing of the arrival of both without affecting the identity of either was what resulted in failure of development. We would further require a methodology for pushing these two cells away from their expected rendezvous in time, without affecting either their identities or the identities of their antecedents. Such a method would allow us to isolate the effects of the robustness system itself, either by challenging its ability to compensate, or experimentally control the timing of the two cells in its absence upon being disabled.

Experimental System: *C. elegans* Embryogenesis

To move forward with our investigation we must find a biological system that can faithfully represent animal development while allowing us the ability to tractably address the “when” of events. This system must afford us the opportunity to identify specific points where the “when” of a particular meeting between cells is necessary, identifiable, predictable, observable, and manipulable. We now turn our attention to an animal that we believe will allow us to address these issues, namely the nematode *C. elegans*.

C. elegans was introduced to the world as a model organism for genetics research by biologist Sydney Brenner (Brenner, S. 1974). Brenner had been looking for an organism that would allow studies of multicellular animal development to be addressed genetically in the laboratory. Brenner introduced a set of genetic tools for the worm, and many have been developed since then.

C. elegans as a model for animal development has a number of very powerful features. The animal is transparent at all stages of development, allowing for the ability to visually track each cell in development. *C. elegans* development is completely cellularized from the first division, allowing for each step of development to be defined in terms of discrete and physically separate components (Deppe et al. 1978). The worm has a fixed number of cells, possessing 558 nuclei immediately after hatching from its egg shell (Sulston et al. 1983), with additional divisions continuing until it completes development with 959 somatic nuclei for the fully formed adult hermaphrodite (White 1988). Many of the cellular divisions, including the very first are asymmetric, allowing for individual cells to be specifically identified during development (Rose and Gonczy 2014). A polarity or directionality is also established in the very early embryo, allowing for identification of a defined anterior and posterior of the embryo (Rose and Gonczy 2014). These properties of asymmetry of division and polarity have allowed every division of every cell to be followed and mapped, and led to the discovery that development is largely invariant in terms of identities and positions of cells as well as sequence of divisions at every step (Sulston et al

1983, Schnabel et al. 1997). The absolute timing of those events at a given temperature is also largely invariant from animal to animal (Bao et al. 2008). *C. elegans* is a poikilotherm that is able to develop normally at temperatures ranging from ~12^{O}C to 25^{O}C (Neves et al., 2015). The rate of development of the entire animal is temperature dependent, with the time for development decreasing by approximately one half for every 10 degrees of decrease in temperature (Deppe et al. 1978, Byerly et al. 1976).

In conjunction with the size asymmetry of many of the early cell divisions, there also exists many temporal asymmetries. Very early in development a distinct characteristic cellular clock (the time it takes from the division of one cell to the division of its daughters), is uniquely defined for five specific cells, the founder cells (Sulston et al. 1983). The subsequent cells in the lineages of each of these early cells will take on the cellular clock of the founder cell for that line (Sulston et al., 1983, Bao et al. 2008). The differences in the clocks can be seen as early as the two-cell stage, where the larger of the two cells, referred to as the AB cell for “anterior blastomere”, will divide earlier than the smaller of the two cells, referred to as P_1 for “first posterior blastomere” (Sulston et al. 1983, Sulston and Horvitz 1987). This sequence of events, AB dividing first followed by P_1, is observed at all temperatures for which the animal is able to develop normally. In addition, two immediate descendants of AB and P_1 physically touch during development. ABp, the posterior daughter of the AB cell, and P_2, the posterior daughters of the P_1 cell, are

not only in contact but are known to share information that will help to establish the trajectory of ABp and its descendents (Priess and Thomson 1987). That AB divides first, giving rise to ABp before P_2 has formed, gives rise to the possibility that this specific sequence of events, AB dividing before P_1, is necessary for the successful interaction between ABp and P_2. This sequence in turn is dependent on the differences in the internal cellular clocks of AB and P_1. As a result, this interaction between ABp and P_2 establishes a situation that fulfills part of our experimental requirements for identifying a system of robustness that ensures the proper timing of particular events within the context of development: the meeting of two cells in space and time, the successful consummation of which is necessary for successful development, in a temporal regime that does not immediately guarantee that they will in fact meet.

Historically the sequence of division of AB and P_1 has been considered to be cell-autonomous and that the time of division for each of the cells is dependent only on the internal conditions of each of the two cells independent of the other. Investigations in which these two cells were removed from the context of the other appeared to result in normal division timing, seemingly precluding the possibility that the time of the division of each of the cells is influenced by the behavior of the other cell (Sulston et al 1983, Deppe et al. 1978, Schierenberg and Wood 1985). However these experiments had two shortcomings. First, the experimental methods used were necessarily either destructive, disruptive, or both, to the developing embryo.

Second, if there is a system in place to ensure the stereotypical sequence of divisions of AB and P_1, it would likely act to modify the existing internal clocks, not necessarily as an integral component of the clock, but rather interfacing with it to return the the entire system back to within acceptable bounds.

The specific hypothesis we propose to test in this work is whether or not the timing of division of AB and P_1 are influenced by cell-non-autonomous events that operate to ensure a reproducible pattern of cell divisions . We postulate that the sequence of divisions of these two cells is so stereotyped, and the subsequent meeting of the immediate daughter cells so critical, that if a system of robustness does exist to ensure proper timing of development events, it is likely to act even at this early juncture. To test this hypothesis, we created an environment where we can modify the developmental timing of the divisions of the AB and P_1 and the subsequent order of divisions, and look for evidence of a system that is able to identify this discordant condition and direct development to accommodate it. We have aimed to modify the relative time of division between these two cells by utilizing the inherent temperature dependent rate of development of the animal. To achieve this, we have placed the embryo into a temperature gradient bringing both to local temperatures sufficient to drive their internal clocks away from their normal relative division times, with both still within the confines of previously established permissible temperatures for the development of the animal.

It is important to note that we do not expect that *C. elegans* embryos in the wild would experience a temperature gradient such as the one applied here. Instead we have used the temperature gradient, and the subsequent temperature-dependent response in division timing of each of the two cells, as an experimentally controllable proxy for the types of variations the cells would ordinarily face that could drive the sequence of divisions away from its characteristic pattern.

Experimental System: Microfluidics

Our technical challenge was to construct a system that allowed us to reproducibly subject the *C. elegans* embryo at the two-cell stage, to a temperature gradient. This task is not a trivial one. The embryo of *C. elegans* is approximately 50 microns long. A difference of temperature between the two cells sufficient to drive them to divide outside of their stereotyped sequence can be estimated at approximately 5 degrees, a number we will seek to flesh out more fully in chapter 3. This means that the temperature gradient required to break the stereotyped division sequence at this stage of development, were it extended to the length of a meter measuring stick, would place one end of the measuring stick at 0 Kelvin, and the other end at 100,000 Kelvin; a temperature more than 17 times hotter than the surface of the sun.

To enable us to achieve this technical requirement we will build and characterize a temperature gradient device by employing a group of technologies commonly referred to as microfluidics or micro electrical mechanical systems (MEMS).

Generally speaking, microfluidics and MEMS systems utilize the technologies introduced by the microcomputer fabrication revolution. With microfluidics, these tools have largely been repurposed to go beyond the original goals of constructing and controlling electrical environments and signals, to allow experimenters to construct and control physical environments on micro scales. Microfluidics in particular, refers to the subset of these types of devices that are constructed to control small volumes of fluid in well-defined ways. The use of microfluidics in C. elegans has been reviewed recently by San-Miguel and Lu (2005).

We have constructed a microfluidic device that allowed us to: 1) create a temperature gradient of more than 5 degrees across 50 microns, 2) introduce and retrieve embryos into and out of the device, 3) position the embryos within the temperature gradient, and 4) record the behavior of the embryos within the temperature gradient.

Conclusion

The remainder of this thesis will proceed as follows. In chapter two, we detail the development and characterization of a microfluidic device that enabled us to subject individual developing embryos to a temperature gradient of up to 7.5 ^{o}C. In chapter three, we detail our verification of this device as a tool compatible with *C. elegans*, build a quantitative model of the rate of development of each of the cells of the two-cell embryo as a function of uniform temperature, and document our results in

applying the gradient to the two-cell embryo. Finally in chapter four, we discuss the biological implications of our findings and put them into the context of existing research, and provide indications on areas of further investigation and development for both the engineering and the biology.

Chapter 2: Design, fabrication, and characterization of a temperature gradient microfluidic device for use with C. elegans *embryos*

Original design objectives and challenges

Our initial design goal was to build a microfluidic device that would allow us to establish a temperature gradient along the long axis of the developing *C. elegans* embryo. Along with this requirement it was necessary to 1) to establish a method of measuring the temperature gradient, 2) establish a way of introducing and retrieving embryos into and out of the device, 3) once in the device, position the embryos within the temperature gradient, 4) verify that the material and environment of the microfluidic device itself does not affect the viability of the embryos, and 5) be able to record the behavior of the embryos within the temperature gradient. In addition we also sought a way to increase the number of experiments that could be run simultaneously.

What is new in this work

While a number of these challenges have been addressed in the literature, several have not. There are several examples in the literature detailing microfluidic-based temperature gradient devices (eg Lucchetta et al. 2005, Mao et al. 2002); however, we believe this work describes the first example of a 7.5^{O}C temperature gradient

across the length scales involved within the temperature range constraints involved. In addition, while there are examples in the literature of using *C. elegans* embryos in microfluidic devices, to our knowledge this is the first device that allows for a single embryo to be selected at an arbitrary developmental stage up to and including pre-pronuclear meeting, reliably loaded into the device and then reliably and identifiably retrieved from the device.

Final device summary

Over several generations of devices and rounds of refinement, we arrived at the current temperature gradient device that we use for embryo temperature gradient experiments (Figure 2.1, 2.2).

A micro-heater is used to establish the high temperature side of the gradient and is created by patterning an approximately 10μm wide, ~100 nm thick, and ~ 5 mm long platinum metal strip on 1mm thick glass utilizing micro photolithography and evaporative metal deposition (Figure 2.1). In addition to the heater, four micro-resistive thermal devices (RTDs) are patterned at the same time on the device using the same material (platinum). Three of these four sensors are 10μm wide, straight traces and range in length from ~3mm to ~ 1mm running parallel to the Joule heater. Each of them is placed at increasing distances from the heater.

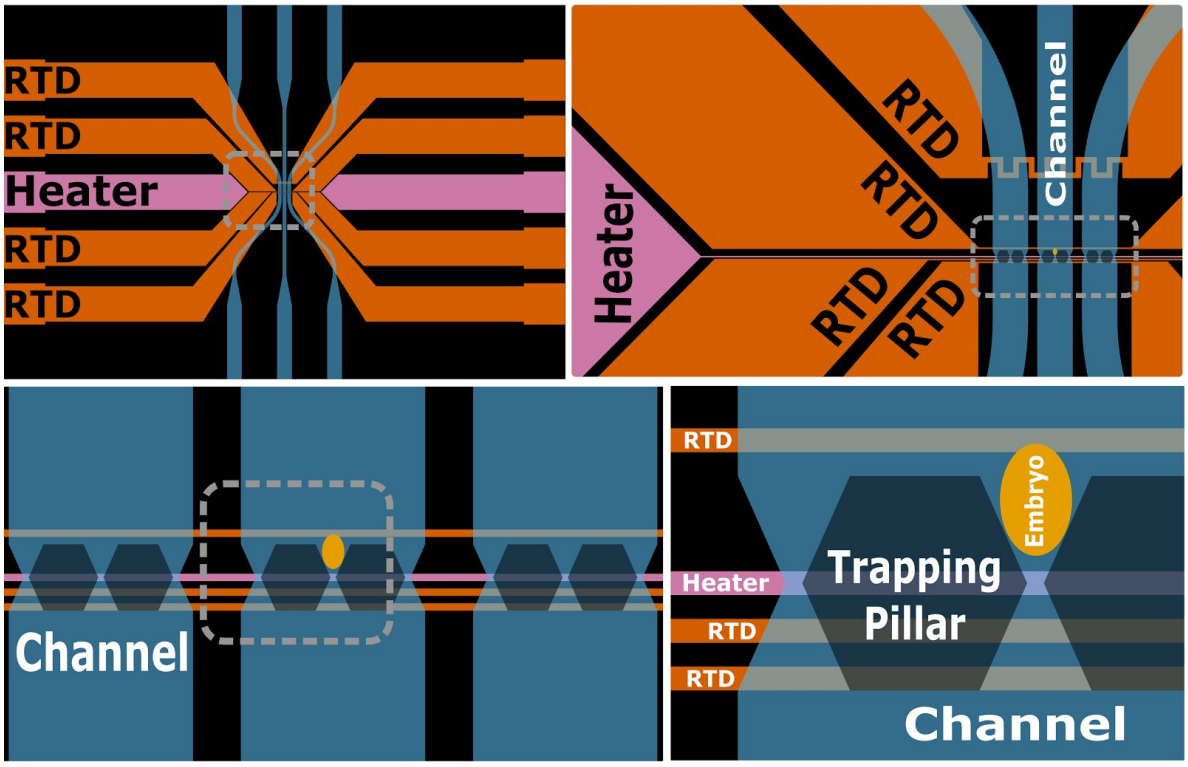

Figure 2.1: Schematic of layout of device at four scales. Top Left: macro view of device. Blue indicates channels, orange indicates temperature sensors (RTD), and purple indicates Joule heater. Callout is found on Top Right: closer view of temperature-sensing regions of RTDs and capture region. Callout is found on Bottom Left: view showing all three channels, capture regions for embryos in each channel, and Joule heater and RTDs close to Joule heater. Callout is found on Bottom Right: closeup of a single capture region and example of embryo size and placement. Spacing between heater and lower RTDs is 10μm. Width of heater and RTDs is 10μm

The closest parallel sensor is placed 10μm between the edge of the sensor and heater, and the furthest is 50μm between the edge of the sensor and heater. A fourth sensor is patterned several millimeters away from the heater to measure the temperature of the device largely outside of the influence of the heater and is constructed as a serpentine trace, allowing for increased spatial averaging (Figure 2.1). The sensors and heaters are covered with ~2-5μm of SU-8 material to isolate

them from the salt water that will eventually be used in the channels of the device, and to prevent hydrolysis as a result of the difference in electrical potentials between the heater and the sensors.

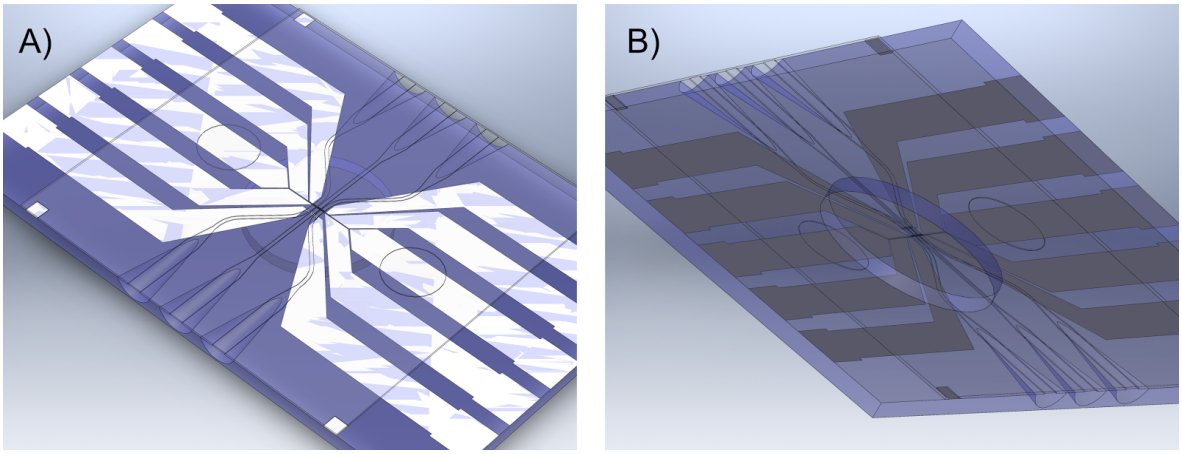

Figure 2.2: Solidworks model of device A) Top view of device showing electrodes, channels, and vias. B) Bottom view of device showing region of thinned glass in center of device.

A microfluidic channel fabricated through soft lithography, using Norland Optical Adhesive (NOA) identified in the literature largely as “sticker devices” (Morel et al. 2009, Bartolo et al. 2008) is placed on top of the heater, with features sufficient to capture and orient a specimen within the temperature gradient. To achieve the heat rejection through the glass, a mixture of chilled water and ethylene glycol (in a ratio of ~ 4:1) is flowed underneath and in contact with the glass. By controlling the flow rate and temperature of the fluid underneath the glass, as well as the power through the Joule heater, we are able to control both the magnitude of the temperature

gradient as well as the absolute temperatures at both the hot and cold side of a specimen.

To increase the magnitude of the temperature gradient within our temperature limits, an ~1 cm diameter and ~ 750-800μm deep disk is removed from the glass on the external underside the device. This disk is immediately underneath the capture and gradient region of the microchannel. This results in glass under the capture region of the channels of approximately 200-250μm thick.

The entire device is mounted on top of a custom built holder that allows for bulk cooling fluid flow to be introduced under and in contact with the external underside of the device. An obstruction is affixed inside of the flow of the holding chamber, underneath the etched disk, to increase the flow of fluid near the external bottom surface of the device (Figure 2.3).

Figure 2.3: Exploded view of holder and device assembly, with top most layer on left, and lower layers spread to the right. A) Top most pressure plate. B) Lower pressure plate with notches to allow for tubing and wiring. C) Top PDMS gasket. D) Device. E) Bottom PDMS Gasket. F) Flow cell body. G) Bottom of flow cell body with flow obstruction in the middle. Flow obstruction sits inside of the flow cell body when

assembled. Device is held in place by placing screws at each of the four corners and through lagers A and B and screwing them into the flow cell body (layer F). Flow obstruction is secured to the bottom of the flow cell body which is itself secured to the flow with two-part epoxy.

The fluidic interface between the macro environment of the lab and micro environment of the microfluidic device is achieved by removing six hemi-conical sections of glass along each of the long edges of a 1mm x 1” x 1.5” piece of soda-lime glass (commercially available microscope slides cut in half) before the microfluidic channel layer is affixed. The hemi-conical sections are perpendicular to the long edge of the glass and project into the glass on the order of five to six millimeters. The sections are approximately 1.5mm in width and 850-900μm deep at the edge of the slide and taper in both width and depth as they proceed into the slide to approximately 100μm wide and deep. Once the microfluidic channel layer is affixed, Polytetrafluoroethylene (PTFE) tubing is inserted into the now completed hemi-conical channels, and secured with adhesive.

Design considerations and choices

A number of methods to establish a temperature gradient inside of a microchannel were initially evaluated, including micro Peltier elements (Maltezos et al. 2005), two temperature flows (Lucchetta et al. 2005), photonic heating (Kim et al. 2009) and Joule heating, and all of which are reviewed by Miralles et al. (2013). We decided that micro Peltier devices would be relatively and potentially prohibitively complex,

while also likely preventing transmitted illumination required for visualization of the developing embryo. We also decided that a two temperature flow system such as used by Lucchetta et al. (2005) for temperature gradients across D. melanogaster embryos would require prohibitively high flow rates to be a reasonable solution, and that photonic heating would limit the number of simultaneous experiments that could be performed. We decided that Joule heating using micro patterning, along with some form of active heat rejection would be the best candidate for relatively low complexity in fabrication, ability to adapt to transmitted illumination and microscopy, and ability to handle multiple embryos simultaneously.

Finite Element Modeling

To further investigate the efficacy of a micro patterned Joule heater as a means of establishing a micro temperature gradient, we constructed a two-dimensional cross section model and numerical simulation of what we considered to be the critical parts of a device: 1) The microfluidic channel itself and immediately constraining materials. 2) The interface between the device and the air on the top of the device. 3) The interface between the device and the heat rejection system on the bottom. And 4) the Joule heater. The model indicated, as was later verified experimentally, that by using commercially available microscope slides of 1 mm thickness we could achieve an approximate 4.5-5^{O}C temperature gradient across 50μm between the temperature ranges of 10-25^{O}C. We also found that by reducing the thickness of the

glass, we would also be able to increase the temperature gradient across this distance and between these temperature ranges (Figures 2.4-2.6).

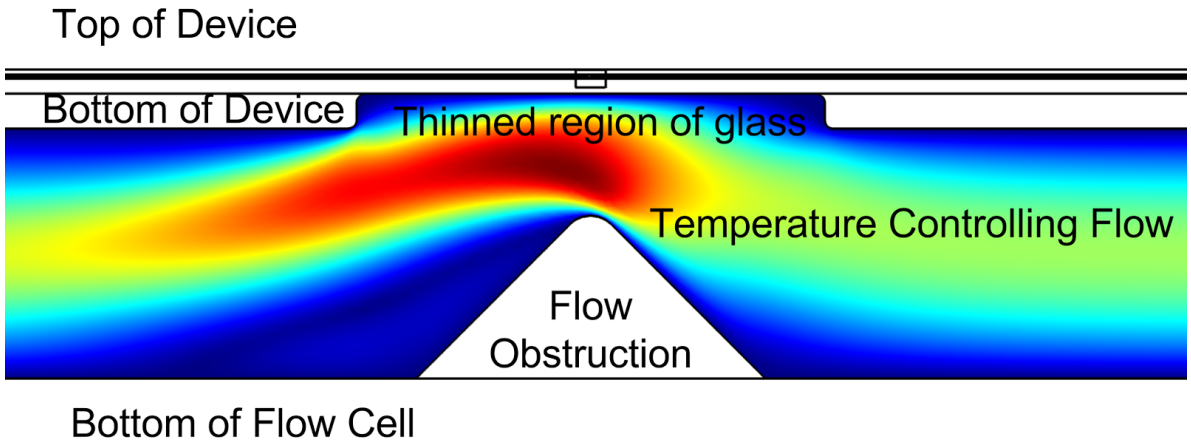

Figure 2.4: Comsol model of cross section of device and device holder during operation. Colored region is indicating speed and path of bulk fluid flow underneath the device. Red is highest flow moving toward lower flow in blue.

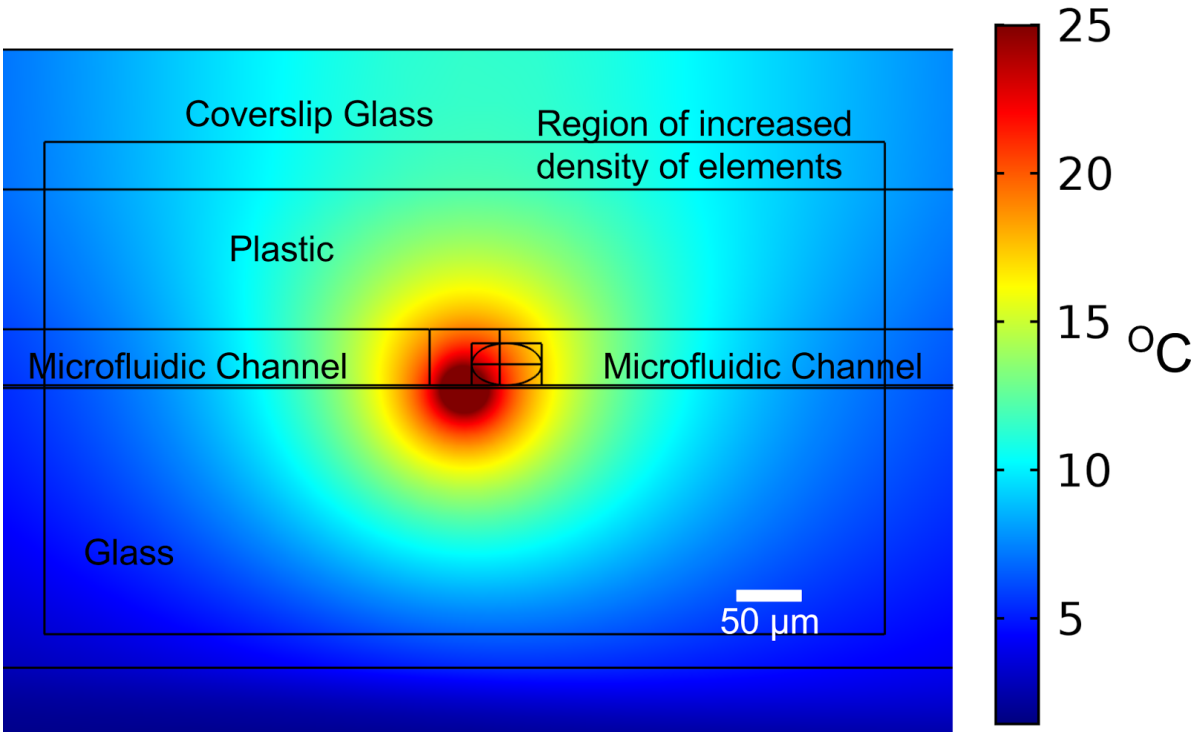

Figure 2.5: Comsol model of cross section of temperature gradient region of device. Oval indicates placement of embryo. Most lines demark separation of material types. Exception is larger rectangle that was used to establish a region of increased density of computation elements.

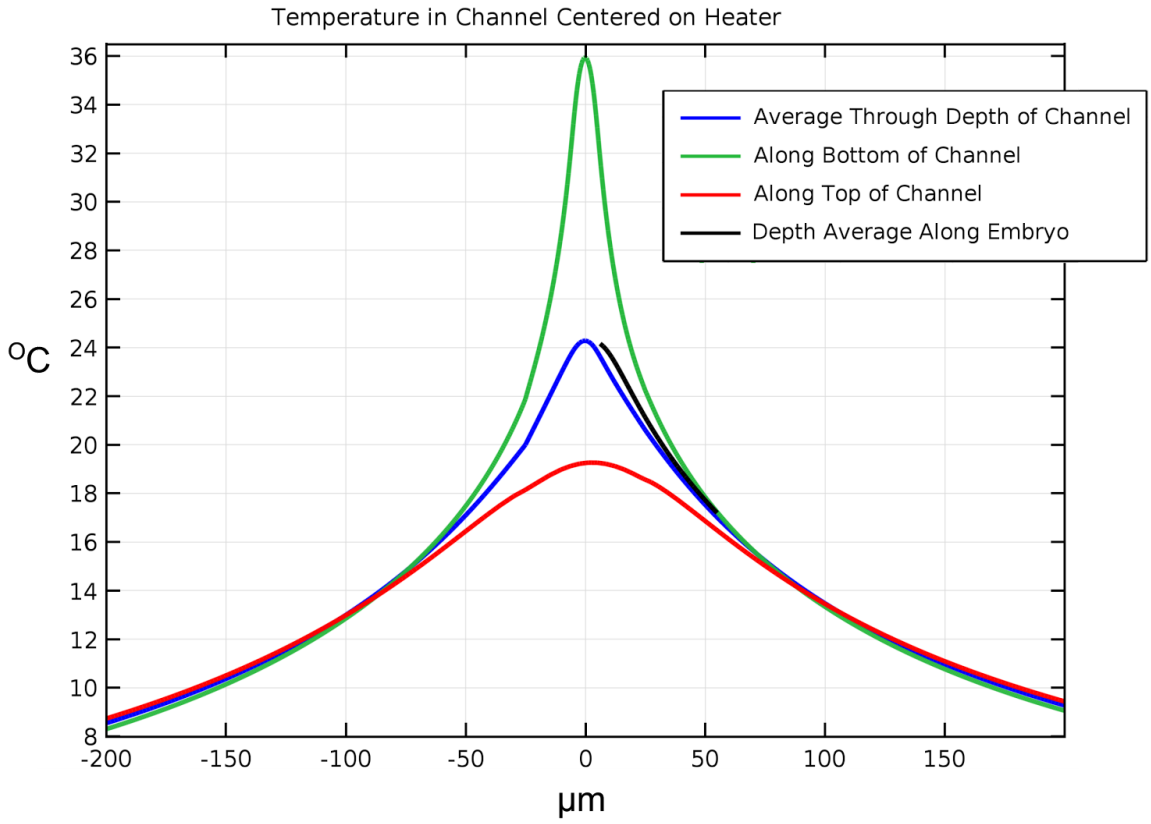

Figure 2.6: Graph of computed temperatures from model. x=0 is center of heating element.

Throughout the development of the device we continued to use numerical simulations to test design changes. Four significant changes were introduced over several design iterations. These were also tested numerically and verified experimentally: heat rejection by high speed fluid flow under and in contact with the bottom of the device, heat absorption on the top as a result of device holding and cooling apparatus, thinning of the glass under the embryo capture and gradient region to increase the magnitude of the temperature gradient, and deposition of a

thin layer of plastic over the electrode layer of the device to separate the Joule heater and sensor electrodes from the fluid in the microchannel.

To determine whether or not a temperature gradient would be experienced within the embryo, we modeled the embryo as a 50x30 μm spheroid with thermal conductivity equal to that of water, $k_{cytoplasm}$=0.6 W/m-K (Croce et al. 2010, Lucchetta et al. 2005), with an insulating eggshell of 300 nm thickness (Johnston and Dennis 2011). Although cytoplasm is a gel matrix, thermal conductivity of a gel is very similar to that of water, where, for example, a concentrated protein solution of 10% gelatin, is only 5% lower in conductivity than that of water (Boggs and Sibbitt 1955). While thermal conductivity of nematode eggshells has not been measured, a model of Drosophila embryos (Lucchetta et al. 2005) used $k_{shell}=k_{paraffin}$ wax =0.25 W/m-K, an extremely conservative estimate that assumes a value that is 10x more insulating than an avian eggshell with a k=2.25 W/m-K (Sun 2007). Using this extreme value in our simulation, the in-embryo gradient was reduced by only 1%. In fact, with an absurdly low value for thermal conductivity that is 10,000x more insulating than avian eggshells (and 60x more than argon gas), the in-embryo gradient in a $5^{O}C$ gradient environment would be reduced by a mere 13%, or $3.6^{O}C$ across 50 μm. We also considered the possibility that extremely active fluid circulation within the embryo might overcome the temperature gradient within the embryo by convective transport. However, the maximum known cytoplasmic streaming velocity of 7 μm/min (Hird and White 1993), cannot overcome thermal diffusion at this scale as the Peclet

number of the embryo with known dimensions and expected possible highest velocity is only $2.5x10^{-5}$.

Material Selection: PDMS v Sticker Material

The channel layer of our initial devices were made by using soft lithography and poly dimethylsiloxane (PDMS) (Duffy et al. 1998; McDonald et al. 2000; Xia and Whitesides 1998). However PDMS posed a number of challenges. Firstly, PDMS has a tendency toward a relatively high amount of compliance, the fluidic analog to electrical capacitance (Kim et al. 2006, Gervais et al. 2006). This generally translates into both delayed initiation and cessation of fluid flow once the microfluidic fluid flow systems are started or stopped (Kim et al. 2006), and results in longer load and unload times of embryos than would be possible without the "fluid compliance". The elastic and deformable nature of PDMS that leads to "fluidic compliance" also results in physical distortions of features under high or low pressures (Gervais et al. 2006). As a result we found that the capture pillars were distorted during testing of loading and unloading embryos, which exacerbated analysis of the unloading and loading. When fabricating PDMS devices in the lab, the PDMS is also frequently used as the structural material for the channel as well as for interconnecting to the outside world (Quaglio et al. 2008). This generally results in the PDMS being relatively thick when compared to the channel depths themselves, and can frequently lead to a good deal of variability in height of the entire device itself. Under a number of circumstances this is not a problem; however,

when trying to create devices that consistently dissipate thermal energy in a predictable manner, this can potentially be a hinderance.

To address some of these challenges, we fabricated a number of devices utilizing Norland Optical Adhesives, specifically formation 81 (NOA81) (Bartolo et al. 2008). This method, along with utilizing PTFE tubing for connecting the devices to the outside world, greatly reduced the amount of “fluidic compliance” in the device and rendered the fluid flow much more tightly coupled with starting and stopping of the control apparati. NOA81 is also much less porous than PDMS which prevented absorption of organic molecules into the material, but did not prevent organic materials from adsorbing to the surface. The manner in which we used NOA81 to construct devices also resulted in a greater consistency in total height of the device. Unlike PDMS, NOA81 is not gas permeable. One of the challenges of this feature is that a biological specimen contained within a device may need to have oxygen replenished. Our investigation of this problem is explored more fully in chapter 3. However this feature also opens up the possibility of tight control of the oxygenation and chemical environment within which the specimen is placed.

Thermometric microscopy

Quantification of temperatures inside of microchannels is frequently achieved by utilizing thermometric microscopy. Thermometric microscopy is any number of techniques that utilizes a microscope to record optically measurable phenomenon

that can be quantifiably correlated to temperature, as partially reviewed by Kim et al. (2015). One frequent method of achieving this is by filling the channel with a fluid containing a specific molecule that, when at a fixed concentration and experiencing invariant lighting conditions, will have measureable changes in fluorescence as a function of a change in temperature. This change in fluorescence is recorded by a camera attached to a microscope. A dilute solution of the temperature sensitive fluorophore Rhodamine B is frequently employed in temperature measurements in microchannels (Kim et al. 2015).

Rhodamine B and Dextran-Conjugated Rhodamine B

The quantum efficiency of Rhodamine B is approximately inversely linear with temperature (Ferguson and Mau 1973), allowing for relatively easy modeling of fluorescent behavior as a function of temperature. However the use of Rhodamine B has several drawbacks including a changing signal over time as it is adsorbed and absorbed onto the surface and into the material that is frequently used for microfluidic applications (Glawdel et al. 2009). Correspondingly, fluorescence measurements taken of the microchannel show a change in fluorescence intensity not solely as a function of the change in temperature, but also as a function of the time the chemical has been in the channel. Problem persists whether or not the fluid containing the Rhodamine B is held to either flowing or non flowing conditions. In PDMS, non flow conditions result in the Rhodamine continuing to diffuse through the PDMS, reducing the concentration of Rhodamine B in the channel over time. Flow

conditions that would hold the concentration of Rhodamine B fixed in the channel result in continued absorption of Rhodamine B into the the PDMS resulting in an increasing fraction of the signal coming from the material of which the channel is constructed instead of from the fluid in the channel.

When the channels of the microfluidic device are constructed with a less or non-porous material such as NOA81, the problem of absorption of Rhodamine into the materials is alleviated. However the problem switches to one of adsorption, as Rhodamine B starts to adhere to the surface of the channel and aggregate on it. A typical attempt to use 100 μM Rhodamine B solution to characterize our sticker-based devices would result in an 11% increase in signal strength at constant temperature over a period of approximately 2 hours; a signal strength that is approximate in magnitude with a temperature dependent change in fluorescence seen with an approximate $10^{O}C$ change in temperature.

Several methods have been previously described to overcome these challenges, including attempting to allow the material of the microchannel to become saturated with the fluorophore and then bleach out the fluorescent signal. (Glawdel et al. 2009). We found that this method resulted in the bleaching of the fluorescent signal coming from the material surrounding the channel; however, we also found that the bleached Rhodamine B became opaque.

While evaluating possible solutions to the challenges that Rhodamine b poses to consistent temperature measurements in our device, it occurred to us that commercially available Rhodamine B conjugated to sugar polymers might address some of these problems. In particular we thought that the long sugar molecule might prevent diffusion of the Rhodamine into PDMS, or the adsorption and aggregation found when using NOA81 to construct microchannels.

To test dextran-conjugated Rhodamine B (DCRB) as an alternative thermometric microscopy option, we first loaded the device with a dilute solution and performed our measurement assay. It has been previously reported that an aggregating fluorophore conjugated to a larger sugar moiety can result in an apparent increase in quantum efficiency of the fluorophore, and that the aggregation rate is temperature-dependent (Filippov et al. 2008). To address this concern we performed our measurements with a flow of the solution running during measurements.

Peclet Number of device

The necessity to have a fluid flow running during temperature gradient measurements opened up the possibility that the flow itself would in some way affect the temperature profile in the device. We initially addressed this concern in two ways: theoretically, by identifying the flow threshold below which temperature would not be affected, and experimentally by measuring the effect of fluid flow above and below this threshold using thermometric microscopy. To identifying the flow level that

would affect the performance of the temperature gradient we estimated the parameters necessary to determine the Peclet Number (Pe) of the device in operation. The Pe number is one of a group of common dimensionless numbers used in engineering to describe relationships between physical characteristics of a system. Pe in particular is a ratio with a domain of 0 to positive infinity that describes the relationship between advective transport of a species by bulk movement, and diffusive transport of a species as it spontaneously moves from a region of high concentration to low concentration. In the system under consideration here, that species is heat. When a system is above a Pe of 1, advective transport is dominant over diffusive transport, and conversely when a system is below 1, diffusion is dominant over advection. We found that for our system a flow rate of approximately 1-2µl/min would correspond to a Pe of 1.

To test this, we performed thermometric microscopy using DCRB and found that at a flow of 2µl/min the temperature profile of the gradient did not appear dependent on the flow, but when the flow was moved to 15µl/min, the temperature profile was shifted with the direction of flow (Figure 2.7).

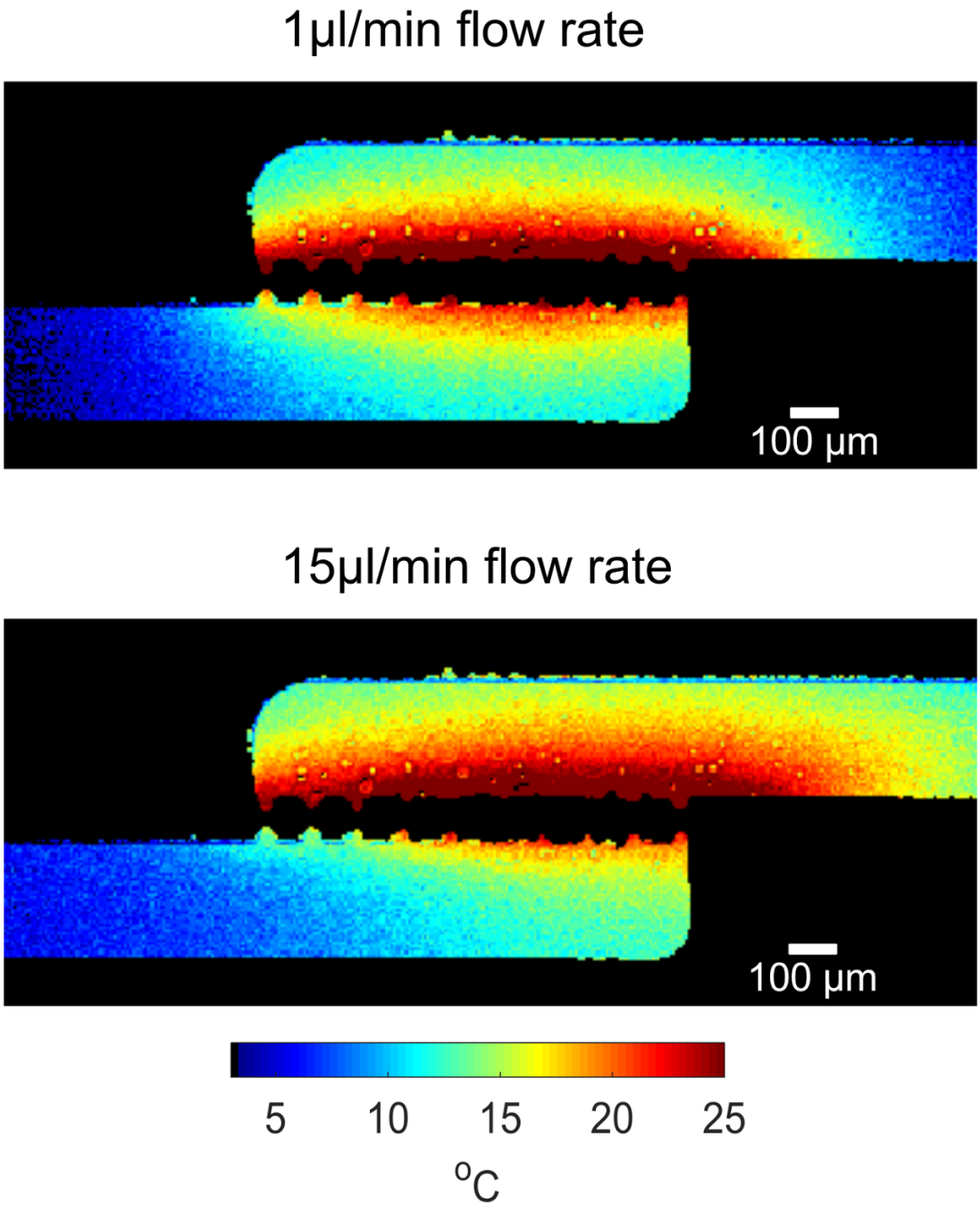

Figure 2.7: False color heat map of temperature distribution in early device for two regimes of fluid flow in microfluidic channel during gradient operation. Flow is from left to right. Top is distribution of temperature with a flow of 1 µl/min resulting in a Peclet number (Pe) of between 0.5 and 1. Bottom is distribution of temperature with a flow of 15 µl/min, exceeding a Pe of 1. Bottom shows shifting of temperature gradient from left to right with the increased flow.

Resistive Thermal Devices (RTDs)

In later devices, in addition to characterization of the temperature gradient with thermometric microscopy, we also included resistive thermal sensors in the region of the device where the temperature gradient was established (Bolker and Sidles 1977).

To characterize the patterned resistive thermal devices we submerged the fabricated devices mounted on a flow cell in a container of well-stirred ice water while simultaneously measuring the temperature of the water and the resistance of each of the patterned traces. We allowed the water to slowly warm to room temperature and compared the resistance measurements of each of the patterned traces to average measured temperature of the water. We found a highly linear correlation between the measured temperature and the measured resistance, and modeled the relationship between the two using a least squares linear model. R^2 values of linear models fitting resistance to temperatures ranging from 0 to 20^{O}C were typically on the order of 0.999.

To verify that the RTDs were primarily measuring the temperature in the region of the temperature gradient, and not the electrode leads leading up to that region, we measured the resistance of the patterned RTDs while flowing fluid through the flow cell of a fixed and measured temperature. We found that our resistance to

temperature measurements were within $1^{O}C$ of the experiment in which the device was fully submerged.

During normal operation, the device is not submerged in fluid, leading to the possibility that the measurement being taken by the RTD is from the bottom of the channel, and not a reasonable estimate of the channel as a whole. To verify that our temperature measurement was a reasonable estimate of the temperature throughout the channel, and not just the bottom of the channel, we constructed a modified flow cell that flowed the temperature setting water both underneath as well as over the top of the device. We found that the average difference in temperature between when the top of the device was exposed to air, and when the top of the device was exposed to fluid flowing at the same temperature and rate as the bottom of the device, was on the order of a third of a degree.

Temperature gradient in device: DCRB, RTD, and model

To allow us to correlate the intensity of DCRB fluorescence with temperature in the channel during operation of the device, we constructed for each pixel, a linear model of the intensity of fluorescence as a function of several fixed temperatures. We found that for the measured area of the device, the average R^2 value was 0.994.

To measure the temperature of the device during operation of the gradient, we next took the inverse of the linear model constructed, and calculated a 97.5% CI and PI

for the inverse model of a typical pixel (Figure 2.8 A). The estimated error of the inverse model is in part a function of the number of images of the gradient for a single condition. While this number of images was somewhat variable when taking a series of measurements at various power levels applied to the heater, or for various temperatures of cooling water under the device, the number of images for these various conditions was never below 30. Given this, we estimated the 97.5% CI and PI intervals for a typical pixel based on 30 images taken at each condition (Figure 2.8 B).

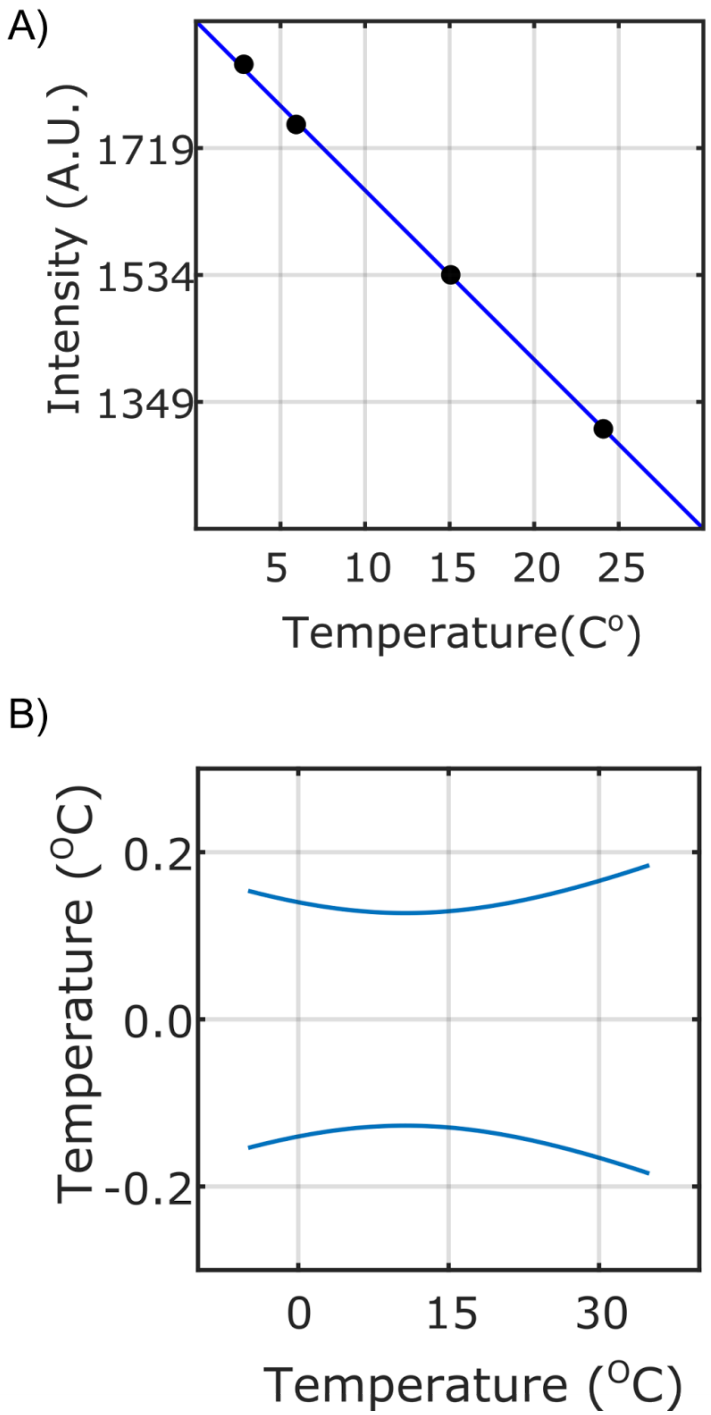

Figure 2.8: A) Linear model relating intensity of fluorescence to temperature for a typical pixel during characterization of the microfluidic device. B) 97.5% confidence interval distance from model for the inverse linear model of intensity to temperature, as a function of temperature.

Using the method described above, were were able to measure the temperature gradient and found that by using a heat rejecting fluid temperature of 1.5^{O}C, and without exceeding an absolute maximum temperature of 25^{O}C in the channel, we were able to measure a maximum temperature gradient of 7.5^{O}C across 50μm (Figure 2.9).

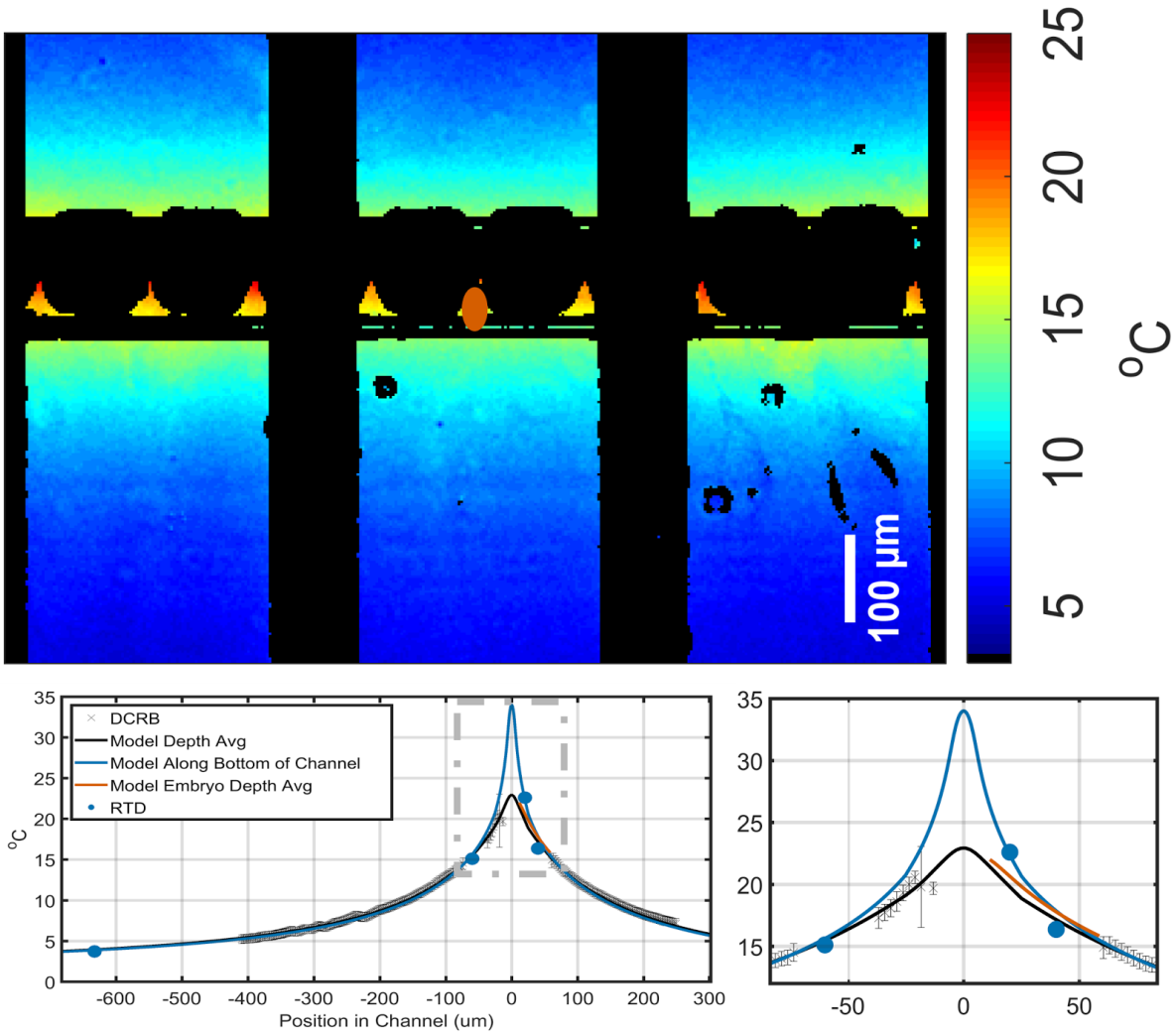

Figure 2.9: Top, false coloring heatmap of temperature distribution in channel during operation of temperature gradient. Orange oval indicates where placement of embryo would be during operation. Bottom Left, black data points and error bars indicate average temperatures and standard error across all three channels as a function of position in channel. X=0 indicates center of Joule heating element. Blue line is the model estimate of temperature along the interior bottom of the microfluidic device. Black line is the model estimate of the depth average temperature in the channel and orange is the model estimate of depth average temperature in the embryo. Blue dots correspond to RTD temperature measurements and their positions relative to the heater.

Loading and unloading embryos

When designing a microfluidic device, one has two general options for the introduction of material into the final device, be it purely fluid or a solid object in a fluid flow: positive or negative pressure. Under positive pressure schemes, fluid is usually introduced to the device by interfacing the device directly with tubing secured by an adhesive, in a manner that allows for a continuous fluid channel from the tubing to the constrained environment of the microfluidic channels. These connections between the macro environment of the lab, and micro environment of the device are generally referred to as “vias”. The tubing is then generally attached to a fluid-filled syringe using any of a number of methods, with pressure either manually applied to the plunger of the syringe by hand or through commercially available or custom-built “syringe pumps”. Under most fluidic based conditions, this is sufficient for operation of the device. However when introducing solid material such as embryos into a microfluidic device, this methodology becomes problematic. In particular, the many orders of magnitude size scales between the loading systems and the micro specimens means that for a single or small number of embryos to be delivered from the syringe into the device, the fluid within the syringe must have a high enough concentration of specimens to ensure that at least one specimen is included in the volume of fluid being pushed into the device, but a sufficiently low concentration to ensure that only a reasonable number of specimens are introduced into the device. In addition, even if one is able to balance between too many and too

few specimens delivered to the device, recovering the individual specimen after treatment becomes problematic, as the fluid network that delivered the original specimen[s] cannot be easily decoupled from the fluid that contains the specimen under consideration. To recover the individual specimen then requires at a minimum a scheme of gating the flow to allow the individual specimen to be recovered and its distinct identity maintained from unwanted specimens. Even if this hurdle were overcome, the highly constrained temporal requirements of the particular types of experiments under consideration i.e., *C. elegans* embryos post-fertilization, at or before the first division, would require that the sample within the loading system would have to be largely enriched for embryos, which would constitute ~ 10% of a general population of embryos, or would require a method of gating to select or reject embryos once they were within the device. Such a gating system would necessarily result in a more complex system and would likely be relatively or even prohibitively slow to operate unless coupled with an automated system for selecting embryos at the appropriate developmental stage. In practice we found these limitations to be real, as “injecting” embryos resulted in either no, or too many, embryos in the device, and the number of times we were able to acquire an embryo at the correct stage of development was zero out of hundreds of embryos attempted.

An alternative method to positive pressure is negative pressure: where material and fluid is moved through the device not by pushing fluid through, but by applying a negative pressure to one end of a micro-channel network, while providing a reservoir

of excess fluid to the other end of the microchannel. The negative pressure can be generated using syringes with or without syringe pumps by pulling on the syringe plunger, or with “vacuum lines” applied to one end of the channel. This method has the distinct benefit that the interface with the microfluidic device that is used to introduce fluid and material into the device is not directly in contact with extraneous apparati, and can be clearly observed under a microscope. The challenges with this method are the propensity for bubbles produced during initial filling of the device, and the limitation on flow rates and levels of vacuum applied, as too high of either will result in generation of new bubbles in the device.

To overcome these challenges, we initially filled the devices with fluid using positive pressure supplied by a fluid-filled syringe driven by a syringe pump coupled to a microbore PTFE tube that was connected to one end of the channel of our microfluidic device. This allowed us to initially and verifiably remove bubbles from the device. To introduce the embryos into the device, a separate microbore PTFE tube that had previously been connected to the other end of the microchannel was immersed in a glass well (~ 1” Diameter x ½” deep) filled with solution. The syringe pump was then operated in “reverse”, creating a negative pressure at what had previously been the inlet, and drawing fluid from the glass well into the device. A fluid flow of 100µl/min was found to be sufficiently low that it did not generate new bubbles in the device (approximate cross section of 50 µm x 250µm), while sufficiently high to allow embryos to be loaded from outside of the device to the

capture region in the device within a few minutes. This method also allowed for individual embryos to be pre-selected for correct development stage, loaded into the device, subjected to conditions of choice, and then unloaded from the device and saved for future analysis, without loss of identity of each embryo. While strict records of failures of loading were not kept, this methodology appeared to be successful in excess of approximately 80% of attempts, with the onset of loading failures generally tightly coupled to a continued inability to load embryos.

One of the challenges of microfluidic devices is interfacing the micro-world of the device, with the macro world of the lab itself. Traditionally in lab-constructed devices, some method of connecting tubing or fluid reservoirs is built into the device as a secondary process. For poly dimethylsiloxane (PDMS) based devices where the microchannel is constructed through soft lithography in the PDMS (Duffy et al. 1998) and before the PDMS is adhered to the substrate (usually glass) (San-Miguel and Lu 2005), a hole is “punched” through the device using a sharp hollow cylinder such as a syringe needle or commercially available biopsy punches (San-Miguel and Lu 2005) such that one side of the hole pierces the embedded microchannel, and the other side is accessible from the opposite side of the PDMS. The PDMS channel can then be adhered to the substrate through various methods (Duffy et al. 1998, Sia et al. 2003) and either tubing or some form of fluid reservoir (for example plastic pipette tips) can be inserted into the PDMS, which is frequently on the order of many millimeters thick, and secured either by using the inherent elastic properties of

PDMS or some form of adhesive. For other types of microfluidic construction techniques such as “sticker devices” (Bartolo et al. 2008), which are generally much thinner, and do not have the elastic properties of PDMS, small holes can be initially drilled into the substrate on which the patterned channels will be mated, again with tubing or fluid reservoirs secured. Both of these techniques necessarily have the connections between the outside world and the micro environment, arranged such that the material being introduced into the device during operation approaches the micro channel perpendicular to the plane of the channels themselves. For fluids that take on a well mixed character, and for experiments involving small particles such as those used in micro-particle image velocimetry (u-PIV), or even experiments dealing with larger particles such as those using adult nematodes, this methodology has shown to be very successful (Devasenathipathy, et al. 2003, San-Miguel and Lu 2005).

However, we found that when using typical microfluidic tubing connection methods, i.e., perpendicular to substrate, only a small fraction of nematode embryos that entered the tubing would reach the capture region. Microscopy inspection indicated that perpendicular fluidic connections frequently lead to “dead spaces” where, although fluid is present, it does not flow. We found that embryos would frequently settle in these areas. To address this challenge, we hypothesized that a via that allowed for the embryos to approach the channels parallel to the plane of the channels as opposed to perpendicular to the plane of the channel, would reduce the

likelihood that the embryo would become unproductively trapped before reaching the capture region. A number of methods were tested to construct this type of interconnection between the macro world and the microchannel device.

We used a diamond-tipped cutting tool to create semi-conical cuts into the side of our substrate, allowing us to connect tubing to the device with the tubing in a parallel orientation to the plane of the channels on the device, with the tubing sealed to the device with two-part five minute epoxy, which wicks into the conical cut up the walls of the cut and along the tubing. As the wicking epoxy reaches the end of the tubing, it largely stops wicking, while continuing to wick up the side of the channel and walls of the cut. This largely leads to tubing connections with little to no “dead” flow area. Additionally, we found that we could flow fluid through the device up to rates of 1 ml/min without failure of either the tubing-to-device connection or the adhesion between the channel layer and the heater substrate.

We found that when attempting to load and unload the embryos into a device that had not first had DCRB introduced into the channel, the embryos would have a tendency to stick to the material of the channel. This is consistent with our increased in background fluorescence signal after loading and unloading DCRB, and is consistent with the hypothesis that the DCRB is acting as a surfactant, with the Rhodamine B molecule more closely coordinating with the material of the channel than the fluid, and with the sugar moiety facing the fluid.

In conclusion we have constructed novel microfluidic based temperature gradient device that allows delivery and recovery of uniquely identifiable specimens on the order of 50μm in diameter into a steep and well defined temperature gradient of up to 7.5^{O}C across 50μm, while maintaining a maximum temperature of 25^{O}C at the high end of the gradient.

Chapter 3: Behavior of C. elegans *embryos in temperature gradient microfluidic device - evidence for compensation.*

With the development of the temperature gradient microfluidic device detailed in the preceding chapter, we will now turn our focus to integrating the device into biological experiments. This chapter will: detail the steps that were taken to verify the device's compatibility with viability of the early *C. elegans* embryo, establish baseline behavior of the early embryo at varying temperatures without a gradient, and measure the behavior of the embryo in the temperature gradient.

Compatibility of microfluidic environment with *C. elegans* embryos

To determine if embryos would be able to survive and develop successfully in the device, we loaded a cohort of early stage embryos (1-8 cell stage) into the device and allowed them to develop to hatching while in the device. We found that in the absence of continual flow of egg salts in the device, and below a certain threshold of flow, the embryos would tend to arrest during development and or not complete development. This finding was consistent with the material from which the device was constructed, NOA81, being gas-impermeable (Bong et al. 2012) and the embryos presumably becoming anoxic. We tested a number of flow regimes, and found that flow rates in excess of 25nl/min would prevent arrest of embryos during development (Figure 3.1 A).

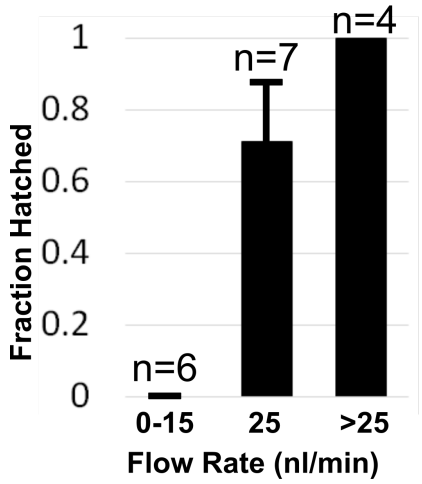

Figure 3.1: Fraction of embryos completing development for several flow regimes in the microfluidic channel

Having previously calculated the Peclet number (Pe) of the device (see chapter 2) and measured the effect of fluid flow below the critical rate, we were confident that a flow rate of 100-500nl/min within the device, a flow rate 4-20x lower than Pe = 1, and 4-10x higher than our observed critical flow requirement to prevent arrested development, would not affect the temperature profile of the device while simultaneously creating a biologically compatible environment. Our real time measurements of temperature in the device in our later experiments also demonstrated that the temperature profile at these slower flow rates remained similar to those without flow.

To determine the effect of loading and unloading on the survival of the embryos, we loaded a cohort of one-cell and two-cell embryos into a room temperature device at 80µl/min, left them in the device for ~ 1hour, with a trickling flow of 500nl/min and

unloaded them at a rate of 300µl/min. Each embryo was then placed on an agar plate and evaluated for whether or not they had successfully developed and hatched 24 hours later. We found that the rate of hatching was 98.4% (61/62) (Figure 3.1 B leftmost column).

Embryos at constant temperature

We hypothesized that if a mechanism exists in the early embryo to compensate for deviations in division times of the individual cells, one way that this system might act would be through continually monitoring and compensating throughout the cell cycle. For two-cell *C. elegans* embryos placed in a temperature gradient, a system that continually monitored and compensated throughout the cell cycle would likely reveal itself as a tendency for one or both of the cells to divide at a rate other than that expected by the temperature experienced by that cell. To allow us to identify compensation in the early embryo in division timing in a manner that might force the individual cells to divide at a rate other than that of their local temperature, we first sought to build a quantitative model of the division time for the second and third (AB and P_1) divisions of the early embryo as a function of temperature (Figure 3.2).

We found that the temperature-dependent time of division was empirically closely described by a modified Arrhenius equation (Equation 2.1). This finding is consistent with findings described by Begasse et al. (2015) for temperature-dependent rate of events observed prior to the division of P_0 in both *C. elegans* and *C. briggsa*e. In this

previous work, as in ours, the data is fit to a model by performing a least squares fit to a linearized version the Arrhenius equation (Equation 2.2).

$$Time\ of\ Event_1 - Time\ of\ Event_0 = \Gamma_1 - \Gamma_0 = A^{B(\frac{1}{T})}$$

Equation 3.1: Arrhenius equation in terms of times of events. Γ_n represents time of event n. B is traditionally expressed as a ratio of E_a (activation energy) and R, the gas constant.

In the linearized Arrhenius equation, the log of the rate of an event (or time) is evaluated as a function of one divided by the temperature at which the rate (or time to division) was measured.

$$ln(\Gamma_1 - \Gamma_0) = B(\tfrac{1}{T}) + ln\ A$$

Equation 3.2: Linearized version of Arrhenius equation with the natural log of length of time of an event taken as y, and inverse temperature taken as x. Parameters B and A are estimated from the data to allow for interpolation and extrapolation.

Our model, however, differs from this previous work in at least one very important aspect. In the earlier work (Begasse et al 2015), the authors used the absolute temperature Kelvin Kelvin to describe the relationship between rate and temperature. While this is consistent with how temperature-dependent rates are

calculated since the introduction of the Arrhenius equation, it inherently makes the assumption that the rate of the event under consideration will continue to move forward, albeit exponentially slower, as the temperature reaches absolute 0. This is true for most systems, but does not pertain to a large number of complex biological processes. An alternative method introduced by Nakamura et al. (1989) allows for greater empirical fitting of data. In this method, an additional temperature term is introduced into the denominator of the independent variable of the linear form of the Arrhenius equation. This additional term, which acts as an offset for the measured temperature of the data, can be thought of as the temperature at which the rate for the system under consideration reaches 0 (Equation 2.3).

$$ln(\Gamma_1 - \Gamma_0) = B(\frac{1}{T - T_0}) + ln\, A$$

Equation 3.3: Modified linear form the Arrhenius equation. A term is added to the denominator of the inverse temperature. T_0 is estimated by finding the best fit to the data.

We sought to find an estimate for this temperature for *C. elegans*. We performed two methods of analysis on our data to find this parameter. The first method was a numerical-simulation-generated general non-linear fit of the data performed in Comsol Multiphysics. The second was a parametric sweep of this offset temperature on the linear model of the data collected. Both methods were in relatively high agreement (~ one part in 100 difference) and showed that the offset temperature

that resulted in the best fit of our data for the N2 strain of *C. elegans* for the second and third division of the embryo was -10^{O}C.

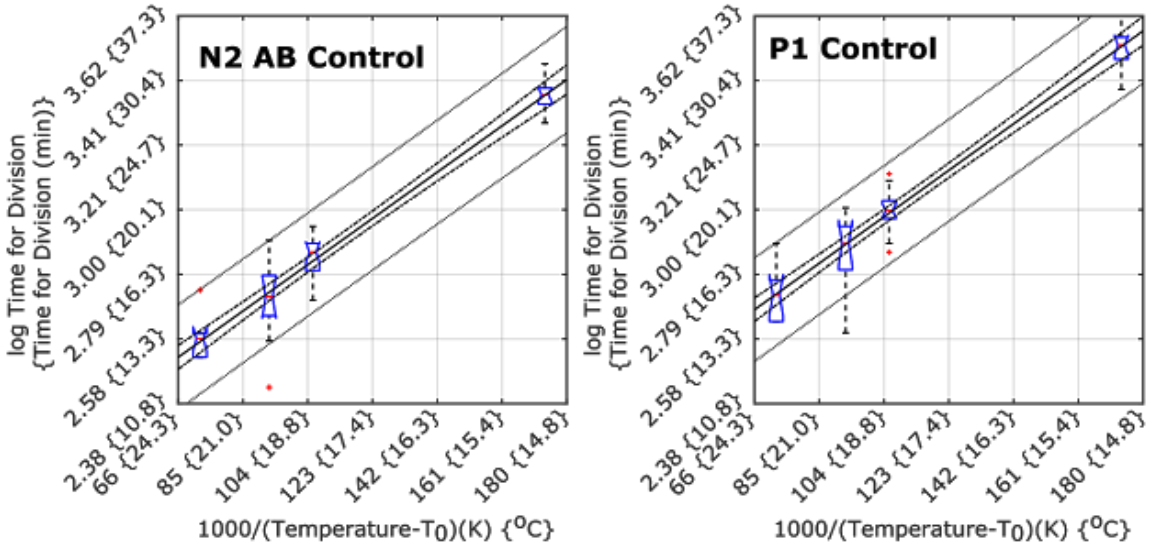

Figure 3.2: Linear model of time of division of AB (left) and P_1 (right) as a function of temperature. Notched box plots are data at various temperatures. Inner most line indicates linear model. Next outermost pair of lines indicate 95% confidence interval of the model. Outermost pair of lines indicate 95% prediction interval.

Embryos in gradient

We tested whether the early embryo would survive in a temperature gradient, by selecting embryos at stages between one and four cells and loading them into an earlier version of the device (Figure 3.3). Once inside of the device we allowed, them to take on a “head-on” orientation in the capture region, so that the anterior-posterior axis of the embryo was perpendicular to the bottom of the channel.

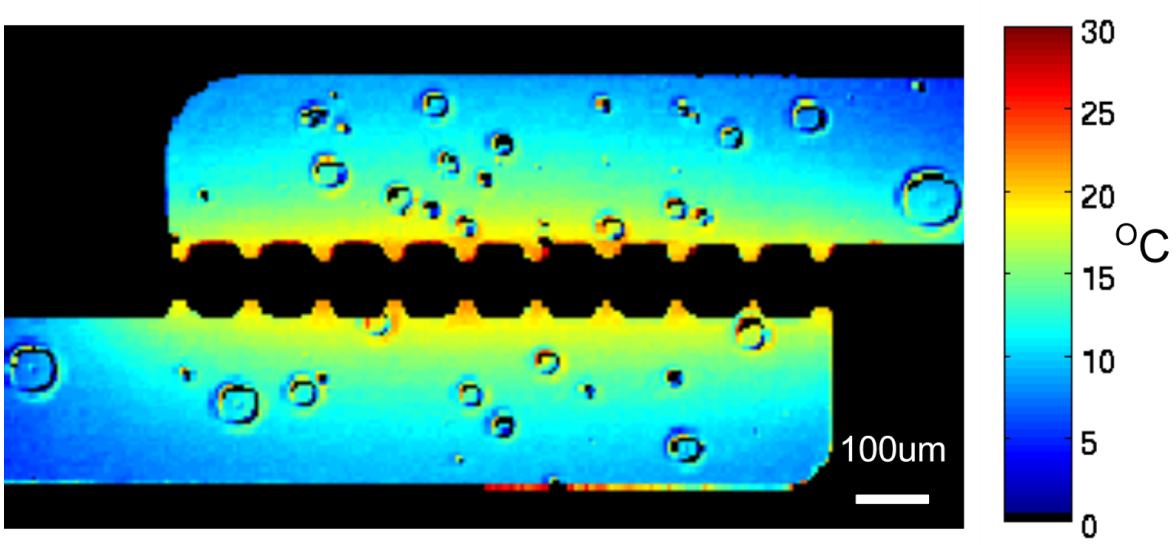

Figure 3.3: False color heat map of temperature in early version of the device. Temperature gradient is not uniform and takes on an ellipse shape, with the steepest gradient along the minor axis of the ellipse.

We allowed them to stay in the temperature gradient for ~ one hour. After an hour they were unloaded, placed on individual agar plates, and scored ~ 1 day later for hatching. The earlier version of the device used for this experiment was constructed in such a way that the magnitude of the temperature gradient differed depending on where in the device the embryo was captured (Figure 3.3). This allowed us to test hatching as a function of several gradient magnitudes without changing experimental parameters. We found hatching rate roughly followed a monotonic decrease as the magnitude of the gradient increased (Figure 3.4).

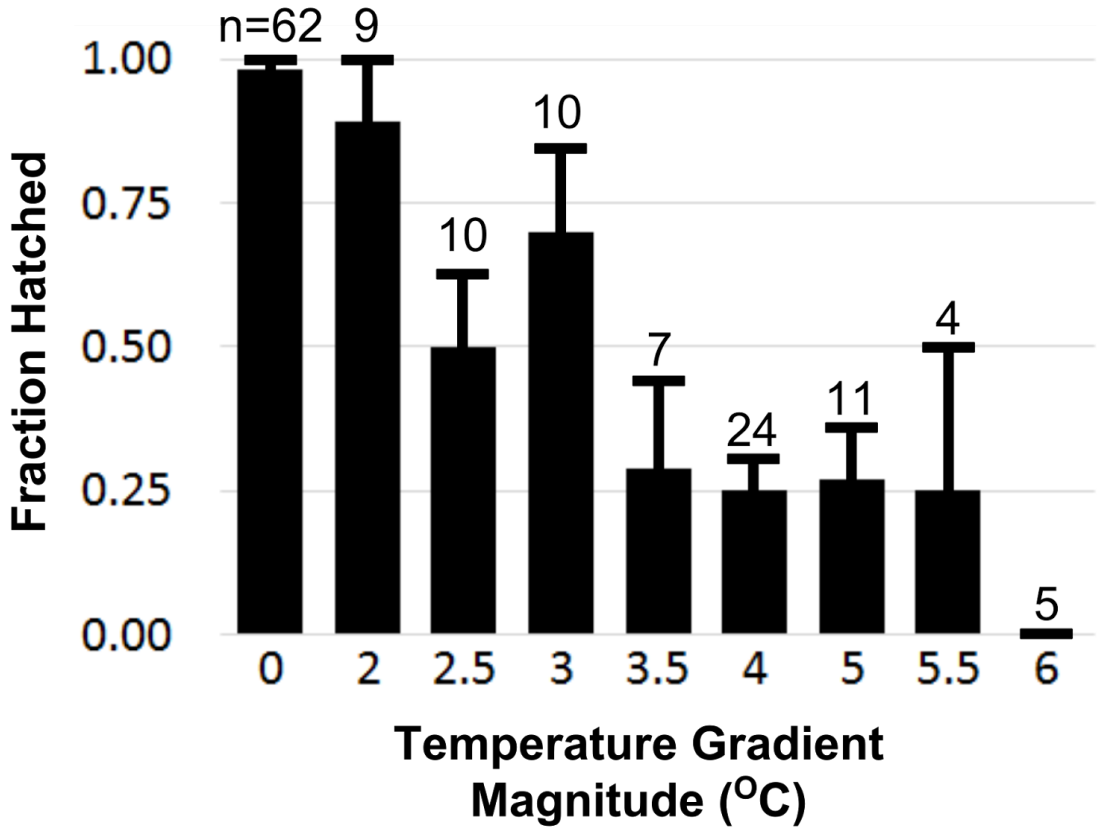

Figure 3.4: Fraction of embryo hatched after ~ one hour exposure to various temperature gradient magnitudes during early embryogenesis. Replenishing flow of 500nl/min was running during experiment.

Next we sought to quantify the temporal behavior of each of the cells of the two-cell embryo in the device. We hypothesized that the temperature gradient may have an effect on the developing embryo even at the one-cell stage. To accommodate this possibility we loaded embryos into the gradient device on their side (anterior-posterior axis parallel to channel) at one of two developmental stages: before the division of the first cell, and after the division of the first cell. For both embryo development regimes, we isolated embryos generally at a stage prior to the

pronuclear meeting. For one-cell embryos we generally loaded them into the device either before the pronuclear meeting or immediately after. For two-cell embryos, we continued to track development until the first membrane cleavage, at which point they were loaded into the device generally reaching the capture region of the device within two to four minutes of the initial cleavage. Room temperature was measured and recorded for embryos that were allowed to develop to the first membrane cleavage outside of the device. For both embryo development regimes we loaded a cohort of embryos into the device with AB positioned toward the heater and P_1 away from the heater, so that AB was warmer than P_1, and another set with P_1 positioned toward the heater and AB away from the heater so that P_1 was warmer than AB. We allowed the embryos to develop in the temperature gradient through at least the division of ABa and P_2, and then unloaded and placed each embryo in its own agar dish. The embryos were then kept at room temperature, and scored for hatching ~ 24 hours later.

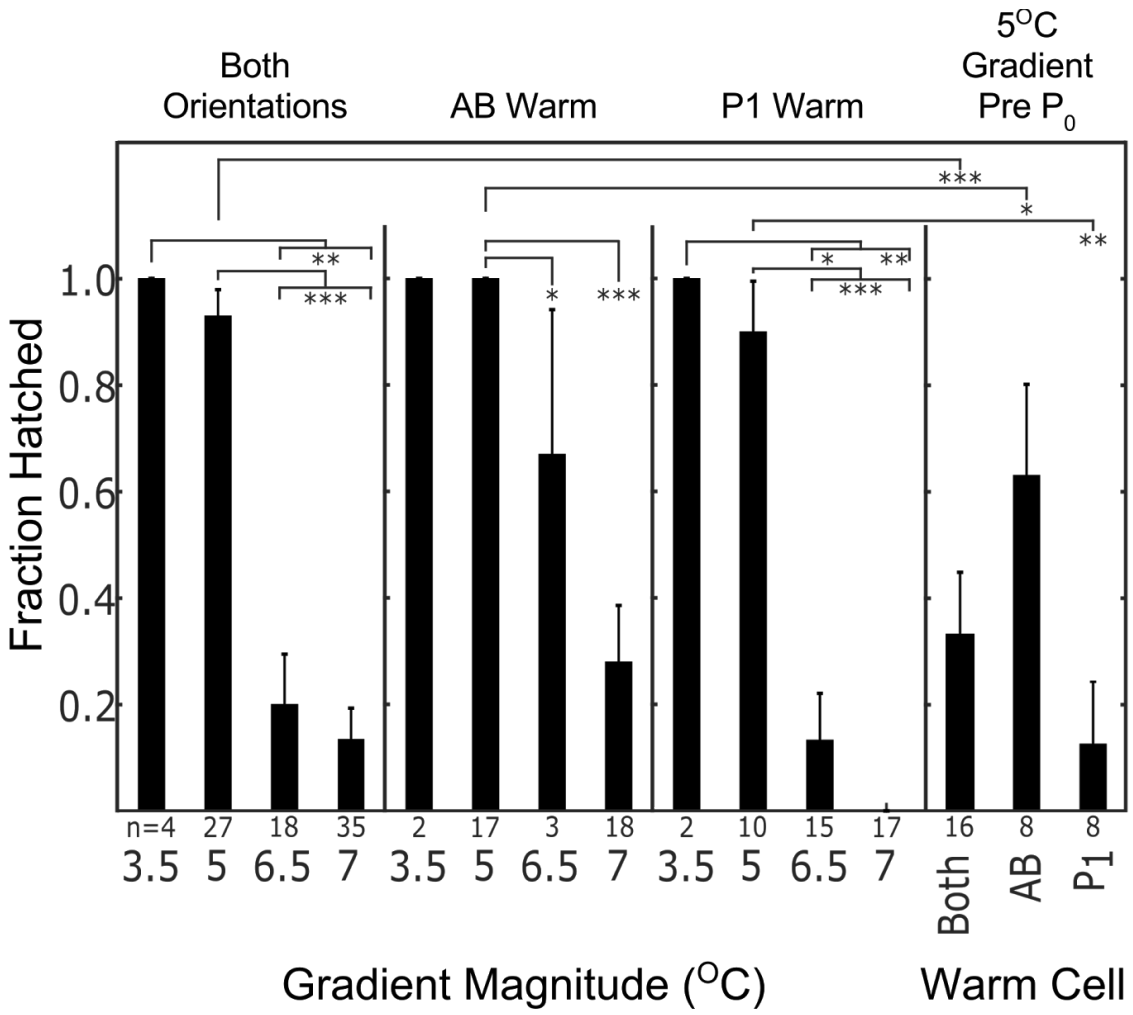

Figure 3.5: Hatching rate of embryos in several gradient magnitudes with indications of levels of statistical significance. Data broken down by gradient for both orientations, as well as AB warm and P_1 warm separately. Embryos loaded prior to first division are broken out separately on the right

As in our earlier study of multiple development stage embryos, we found here that without regards to orientation in the gradient, the rate of hatching of embryos subjected to a gradient at the two cell stage was roughly monotonic: as the magnitude of the gradient increased, the hatching rate decreased. We also found that embryos oriented in the gradient such that AB was warmer than P_1 had a higher

rate of hatching when compared to embryos oriented such that P_1 was warmer than AB. A Fisher's Exact test indicated a p value of ~ 0.1 when comparing the orientation-dependent hatching rate of embryos subjected to a 6.5^{O}C gradient, and a p value of ~0.11 when comparing the orientation-dependent hatching rate of embryos loaded prior to the first cleavage and subjected to a 5^{O}C gradient. However a p value of 0.045 was found when comparing orientation-dependent hatching rate of embryos at 7^{O}C (Figure 3.5 and Table 3.1) .

All embryos

	3.5	7	6.5	5
3.5	-	-	-	-
7	0.0015	-	-	-
6.5	0.0096	0.469	-	-
5	1	<0.0001	<0.0001	-
5 pre P0	0.0867	0.0778	0.4569	<0.0001

P_1 Warm

	3.5	7	6.5	5
3.5	-	-	-	-
7	0.0058	-	-	-
6.5	0.0441	0.2117	-	-
5	1	<0.0001	0.0002	-
5 pre P0	0.0667	0.32	1	0.0029

AB Warm

	3.5	7	6.5	5
3.5	-	-	-	-
7	0.1105	-	-	-
6.5	1	0.2474	-	-
5	1	<0.0001	0.15	-
5 pre P0	1	0.1892	1	0.0243

AB Warm V P_1 Warm

	3.5 AB	7	6.5	5	5 pre P0
3.5 P1	1	-	-	-	-
7	-	0.0455	-	-	-
6.5	-	-	0.1078	-	-
5	-	-	-	0.3704	-
5 pre P0	-	-	-	-	0.1189

Table 3.1: Fisher's Exact test multi-way hatching comparison. Top Left, p values for hatching rates for combined orientations at different temperature gradient magnitudes. Top Right, p values comparing hatching rates of embryos with P_1 warmer than AB. Bottom Left, p values comparing hatching rates of embryos with AB warmer than P_1. Bottom Right, p values comparing hatching rates for embryos with same gradient magnitude, but different orientation in temperature gradient.

Un-division of two celled embryos

We also observed, that about 10% of the time (5/50) we loaded two celled embryos into the device with a gradient established, the embryos appeared to undergo an “un-division” phenomenon. The cleavage furrow that had previously formed and been observed under the dissecting scope before the embryo was loaded into the device appeared to dissolve. To more fully visualize what was happening, we loaded a cohort of embryos which have been genetically modified to contain a gfp tagged histone that marks the chromosomes. This allowed us to view the behavior of the nuclei of the two cells. We found this strain also underwent an “un-division” part of the time and that in doing so the two nuclei of the newly formed AB and P_1 migrated back toward each other. We further found that the nuclei would then later break into six parts. None of the embryos that demonstrated this behavior hatched (Figure 3.6).

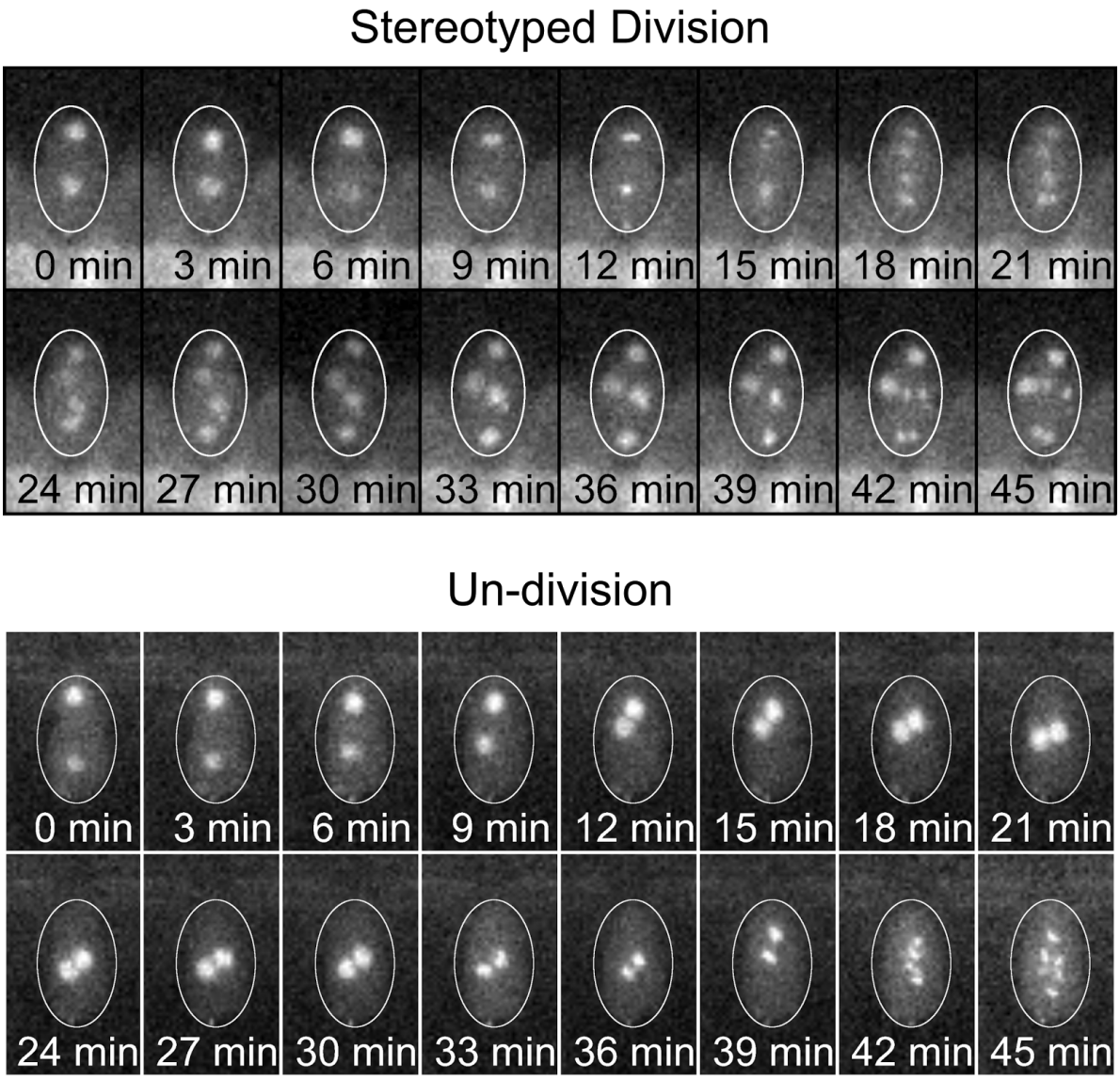

Figure 3.6: Fluorescence imaging of C. elegans embryos starting at the two-cell stage expressing GFP-tagged histones. Top, stereotyped division showing division of nucleus of AB starting approximately at 15 minutes, with P_1 nucleus starting to divide at approximately 18 minutes. Bottom, “un-division” event showing nuclei migrating back toward each other starting between 6 and 9 minutes, and then breaking into 6 parts at 45 minutes.

Quantitative behavior of embryos in the gradient

A number of qualitative trends were observed in the quantitative behavior of the individual cells within the gradient (Figure 3.7-3.9). First, the variability of the timing of the divisions for the embryos in the gradient generally exceeded that of the embryos at constant temperature. In addition, both cells, independent of their orientation, appeared to slow down in the temperature gradient relative to their expected behavior. The exceptions to this general trend were the behavior of P_1 at the highest gradient used, and the general behavior of the embryos loaded at the one-cell stage and experiencing a 5 degree gradient (Figure 3.8 and 3.9). In these cases the cells seemed to track closer to the expected behavior at that temperature.

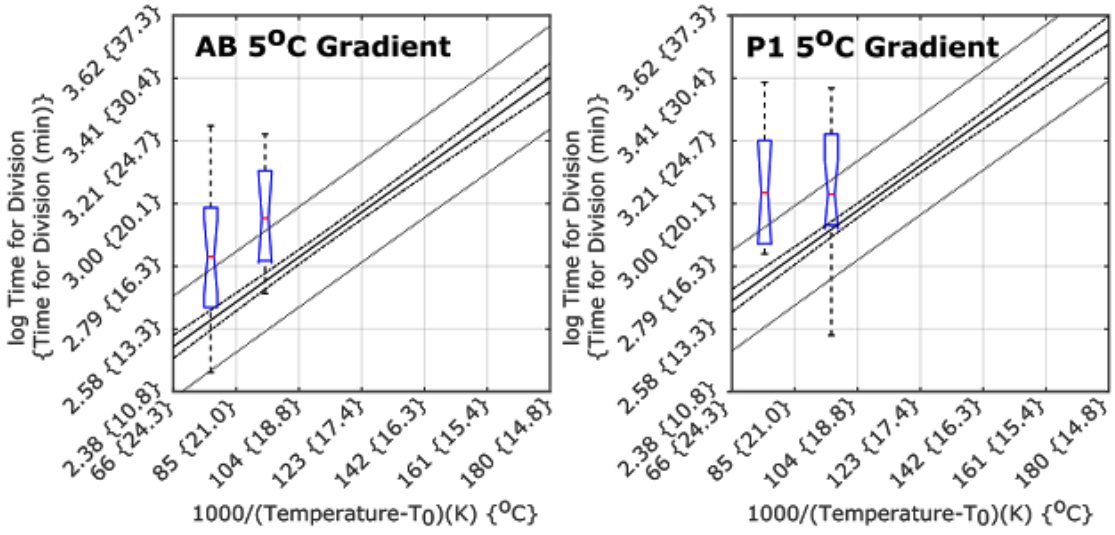

Figure 3.7: Notched box plot of time of division of AB (left) and P_1 (right) at the corresponding temperature plotted over the corresponding model. In both AB and P1 plots, left box is for the orientation of that cell next to heater, and right box is for that cell away from the heater. Both plots are for a temperature gradient magnitude from end to end across the embryo of 5 degrees celsius. This cohort of embryos was loaded into the device after the formation of the first cleavage.

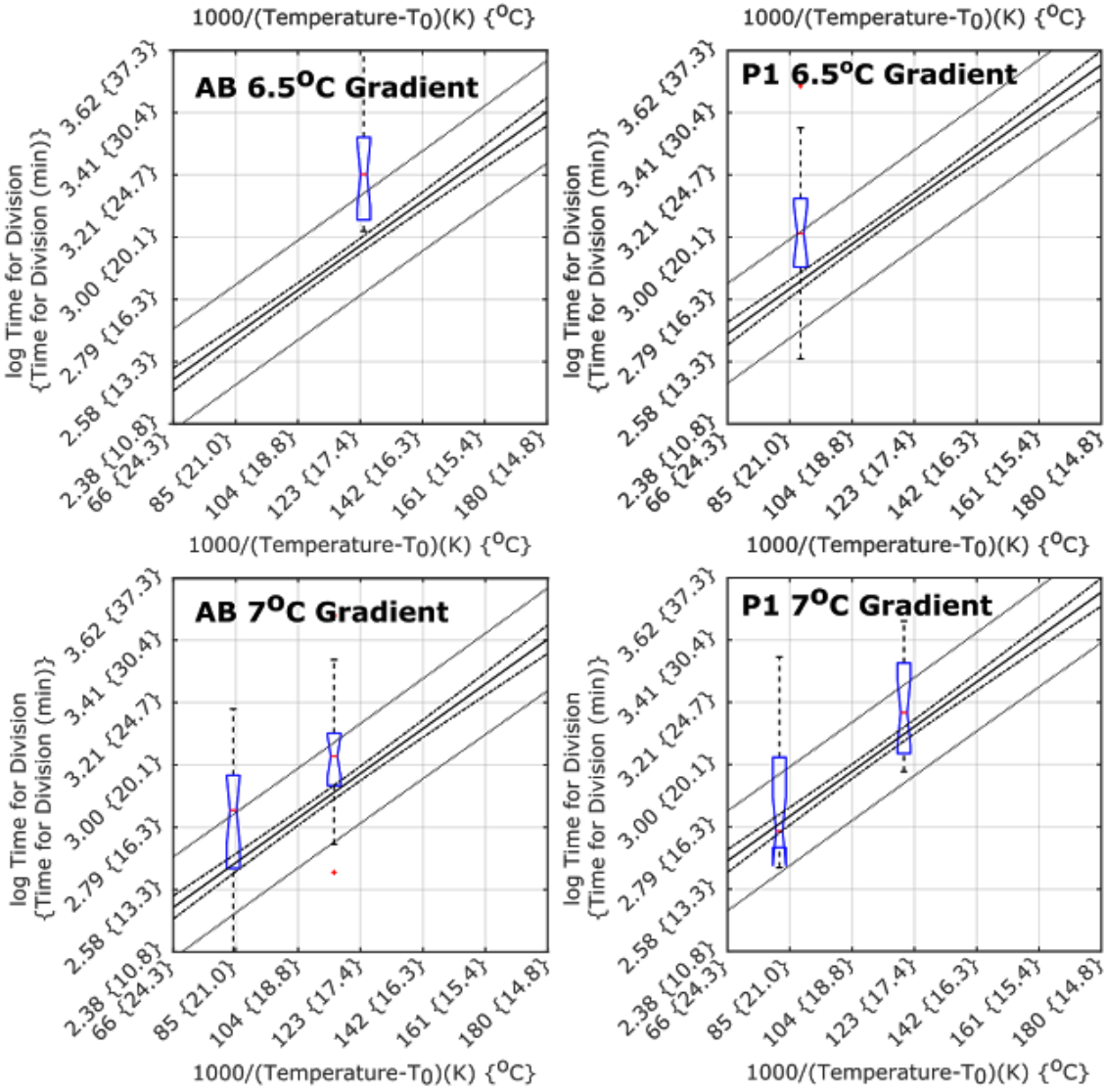

Figure 3.8: Notched box plot of time of division of AB (left) and P_1 (right) at the corresponding temperature plotted over the corresponding model. In both AB and P1 plots for the 7 degree temperature gradient, left box is for the orientation of that cell next to heater, and right box is for that cell away from the heater. These cohorts of embryos were loaded into the device after the formation of the first cleavage.

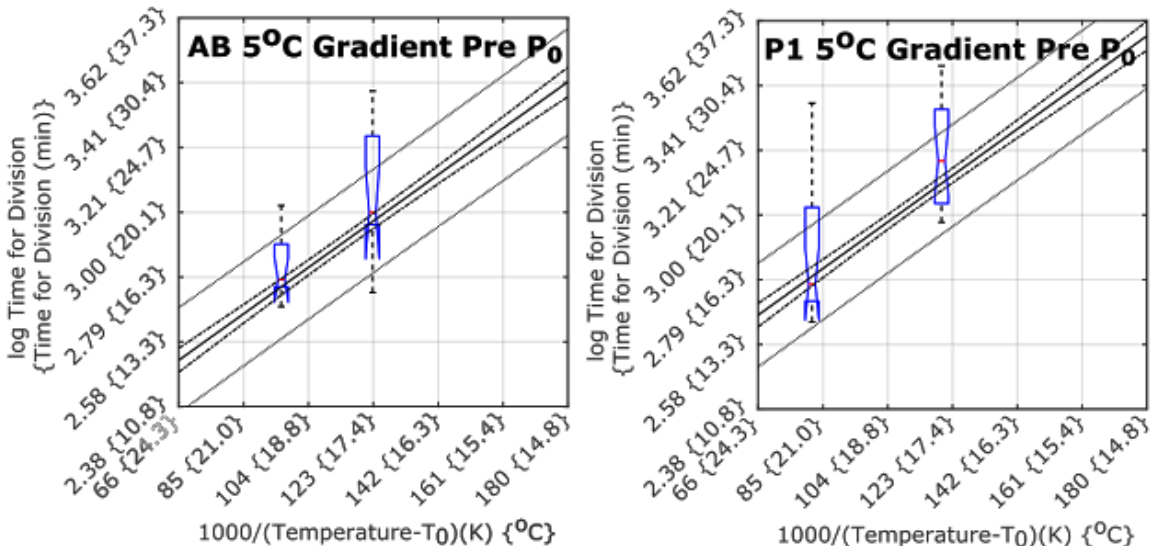

Figure 3.9: Notched box plot of time of division of AB (left) and P_1 (right) at the corresponding temperature plotted over the corresponding model. In both AB and P1 left box is for the orientation of that cell next to heater, and right box is for that cell away from the heater. These cohorts of embryos were loaded into the device prior to the first cleavage.

Given the spread of the division times of the cells when evaluated on their own, it is possible that for a given embryo, AB might be slower than normal and P1 might be faster than normal, or vice versa, in either of the two orientations. To allow us to analyze the relationship between the behaviors of each cell in the gradient we calculated the linearized fold change in time of division for each of the two cells of the two-cell embryo. We made this calculation by taking the $\log_2$ of the ratio of observed time of division and the expected time of division at the cell-specific temperature for each cell of each embryo.

$$Linearized\ Fold\ Change\ in\ Time\ of\ Division = log_2\left(\frac{Observed\ Time\ of\ Division}{Expected\ Time\ of\ Division}\right)$$

Equation 2.4: Calculation for determining fold change in time of division away from expected time of division at temperature experienced by the cell. Taking the log of the ratio of the observed and expected time of division allows a doubling in time of division to be the same distance from the origin and a halving of the time of division.

We then graphed the behavior of each embryo as a single point, with the x axis as the behavior of AB, and the y axis as the behavior of P_1. With this methodology a division time that is twice the length of the expected division time is the same distance from the origin as a division time that took half as long. This methodology allows us to simultaneously identify how each cell is behaving relative to the other as well as relative to its expected behavior (Figure 3.10).

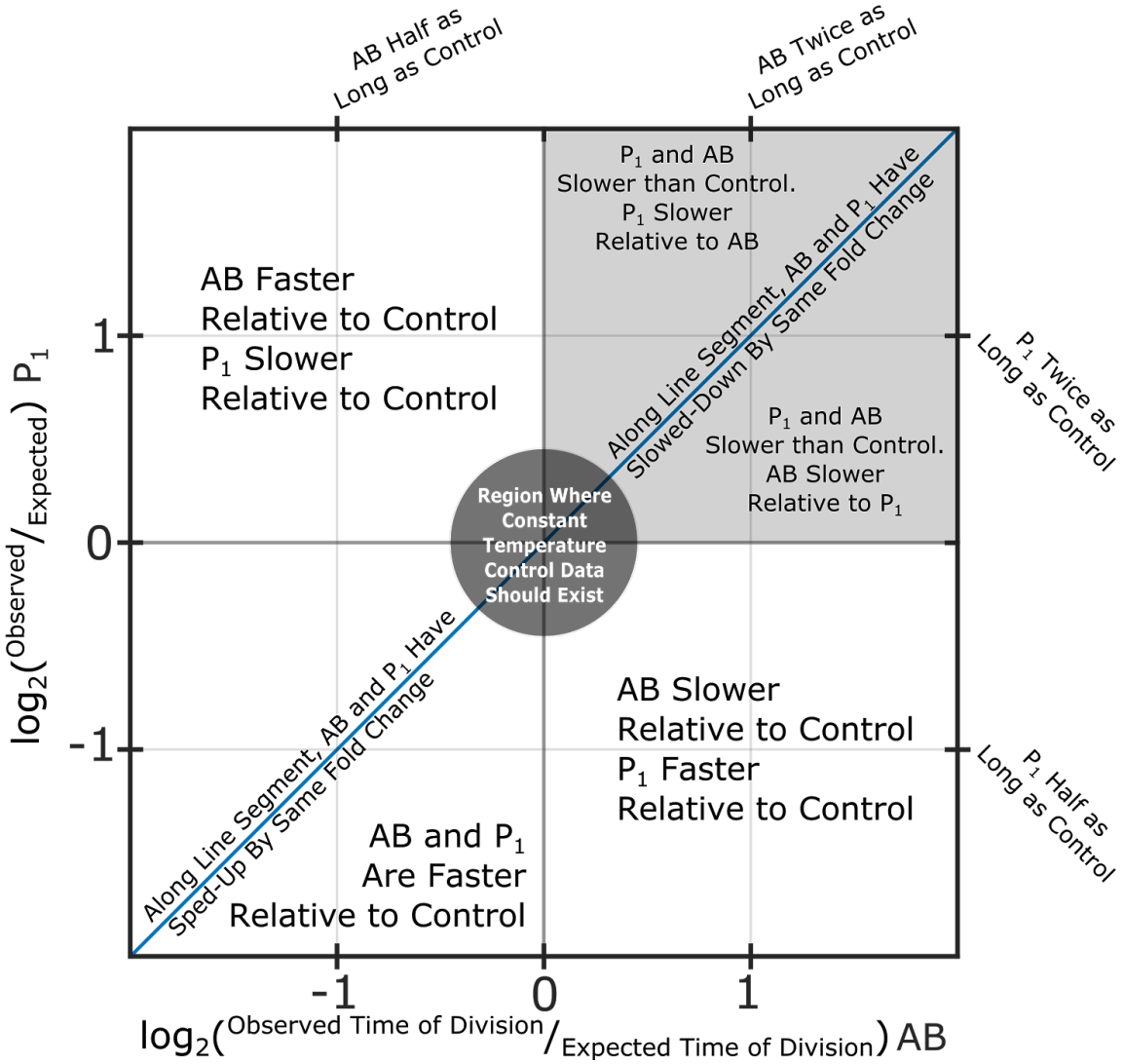

Figure 3.10: Explanatory graph for visual representation of fold change in time of division for embryo as a whole

We found that embryos in the temperature gradient largely fell in one of three areas. Those that did not hatch tended to cluster closer to the origin with a greater fold change in length of time for division in AB when compared to P_1. This trend held true for both orientations, with cohorts of embryos that did not hatch clustering closely together independent of orientation. For embryos that hatched, we found that both

cells were even slower than should be expected for their local temperature when compared to those that did not hatch. We also found a qualitative difference in behavior of the two orientations for embryos that hatched. For embryos that hatched and were positioned in the gradient with P_1 warmer than AB, the magnitude change in behavior away from expected was higher for P_1 than AB. The converse was true for embryos that were positioned with AB warmer than P_1; the magnitude change in behavior away from expected was higher for AB than P_1 (Figure 3.11). However the orientation behavior of the populations that hatched were not reflections of each other about the line of x=y. Embryos that hatched where P_1 was warmer than AB, experienced a greater magnitude in slowdown of P_1 relative to AB, while the behavior of AB in this orientation was similar to the behavior of AB when AB was warmer.

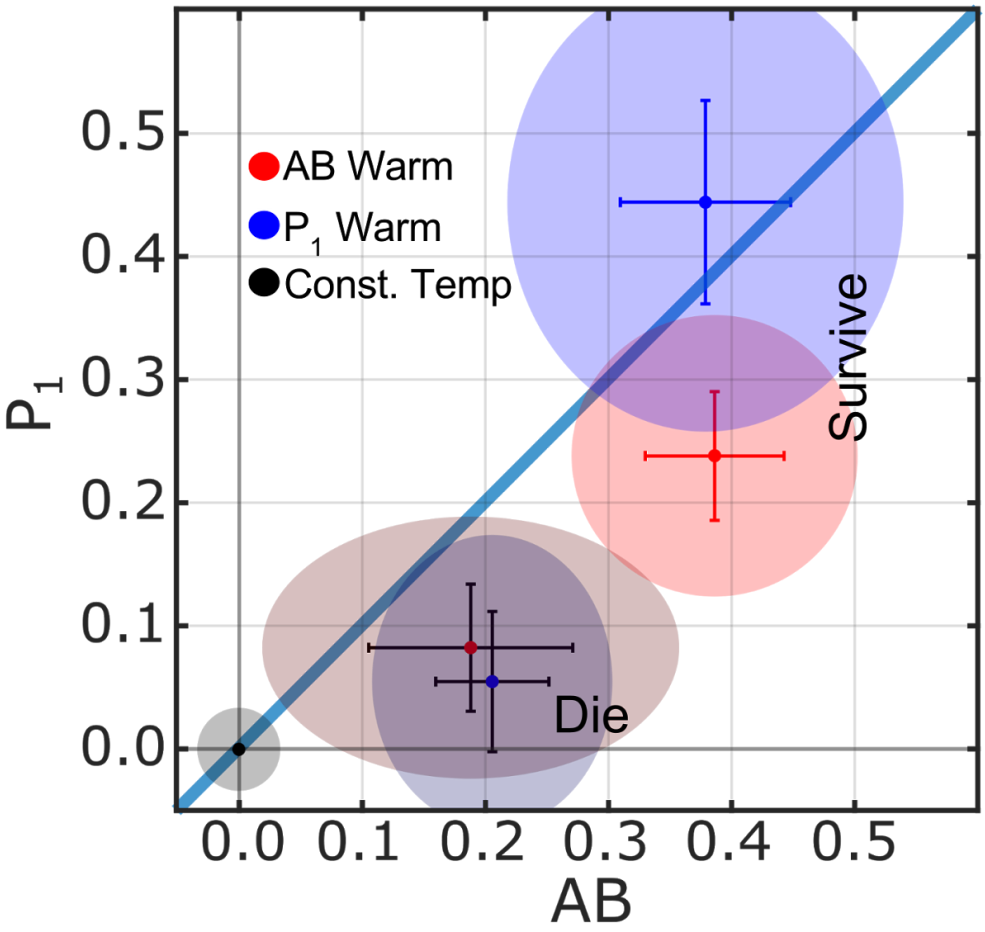

Figure 3.11: Graph of the mean, standard error, and 95% confidence intervals for fold changes in behavior of AB and P_1, broken down into orientation in the temperature gradient, and whether or not the embryo survived to hatching. Blue is for embryos with P_1 warmer than AB, and red for embryos with AB warmer than P_1. Black standard error bars were used to identify the populations that did not hatch, and colored ellipses were used to portray the two dimensional 95% confidence interval for each population. Black data point at origin, and surrounding gray ellipse are mean and 95% confidence interval of behavior of constant temperature control embryos.

Reversal of Division Sequence

Under certain conditions we were able to force a reversal of the stereotyped division sequence between AB and P_1 (Figure 3.12). For embryos oriented with P_1 warmer than AB and loaded after the cleavage of P_0, we found that a temperature gradient magnitude of 6.5^{O}C was sufficient to drive P_1 to divide before AB. For a 6.5^{O}C temperature gradient with P_1 warmer than AB, we observed a division sequence reversal rate of 60% (9/15), and for 7^{O}C we found a reversal rate of 71% (12/15). For embryos loaded before the division of P_0 and oriented with the posterior side toward the heater, we observed sequence of division reversals for AB and P1 at a rate of 90% (9/10). None of the embryos that experienced a reversal of sequence of division hatched. However, a surprisingly high percentage the embryos did proceed through morphogenesis. Of the embryos that experienced a reversal in sequence of division of AB and P_1, 32% (9/28) resulted in an embryo that appeared wormlike and had therefore undergone nearly normal morphogenesis. Embryos with AB warmer than P_1 that did not hatch, proceeded through morphogenesis approximately 43% of the time (6/14).

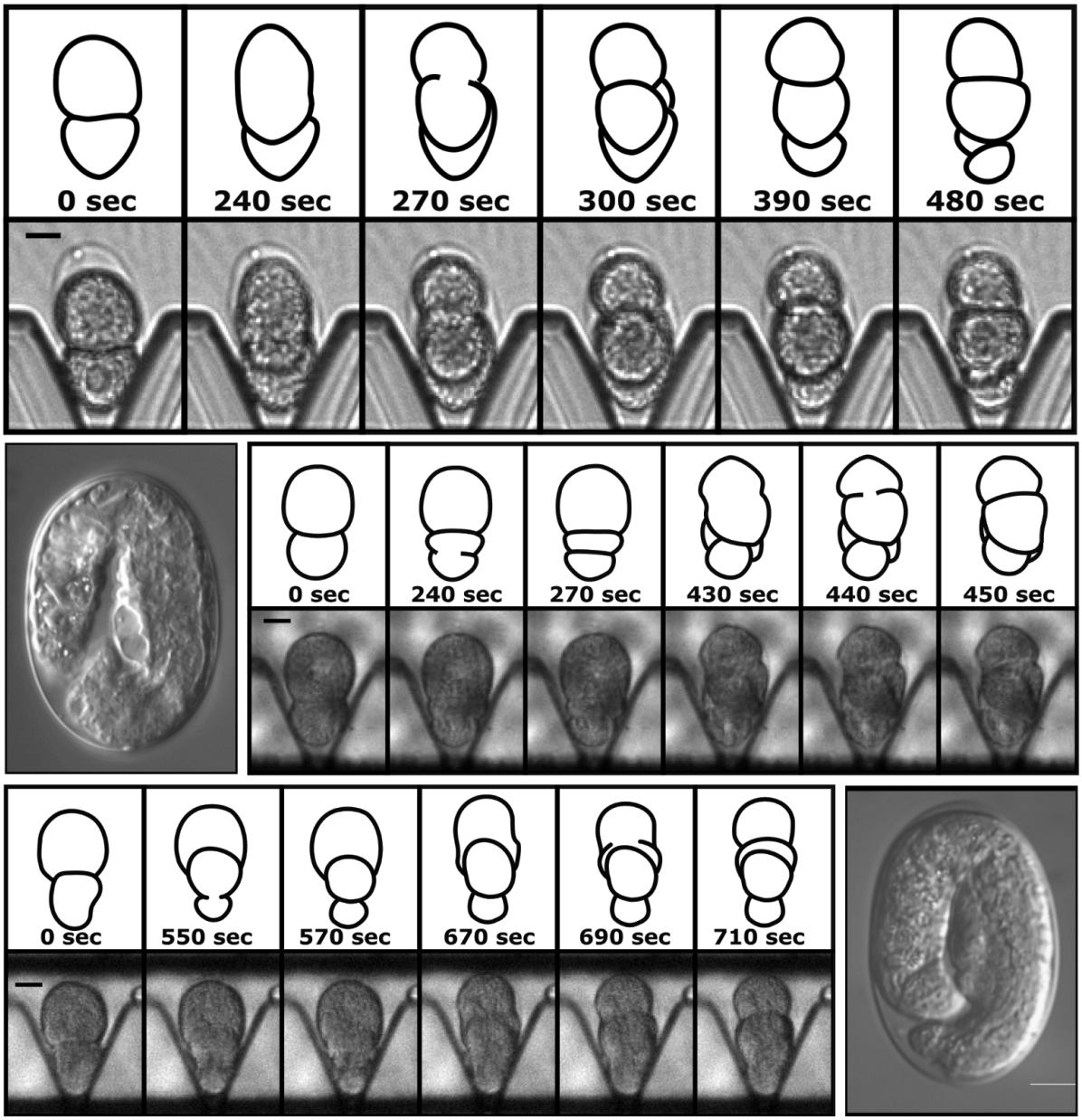

Figure 3.12: Top panel; time lapse panel of images and outline for a stereotyped division of the AB cell (larger) dividing before the P_1 cell (smaller) during *C. elegans* embryogenesis at a constant permissive temperature. Middle and Bottom panels; two examples of time lapse and outlines of two embryos experiencing a reversal of sequence of the stereotyped division pattern of AB and P_1, along with 100x DIC image of embryo ~ 24 hours after being in temperature gradient.

Chapter 4: Discussion and Conclusions

Interpretation, implications, and future directions of the biological findings

As was discussed in chapter one, a system that worked to ensure that certain events during development occur in a stereotyped sequence, or compensate when they do not, could potentially act in two ways: by identify deviations in acceptable rates and timing of events and act to correct the deviations immediately after or during their occurrence, or by identifying at pre-established checkpoints along development, aberrant conditions that have occurred in the past, and attempt to counteract them in the present or at some point further in development. We believe our data are consistent with a model in which both types of systems are in play.

In particular, the general trend for both cells of the two-cell embryo to slow down relative to their expected behavior when in the gradient, is consistent with a system in which the cells coordinate their division timing. As there is no third cell at this point that could in effect supervise the other two cells, it is reasonable to conclude that this system must be comprised of some level of communication between the two cells and involve components of both cells. The data is also consistent with a model where this sharing of information is bidirectional, as both cells slow down relative to their expected behavior. Were the information only unidirectional, we would expect that only one of the two cells would deviate from its expected behavior.

The quantitative difference in behavior between the embryos that hatched and those that did not would also argue for a maximum compensatory capability for this system. For the cohort of embryos that did not hatch, the data indicates that the system slowed in general, consistent with a model where a disparate condition has been detected and activated a compensation process. However, the reduced magnitude of compensation amongst the cohort of embryos that did not hatch would seem to indicate that conditions are excessively discordant, i.e., outside of the bounds of a “dynamic range” for the system, the system is no longer able to compensate to the point of recovery. The data also argue for a difference in the system between the two cells AB and P_1. If this were not the case and the system for detection and compensation between the two cells was symmetric, we would have expected the orientation-dependent behavior of the two cells to have been reflections of each other along the line of x=y in our graph of fold change in division time for AB and P_1. Instead we observed that for both orientations, for those embryos that survived, AB experienced approximately the same slowdown, while the slowdown of P_1 became more exaggerated when it was being thermally driven faster than AB. This may indicate that the system in play is comprised of two independent and distinct monitoring and compensating systems: one that can influence the division timing of AB while monitoring the progress of P_1 and vice versa.

Our data also supports the existence of a later-acting checkpoint compensation system. Embryos that were subjected to the gradient but did not hatch, largely

demonstrated a reduced capacity to compensate for the adverse conditions. Nonetheless, even embryos that experienced a reversal in their stereotyped division sequence in which AB divided before P_1, were able to proceed through development to the point where the end product was strikingly similar to a worm. Such a response is consistent with a model where at some point in development after the division of AB and P_1, a system is recognizing that the outcome of the previous steps is not sufficient for successful completion of development, and is moving the system back to a stereotyped pattern of development.

The possibility of compensation of developmental timing may help explain previously identified phenomenon. For example, constant temperature quantitative cell division timing studies in *C. elegans* by Richards et al. (2013) had identified potential cell timing compensation mechanisms in the form of a negative correlation between cell cycle timing in a cell and its later descendants: cells that divided early gave rise to grand daughters that were more likely to divide late. This negative correlation implies that the developing embryo can identify that an earlier process had taken either too much or too little time and compensates by changing the timing of subsequent processes in the opposite direction. In *C. elegans,* cytokinesis and the cell cycle are tightly coupled even in early embryogenesis, as it is in mice where evidence suggests that DNA damage and spindle assembly checkpoints are active (Wei et al. 2011, Shimura et al. 2002 Artus and Cohen-Tannoudji 2008) in contrast in *Xenopus* and Zebrafish (Clute and Masui 1997, Ikegami et al. 1997) where these systems are

enabled only after the midblastula transition. It is possible that the compensatory system identified in our work may then be an integral part of cell cycle checkpoint mechanisms in general. This may account for the previous observation that human embryos are particularly susceptible to failure early in embryogenesis, and that the failure appears to be tightly coupled with mismatches in cellular timing of the very early embryo cells (Cruz et al. 2012). It would not be hard to envision how the compensatory system described here could be directed toward a more global developmental abort system in higher organisms.

The next logical steps for moving this work forward would be to look for genes responsible for the slow down in time of division response of the two celled embryo placed in the temperature gradient. The asynchrony of AB and P_1 within is known to be comprised of at least two systems. One of these systems is cell size dependent, comprised of ATL-1 and CHK-1, and accounts for approximately 40% of the difference in cell cycle timing between AB and P_1 (Brauchle et al. 2003). The other system is independent of cell size, and dependent on localization of PLK-1 and CDC-25.1 in P_1 (Budirahardja et al. 2008, Rivers et al. 2008). Both systems are known to be checkpoint based systems. Candidate genes for the putative timing compensation identified in our work, would likely include a list of genes known to interact with either the ATL-1/CHK-1 checkpoint system or the PLK-1 checkpoint system.

The work on Notch signalling in somite development, published by Palmeirim et al. (1997), and Jiang et al. (2000), would indicate that genes involved in Notch signalling would be likely candidates as members of the system of timing compensation identified in our work. The lin-12 gene, which in *C. elegans* encodes a member of the Notch/LIN-12/glp-1 transmembrane receptor family is known to be expressed in the 1.5 fold developmental stage of *C. elegans* (Regos et al. 2013, Hermann et al. 2000). CEL-Seq analysis of the transcriptome of the early embryo by Hashimshony et al. (2012) indicated that while lin-12 presence is relatively low during the one and two celled stage embryo, it is present (Hashimshony et al. 2012, 2014). Its presence before the maternal to zygotic transition (Robertson 2015) would indicate that, at least early on, its presence is only maternally derived. As the known function of lin-12 is thought to only occur in the 1.5 fold stage of development of the *C. elegans* embryo, long after the embryo has started utilizing its own transcription machinery, it raises the question what is its function at the earlier stages. In addition GLP-1 also exists as a maternal product in the early embryo, where it is segregated to the AB lineage (Evans et al. 1994).

Our work here also indicates a handful of additional avenues of investigation that may prove fruitful. An interesting question that the work here makes it possible to ask what factors dictate the temperature limits within which *C. elegans* and other poikilotherms are able to develop successfully? The trivial answer is generally accepted to be, that outside of this temperature range, critical cellular components

encounter a critical thermal threshold, outside of which they are unable to properly perform their function. The studies by Begasse et al. (2015) and Kuntz et al. (2014) demonstrate the uniform scaling of development in time as a function of temperature when comparing closely related species of nematodes and flies respectively. In conjunction with this, the exponential nature of the temperature-dependent rates of events in the one-cell *C. elegans* embryo (Begasse et al. 2015) and the temperature-dependent models of the divisions of AB and P_1 presented in our work here, raises the possibility that the permissive temperature ranges of those species may be the result, not of protein function failure, but of a divergence of differing clocks within the developing animal outside of an allowable range. An interesting way to test this would be to subject the two-cell *C. elegans* embryo to a temperature gradient, where the entire embryo would experience temperatures outside of the permissive range, but with P_1 slightly warmer than AB. This would establish an environment where the normally exponentially diverging clocks of AB and P_1 at elevated temperatures, were no longer exponentially diverging. Hatching rates of embryos subjected to such conditions could be compared to hatching rates of embryos subjected to elevated uniform temperatures during the division of AB and P_1.

Additional experimental avenues made possible by the tightly controlled thermal environment of the microfluidic chip, would be to further characterize the behavior of the two-cell *C. elegans* embryo outside the permissive temperature range. The offset

parameter introduced in our model of temperature-dependent division timing of AB and P_1 could be further verified and made more precise, with the possibility of extracting biological significance out of the number itself. An interesting comparison would be to perform a similar characterization of *C. briggsae* or *C. elegans* wild isolates.

Problems with Titanium

The devices were initially fabricated without a protective layer between the fluid in the channel and the metal of the heater. We found that the electrodes would corrode and unpredictably and catastrophically fail over time. This failure would frequently be preceded by the generation of bubbles in the channel which appeared to emanate from the side of the electrodes. These bubbles would occur both in the presence and absence of a voltage applied along the heater, eliminating the possibility of electrolysis by externally applied voltage. Estimations of the volume of gas generated from the metal of the heater approximately corresponded to the quantity of gas that would be generated if a monolayer of the titanium exposed to the fluid were to react with water, generating hydrogen gas and titanium dioxide. Extensive literature review on the possible causes of the evolution of gas emanating from the heater bore few results. The most promising leads for causes came from a series of three papers. The first, from Firebaugh et al. (1998) found that thin platinum films deposited on thin titanium films degraded at temperatures of 700^{O}C and higher.

Subsequently, a set of papers sought to characterize this process in time, also at elevated temperatures, and found that overall resistance of the film increased as titanium migrated into platinum (Schmid and Seidel 2008, Grosser and Schmid 2010).

The device that we have presented here does not experience temperatures near those of the experimental conditions cited above, either during fabrication or use. However the degradation of the electrodes in the absence of a plastic covering layer, and in contact with the salt water of the experiments would indicate that a similar process is happening in our devices. In addition to this, RTDs in a number of our devices did experience general increases in resistance over time, independent of temperature. These increases in resistance did not appear to be gradual, but rather appeared to happen in a stepwise fashion at random time points. After each of these occurrences the devices were re-calibrated for their change in resistance as a function of temperature. We found the relationship between temperature and resistance for the sensors remained highly linear, and that the slope describing the change in resistance as a function of the change in temperature remained approximately the same. However we found the offset parameter of the linear model (resistance expected at a temperature of $0^{O}C$) had increased. This is consistent with the time course findings of Schmid and Seidel (2008) and Grosser and Schmid (2010), in general but not specifics. The spontaneous evolution of gasses from our early unprotected electrodes is also consistent with the findings of Grosser and

Schmid (2010), that titanium from thin film Ti underlayers migrate through platinum thin film top layers predominantly resulting in Ti_XO_Y species. Pure titanium in water would spontaneously oxidize water giving off hydrogen gas. A potentially fruitful and generally helpful project could be to investigate the hypothesis that 1) titanium does migrate into platinum thin films even at these low temperatures, and 2) measurably does so in a stepwise and stochastic manner.

Modular Chip Design

The challenges of the current microfluidic device design are the number of critical steps that are error-prone and or do not lend themselves well to scaling. The cutting of vias for the tubing and the etching process that removes the material from the underside of the device are two examples of these types of problems. For the via construction, we have found that it takes several days at a minimum for someone who has never constructed a device to be able to proficiently form the glass cutouts at a usable quality. Even with skilled hands the time it takes to form usable vias for a single device can take on the average of an hour or more. The etching process that removes the material from the underside of the device to allow for creation of the gradient is also error-prone. Even though multiple devices can be etched simultaneously, the etching rates are variable from device to device even within the same treatment. The process also requires constant monitoring and re-etching to create a cutout that is thermally, structurally, and optically sufficient. In addition neither of these processes are ones that could be easily outsourced to a third party.

One potentially fruitful next step, would be to take the current design and modify it to a more multi-layered design, with the material and thickness of each layer selected for scalability and ease of handling. This could potentially increase the number of devices that can be constructed simultaneously, and allow for the possibility of outsourcing some or most of the construction of the device to traditional MEMS fabrication facilities.

Conclusion

We have successfully designed, characterized, and demonstrated the use of a microfluidic temperature gradient device and system sufficient to establish a 7.5^{O}C gradient across the ~ 50 μm long axis of the *C. elegans* embryo. We have characterized the division time of the two celled embryo as a function of temperature and established a mathematical model describing the relationship. We have demonstrated that the cells of an embryo placed in this temperature gradient in the two-cell embryo are in different temperatures, behave inconsistent with the expected behavior at the local temperature of each of the cells. We have shown that this inconsistency is in the form of both cells slowing down relative to their expected behavior based on their own local conditions, and that the magnitude of this slowdown is increased for embryos that survived to hatching after being subjected to the temperature gradient. We have shown that the quantitative and qualitative behavior of the cells in the embryos is dependent on the orientation of the embryo in

the temperature gradient. We have demonstrated that the temperature gradient under certain conditions is sufficient to reverse the sequence of divisions of the two-cell embryo, and that although embryos that experience this condition have not hatched, we have shown that a fraction of the time they nonetheless undergo morphogenesis. We have also demonstrated an interesting physical phenomenon that results in an “un-division” of an embryo that appears to have already completed cytokinesis.

Appendix A: Materials and Methods

Device: Backplane (Electrode Layer)

Device design for lithography masks was performed in autocad and saved as DXF format for printing (Figure A.1). For backplane design (electrode layer), masks were obtained from CAD/Art Services,Inc. (Bandon, OR). A 1:1 scale black and white printout is produced for placement of vias.

Via cutting

A 1”x3” microscope slide (eg Model No. 12-550B, Fisher Scientific, Canoga Park, CA) is marked to indicate position of vias. A diamond coated conical drill bit (kit #97626, Harbor Freight Tools, Ventura CA) mounted in a variable speed Dremel rotary tool (Dremel, Mount Prospect, IL), held vertical by a drill press jig (Model # 220-01, Dremel), is operated at ~ 5K-10K RPM, and used to grind a tapering hemi conical cutout at each of the via locations. Cutout starts at the edge of the microscope slide and projects perpendicularly from the edge into the microscope slide. Microscope slide is held with the long axis in either hand and held parallel to the bit. The vias marked on the top side of the glass are cut first by bringing the top edge and bit facing face of the slide into contact with the bit at a slight angle. The slide is gently pressed and rotated until a tapered cut is achieved. Depth and width of cutout tapers from the edge of the slide, terminating on the surface of the slide approximately 1cm from the edge. Maximum depth and width at the edge of the

slide is approximately 800-900 μm, and 2 mm respectively. Sufficiency of depth of cut is confirmed by placing a clean microscope slide on top of the vias, and inserting a length of PTFE 0.030" outer diameter tubing (Cole Parmer, Item # EW-06417-11) that has been pinched flat on the end, about ½ way into the cutout.

SiO_2 Deposition

To prevent migration of impurities from the glass of the microscope slide into the metal that will deposited onto the device, a layer of SiO_2 is reactive sputter deposited on the eventual electrode containing faces of the backplanes. Backplanes are transferred to a clean room environment, DI rinsed and scrubbed with a dilute surfactant solution using a cleanroom swab. Backplanes are then sonicated in a bath of clean room grade acetone, for 5 minutes, followed by 5 minutes of sonication in a bath of isopropanol. They are then rinsed with DI for approximately two minutes and dried with compressed N_2 gas. Backplanes are then placed on a 150^{O}C hotplate for five minutes to dehydrate. They are then placed in an asher (PEII-A, Technics) and subjected to a 300 mTorr, 100W O_2 plasma for 60 seconds. Backplanes are then loaded into a an RF sputter machine (ATC 2200-V, AJA International). The system is brought down to vacuum, the backplanes are brought to 250^{O}C for 10 minutes, and then cleaned with an ionized argon gas backsputter. 100-150 nm of SiO_2 is then sputter deposited.

Photolithography for metal deposition.

Photolithography for metal deposition is performed similar to cleanroom recipe available at the UCSB clean room facility website[1]. Devices are spin coated (PWM32 Spinner, Headway Research, Garland, Texas) with negative resist AZnLOF2020 (MicroChemicals GmbH, Ulm, Germany) to allow for patterned features, with an adhesion promotion layer of Bis(trimethylsilyl)amine (HMDS) applied before the photoresist. Pattern is exposed onto photoresist covered backplane with a custom made mask on an SUSS MJB-3 aligner (Karl Suss America). Aligner is configured for near-UV window (365 and 405 nm).

1. 200^{O}C 5 min dehydration bake on hot plate.
2. Move to spinner and dispense ~1 ml HMDS onto backplane.
3. Allow to sit for 40 seconds to allow for surface chemistry between glass and HMDS.
4. Spin at 3K RPM for 30sec.
5. Place on 100^{O}C hot plate for two minutes.
6. Allow to cool for two minutes.
7. Move back to spinner and dispense approximately 1.5-2 m of photoresist so that entire backplane is covered with a shallow pool.
8. Spin at 3K RPM for 30 seconds.
9. Along the sides of the backplane, gently drag a cleanroom swab soaked with edge beam remover (AZ EBR Edge Bead Remover, MicroChemicals)
10. Place on 110^{O}C hot plate for 90 seconds.
11. Allow to cool for two minutes.
12. Place backplane in aligner on top of a black chuck and align mask to drilled vias.
13. Expose for 10 seconds.
14. Perform post exposure bake on a 110^{O}C hotplate for 60 seconds.
15. Allow to cool for two minutes.
16. Develop for 60 seconds in a bath of AZ300MIF (MicroChemicals)

[1] https://www.nanotech.ucsb.edu/wiki/index.php/Contact_Alignment_Recipes#Positive_Resist_.28MJB-3.29

17. Rinse with DI, and dry with compressed N2
18. Inspect under microscope.

.

Metal Deposition and Liftoff

Devices are subjected to a 300 mTorr, 100W O_2 plasma clean, and immediately transferred into electron beam metal deposition machine (Temescal). 10nm of Ti is deposited followed by a 10 minute cool down period and 100nl of Pt is deposited. Devices are unloaded from the machine and placed in a bath of AZNM liftoff solvent (MicroChemicals), and sonicated for 15 minutes. Devices are rinsed with acetone, isopropanol, and DI for several minutes each, and dried with compressed N_2.Devices are then inspected under a microscope.

SU-8 Deposition

To isolate the electrodes from the water of the microchannels of the final device, the electrode containing face of the device is covered with an approximate 2 μm layer of SU-8 2002(MicroChem Corp.,Westborough, MA). The following recipe is adapted from the MicroChem website[2]. To prevent covering of electrodes with SU-8, a crude mask made from a 2" x 3" microscope slide and aluminum foil that sit over the electrodes, is placed over the device during UV exposure.

1. 5 minutes 200^{O}C dehydration bake on a hot plate.
2. Move to spin coater and dispense ~ 1ml of HMDS.
3. Allow to soak for 40 seconds.

[2] http://www.microchem.com/pdf/SU-82000DataSheet2000_5thru2015Ver4.pdf

4. Spin at 3K RPM for 30 seconds.
5. Place on 100^{O}C hot plate for 2 minutes.
6. Allow to cool off of hot plate for 2 minutes.
7. Place back in spin coater and dispense ~ 1.5-2 ml of SU-8 2002 (enough to cover device.
8. Spin Recipe: accelerate at 100 RPM/sec to 500 RPM and spin for 10 seconds. Accelerate at 600 RPM/sec to 3K RPM and spin for 30 seconds. Decelerate at 500 RPM/sec until stopped.
9. Along the sides of the backplane, gently drag a cleanroom swab soaked with edge beam remover (AZ EBR Edge Bead Remover, MicroChemicals)
10. Place on 95^{O}C hot plate for 1 minute.
11. Allow to cool off of hot plate for 2 minutes.
12. Place backplane in aligner with mask covering electrodes and expose for 15 seconds.
13. Place on 95^{O}C hot plate for 2 minutes.
14. Allow to cool off of hot plate for 2 minutes.
15. Place in bath of SU-8 Developer (MicroChem) with gentle agitation for 2 minutes.
16. Rinse with acetone and inspect.
17. Sonicate in a bath of acetone for 2 min.
18. Sonicate in a bath of isopropanol for 2 min.
19. Dry with compressed N_2 gas.
20. 300 mTorr, 100W O_2 plasma clean.

HF etch for thinned temperature gradient region.

Backplanes are sandwiched between two layers of poly-olefin based dicing tape (eg Model No. F42, Microworld, Grenoble, France) on both sides. An ~ 1cm diameter circular cut centered on the center of the electrodes, is made in the dicing tape of the non electrode containing face of the backplane. The cut is made with a Trotec Speedy 100 laser cutter (Trotec Laser Inc., Plymouth, MI). The device is then placed in a plastic cylindrical container such that the height of the container is approximately 2x the height of the device, and the base of the container is approximately 2x wider than it's height. Device is positioned so that it is at the edge of the container, with the

cutout facing the inside of the container. An ~ 1” stir bar is added to the container, and the container is filled with 49% hydrofluoric acid. Container is placed on a stir plate and stir bar is rotated at ~ 2 Hz. After 15 minutes device is removed from HF solution, rinsed, dried and the depth of the hole is measured. Second etching is performed with the device oriented “upside down” relative to its initial orientation. This process is continued until depth of etch reaches ~ 750-800 μm.

Devices are thoroughly rinsed with DI and dried with compressed N_2. Olefin tape is then exposed to UV (releasing the tape adhesive) and the device is removed from the tape.

Microfluidic channel mold fabrication

The microchannel device is designed in autocad and a DXF file is produced. In addition to the microfluidic channels, and embryo capture structures, the design has a number of registration marks that allow for proper placement on the backplane. A silicon wafer mold is obtained from the California Nanosystems Institute (CNSI) Clean Room facility wafer processing services (CNSI, UCSB, Santa Barbara, CA) utilizing the premade design. Design is etched into the wafer approximately 40-50 μm deep. A final PDMS mold is made from the silicon wafer using standard soft lithography techniques (Xia and Whitesides, 1998).

Microchannel Fabrication

Microchannel layer of device is constructed consistent with methods developed by Bartolo et al. (2008). PDMS channel mold is placed on 2”x3” microscope slide and placed on a scale (Model # ML1502E, Mettler Toledo). Approximately 0.20 grams of NOA 81 (Norland Optical Adhesives, Cranbury, NJ) is dispensed in center of mold. Any bubbles present are removed with either 100 µl or 1 ml pipetman with disposable tips, and polymer is removed until mass of deposited polymer is approximately 0.18g. A 25x25mm No1 coverslip (Thermo Scientific model No. 3307) is gently lowered onto the polymer, and edges of coverslip are moved with forceps so that the corners are aligned with registration marks pre patterned on the mold. Mold, NOA 81, and coverslip are allowed to sit until the thickness of the polymer is roughly uniform underneath the coverslip. Device is placed on an aluminum foil covered flat platform approximately 2” high and placed in a UV lamp housing (Model No 5200, Norland Optical Adhesives, Cranbury, NJ), containing a 4 Watt UV bulb. Device is cured from 30-70 seconds depending on age of UV bulb. Device is removed by peeling back the PDMS mold, releasing the channel layer and coverslip.

Device Assembly

Sticker device channel layer is placed coverslip side down (feature side up) on a ⅛” thick piece of soda-lime glass approximately 4” x 8” in dimension. Glass and channel layer of device are placed on an inverted microscope configured for epi illumination

(Eclipse TE200 inverted scope, Plan Fluor 4x Objective, WD 17.1, Nikon, Tokyo, Japan). An in house made jig (Figure A.1) is used to hold the electrode covered backplane (features side down) through coupling to a vacuum pump (Model No DOA P794, Gast Manufacturing, Benton Harbor, MI). The backplane is then lowered onto the channel layer, while positioning of channels, and capture region of the device are aligned with the Joule heater patterned on backplane. After backplane is aligned and in contact with the channels, the vacuum is released, the device is flipped over, and the handle of small metal forceps are used to press the channels onto the device until full contact is made between the two. Regions of non-contact are visible through the microscope as “newton rings”.

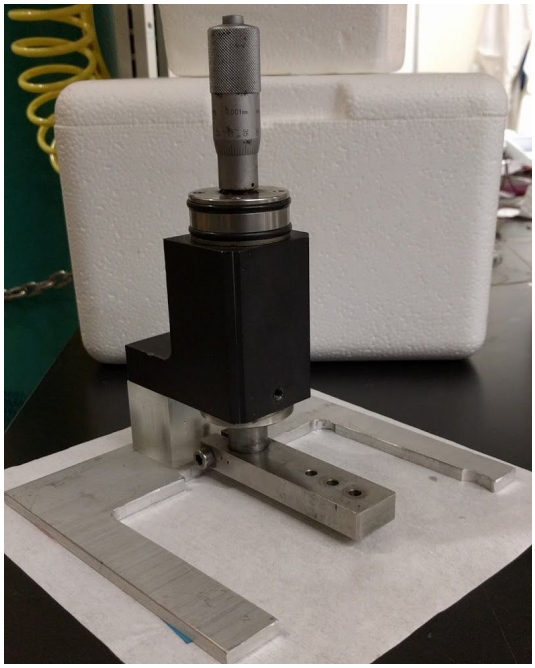

Figure A.1: Custom built device assembly alignment tool. A vacuum line is connected to the innermost of the three holes on the center block. Device is placed on the bottom of the block, feature side down, and held in place by the vacuum. Micrometer dial on the top is used to lower the device backplane toward the microfluidic channel layer.

Device is again placed on the aluminum foil covered flat platform and placed inside the UV lamp housing and exposed to UV for 5 minutes. Device is then exposed to full sunlight for an additional 15 minutes. Device is then placed in a 50^{O}C over for 12 hours.

Tubing

A 4” x 8” x ⅛” piece of soda-lime glass is tightly wrapped in a single layer of aluminum foil (shiny side up). Device is placed in center and secured with paper tape.

Six, Approximately 1.5 meter lengths of PTFE 0.030" outer diameter tubing are cut, and ~ ½ - 1 cm of the ends are flattened with metal forceps. Under a dissecting scope, flattened tubing is inserted into each of the vias. Tubing is taped to the aluminum 1-3” from the edge of the device to prevent the tubing from falling out of the device. Approximately 2 ml of two part epoxy (Devcon 5 min Epoxy, ITW Polymers Adhesives North America, Danvers, MA), is mixed and loaded into a 1 ml syringe (Model No. 309659, Bechtel Dickinson, Franklin Lakes, NJ). A 200 µl disposable pipetman tip is shortened at the wide end with a razor blade, and placed onto the tip of 1ml syringe. Epoxy is dispensed with the pipet tip positioned at either side of the junction between the PTFE tubing and the device itself. This is repeated for both sides of the tubing and for all tubing in the device. Epoxy is allowed to cure overnight, afterwhich device is removed from the aluminum foil.

The tips of 27 gauge ½" needles (Terumo Medical Products, Somerset, NJ) are cut off and the shafts rounded with a standard "cutoff wheel" on the Dremel rotary tool (eg. Model No. 420, Dremel, Mount Prospect, IL). Needle is cleaned and inspected. One modified needle each is inserted into the tubing from one side of the device for future fluid loading.

RTD characterization

Two insulated wires, of either 26 or 28 AWG are soldered to each end of each RTD. Device and wire are placed in a 170x90 cm Pyrex glass dish (Model NO. 3140, Corning, Corning, NY), with ellipsoid magnetic stir bar ~ 1.5" x 0.75". Dish is filled with a mixture of deionized water and ice and placed on a stir plate (Model No. PC-351, Corning, Corning, NY). Stirring is set to approximately 5 Hz. A K type thermocouple is placed inside of the bath (Model No. 5sc, Omega Enterprises, Norwalk, CT). Thermocouple and unsoldered wire ends are connected to a National Instruments DAQ thermocouple or RTD measurement module and housing (Model Nos. NI 9211, NI 9217,NI cDAQ-9172 respectively, National Instruments, Austin, TX). Resistance measurements are performed in "4-wire" mode. Resistance measurements and temperature readings are recorded by a custom Labview software (Labview v8.6, National Instruments, Austin, TX). Water in bath is allowed to come up to room temperature while bath temperature and device resistance measurements are recorded. Measurements are used to determine a linear

relationship between the temperature and resistance of the sensors utilizing standard least squares fitting.

Device Holder

Device is mounted on a custom built device holder/flow cell. Device holder is constructed so that bulk fluid flows underneath and in contact with the outside bottom surface of the microfluidic device (Figure A.2).

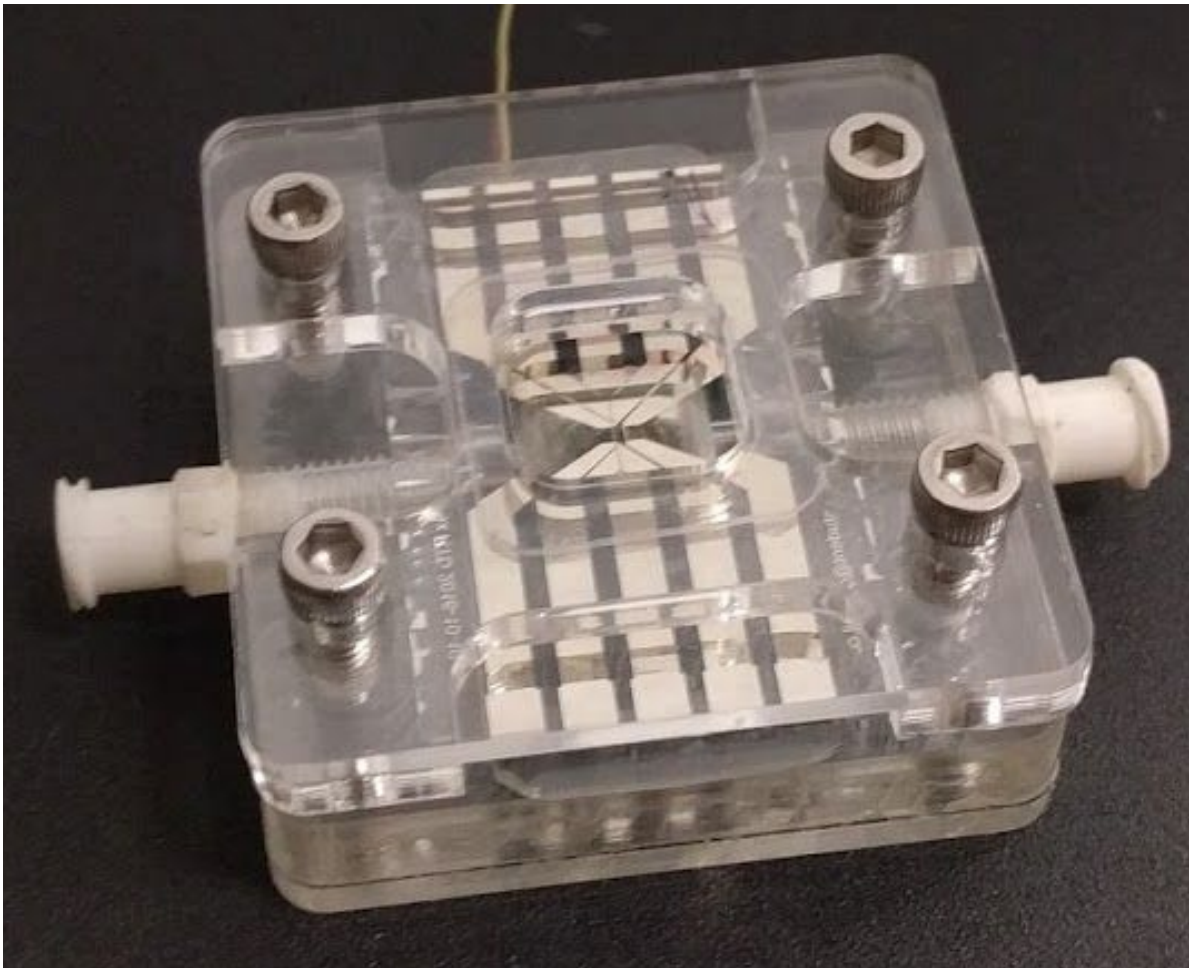

Figure A.2: Fully assembled device holder and bulk fluid flow cell with device in place. Swagelok connectors attach to tubing leading to a bulk water circulator.

Thermometric Microscopy

Bulk fluid flow tubes are connected to flow cell and to a heated and refrigerated water circulator (Model No. A82, Haake, Thermo Fisher Scientific, Waltham, MA). Circulator is filled with DI water and ethylene glycol in a ratio of 4:1. Flow rate of water through the fluid cell is on the order of 19 ml/sec.

Device holder/flow cell and device are loaded into a custom built holder attached to an upright microscope (Eclipse E600 FN upright scope, Plan Fluor 10x Objective, WD 16, NA 0.30 Nikon, Tokyo, Japan) (Figure A.3).

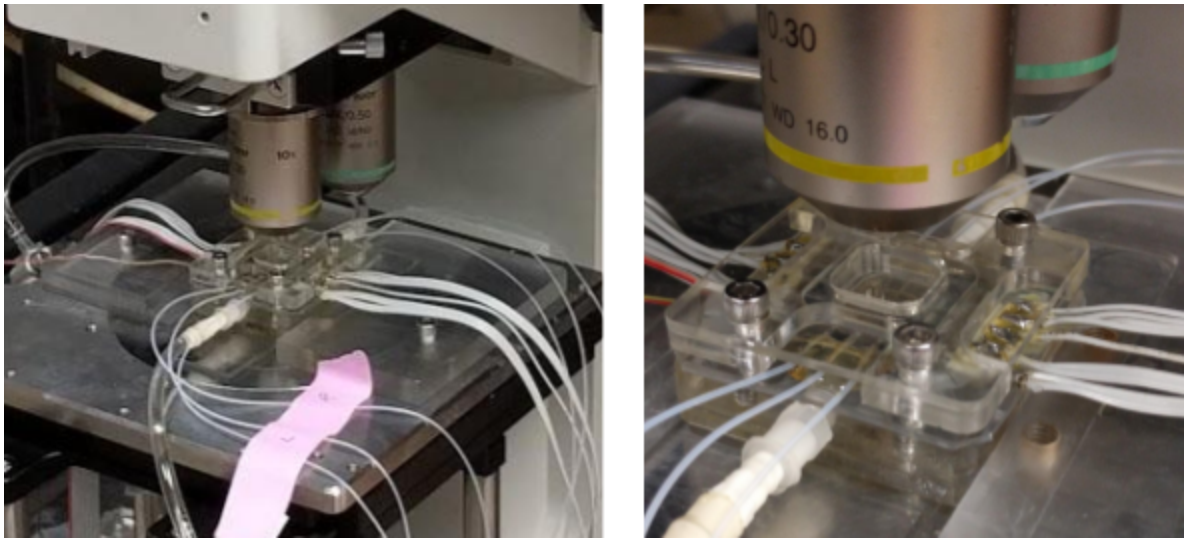

Figure A.3: Left, Device Holder/Flow Cell and Device secured to stage of the microscope. Right, Close up of Device Holder and device secured to stage.

Deionized water is loaded into the microchannels of the device at a rate of 300 µl/min utilizing a syringe pump (eg Model No. NE-1000, New Era Syringe Pumps, Farmingdale, NY), and either a 1 ml or 3ml syringe DI filled syringe. Channels are inspected under light microscopy for expression of bubbles.

A solution of 1 mg/ml of dextran conjugated Rhodamine B (DCRB) (Model No. R9379, Sigma Life Sciences, St. Louis, MO) is mixed. Four 1.2 ml aliquots are

decanted into 1.5 ml microfuge tubes and spun at 17G (accuSpin micro 17, Fisher Scientific, Canoga Park, CA) for 5 minutes to remove particulates. Solution is transferred to four, one ml syringes. Approximately 600 µl of solution is loaded into each channel of the device at 300 µl/min.

Microscope and device are sealed within custom built environmental enclosure, which is filled with laboratory supplied air with a sub $0^{O}C$ dew point to prevent condensation on device during operation. Environmental chamber is maintained at a slight positive pressure (Figure A.4).

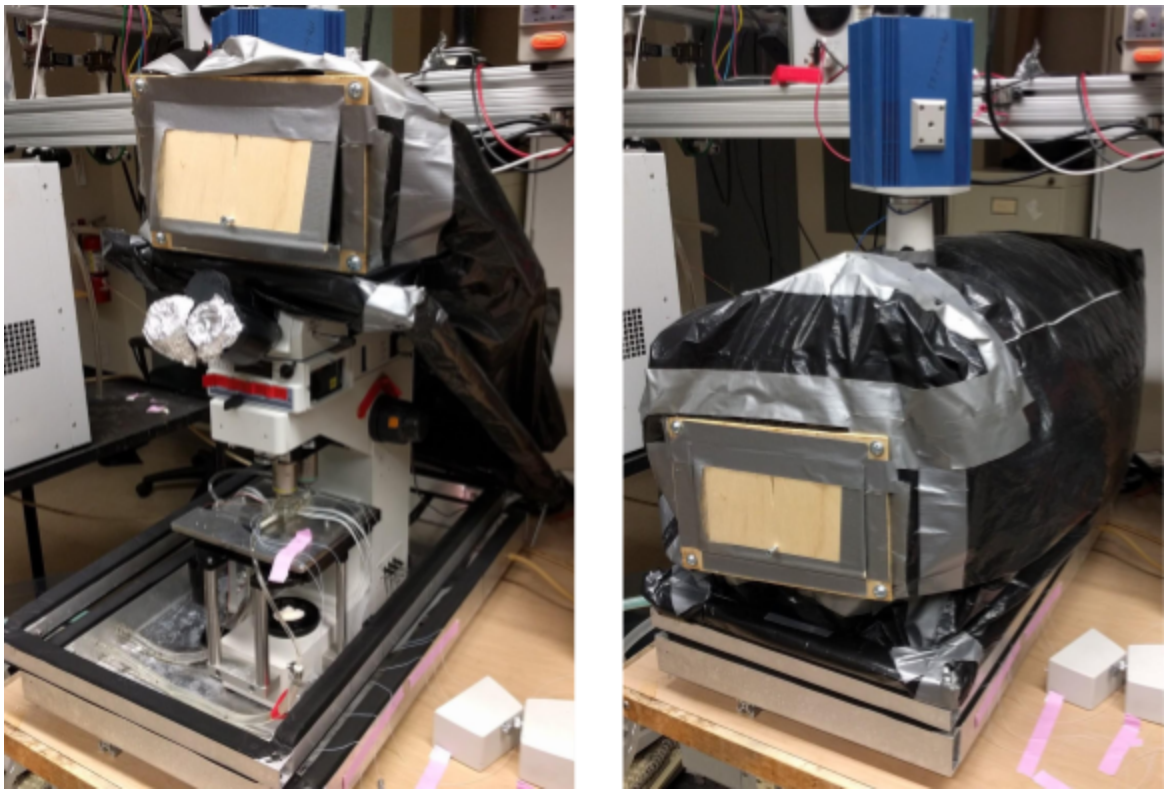

Figure A.4: Left, Microscope with environmental isolation chamber unsecured for device setup. Right, environmental chamber for microscope secured for control of humidity around microscope.

Circulator temperature is brought down to approximately 5^{O}C and flowed through the fluid cell. Temperature of the water in the fluid cell is measured by a thermocouple embedded in the flow of the fluid cell. Temperature inside of the device is measured by taking temperature (resistance) measurements with the RTDs. DCRB solution was flowed at a rate of 500 nl/min during data acquisition. To construct a standard curve of fluorescence to temperature 30-60 images are taken with a TEC cooled fluorescence CCD camera (COOL Snap HQ2, Photometrics, Tucson, AZ) , and Rhodamine microscope filter (Nikon R/DII 31002), at each of a series of temperature between 30^{O}C and 1.5^{O}C. Illumination is achieved through an “epi” illumination configuration, with a custom built light source consisting of a white 1 Watt LED (Model No 518, Adafruit industries), housing and power supply, driven at 200mA and rated for between 90 and 140 lumens. A fiber optic cable is run from the light housing to a collimating lense attached to the microscope.

To measure the temperature gradient, the circulator temperature is brought down to 1.5^{O}C and a voltage is applied to the Joule heater. A series of 30-60 images is taken at each of a number of voltage steps.

Thermometric Microscopy Data Analysis

During image acquisition for fluorescence data, it is typical for the device to move to some degree. This movement is particularly apparent when comparing images from

different temperatures. This can give rise to the situation where a temperature measurement during gradient operation can be based on a model between temperature and fluorescence, where the data used to generate the model is based on a different physical point in the device then that under consideration. To limit these effects the images are manually aligned utilizing imagej version 1.47 (Schneider et al. 2012). This generally results in image sets that are off by no more than one pixel from each other.

The data for each image taken for the standard curve, along with the temperature measurements for that data are loaded into a custom matlab script, and classical least squares model between fluorescence to temperature is constructed for each pixel. The data is then filtered to remove any pixels that have a poor R^2 value (generally anything lower than 0.98). Additional filtering includes removing pixel that are neighbored by pixels where the models for the two pixels are significantly different. This reduced the possibility that data taken during temperature gradient measurement is evaluated with an inappropriate model.

To estimate the temperature in the device during operation of the gradient, the images taken at each applied voltage are averaged. The final average image at a particular voltage is then aligned with the images of the standard curve as described above, and a temperature is predicted for each pixel utilizing a custom matlab script.

Comsol simulation

2D Finite element analysis was performed on a model of the microfluidic device and heat rejection system to estimate the magnitude and performance of putative and produced designs. Comsol Multiphysics version 5.1-5.2a were variously used. Built in material properties were used, with the notable exceptions being the physical parameters for SU-8, and NOA 81, which were both estimated to behave like poly ethylene. Cooling fluid flow under the device was assumed to be laminar.

Worm handling and maintenance

Strains used

Experiments were either conducted with the canonical N2 strain or with AZ212: *ruIs32 [pie-1p::GFP::H2B + unc-119(+)] III* (Homozygous expression of GFP::H2B histone fusion in germline. pAZ132).

Worm maintenance

C. elegans were maintained as described by Stiernagle (2006). Plates were kept at either room temperature (18-22^{O}C) or in a 15^{O}C incubator.

Egg Salts

Egg salts solution is created consistent with Edgar and McGhee (1986). pH is adjusted to 7.3 by dropwise addition of 100mM NaOH or HCl.

Loading, positioning, and unloading embryos into, inside, and from the device

Each well of a 3 Depression Glass Spot Plate (Model No. 7223-34, Corning, Corning, NY) is filled with approximately 1 ml of “egg salts”. 9-10 young adults are transferred into the first well with a platinum worm pick (Stiernagle 2006). Under a dissecting microscope 5-6 are then transferred from the first well to the second with a mouth pipette (Junkersdorf and Schierenberg 1992,Edgar 1995). 27 gauge, ½” (Terumo Medical) needles are then placed on 1 ml syringes (Bechtel Dickinson) and used as scissors to cut the worms in the well in half just to either side of the vulva. Embryos consistent with having pronuclei are isolated in the well and loaded into the device.

To load the embryos into the device, a second 3 Depression Glass Spot Plate is placed in a custom holder (Figure A.5). The three channels of the the device are filled with egg salts from three different 1 or 3 ml egg salt filled syringes at a rate of 300 µl/min powered by syringe pumps, with the flow-through emptying into the wells of the spot plate. The ends of the tubing from the device are held so that each of the three is held within the cavity of its own well, with the end of the tube submerged below the surface as the well fills from the flow-through of the device. The wells are filled the remained of the way with egg salts utilizing a standard 1 ml pipetman. Once a continuous fluid circuit is established between the egg salt filled syringes in the syringe pumps, and the wells of the spot plate, the syringe pumps are operated in a reverse manner at a rate of 100 µl/min so that the fluid from the wells are drawn into

the tubing, device, and syringes. Under the dissecting scope, the mouth pipette is used to transfer an embryo from the well in which it was cut to one of the wells that has tubing submerged. The embryo is expelled from the mouth pipette into the fluid of the well near the tube, and the embryo is observed entering the end of the tube, and eventually reaching the capture region of the device, wedged between two of the pillars. Each well has one embryo loaded in this manner.

Figure A.5: Custom housing to hold end of the tubing attached to the device in the wells of the 3 Depression Glass Spot Plate

Once the embryos have reached the capture region, the syringe pumps are stopped and the flow is allowed to come to a stop (~30 seconds to 1 minute). If any of the embryos are not in the correct orientation, the tubing that corresponds with the particular embryo is “flicked” with the finger, causing a short rapid movement of the flow in the channel, and pulling the embryo away from and then back toward the

capture region. The new orientation is to some extent random, and so frequently several “flicks” are necessary to achieve the correct orientation and placement of the embryo.

To unload the embryos, the syringe pumps are again operated in the forward direction (expelling) with fluid moving toward the wells from which the embryos were initially loaded. The syringe pumps are operated at a rate of 100 µl/min, and the end of the tubing still submerged below the surface of the egg salts is observed until the embryo is seen emerging from the tubing, into the well itself. The embryo is then captured with the mouth pipette and transferred to a standard agar plate for further analysis.

Embryo division timing expt

For embryo division timing experiments, embryos are loaded into the device as described above. Once the embryos are positioned, a trickling flow of 500 nl/min is started from the device, with the fluid being drawn from the wells in which the embryos were loaded. Positioning embryos is the same for both constant temperature and temperature gradient experiments, with the exception that for temperature gradient experiments, the repositioning is continued until the desired orientation in the gradient is achieved.

For constant temperature experiments, the temperature of the device is set by the temperature of the bulk fluid flowing underneath the device in the device hodler/flow cell. For temperature gradient experiments, the temperature distribution in the device is achieved by setting the temperature of the bulk fluid flowing through the flow cell to relatively low temperature, and then applying a voltage to the Joule heater consistent with the desired temperatures. For both types of experiments real time temperature measurements are taken with the RTDs. These temperature measurements indicate that the temperature profile within the device is affected by the flow of the fluid in the microchannels during embryo loading and unloading while the fluid in the microfluidic channel is running at 300 µl/min, but not channel flow is at 500 nl/min. In either type of experiment, the temperature of the bulk flow is measured by a thermocouple embedded in the flow, and temperature measurements are recorded in the device and microfluidic channels by the RTDs.

Images of the embryos are taken by the same microscope and camera used in thermometric experiments, with the exception that a neutral filter is used instead of a fluorescent filter, and illuminated is transmitted instead of epi configuration.

Temperature estimation in gradient.

The maximum temperature gradient in our device that has been measured by our RTDs and thermometric microscopy method was 7.5^{O}C without exceeding a maximum temperature with which the embryo would be exposed of 25^{O}C. However,

any arbitrary temperature gradient below 7.5^{O}C is possible with the maximum bound of 25^{O}C, and even greater gradients are possible if the upper temperature is allowed to go higher. To allow us to estimate the temperature gradient under arbitrary conditions, the temperature distribution within the device is estimated by inputting the known parameters of the system, such as fluid flow rate and temperature of the fluid moving through the fluid cell, and current density through the heater. The temperature measurements of the RTDs are used to confirm these values. Under normal operating conditions for our *C. elegans* embryo experiments however, the temperatures as measured by the closest and furthest straight RTDs (Figure A.6) were found to be reasonable approximations of the temperature experienced at the extreme polls of the embryo as predicted by the Comsol model for a given set of conditions.

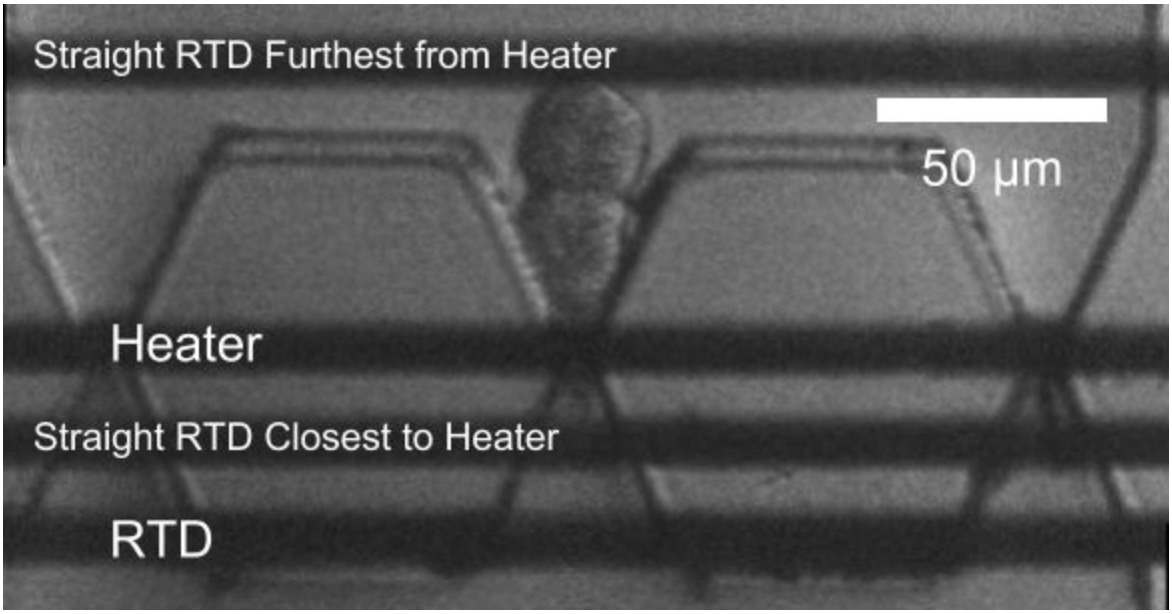

Figure A.6: Position of embryo in the capture region of the device. Estimate of the temperature at the extreme ends of the long axis of the embryo when positioned this way, can be reasonably approximated by the RTD measurements of the closest and furthest straight RTDs.

Temperature gradient data analysis

Division time calculation

Time of division for cell is determined by watching time lapse images the embryo in the capture region. Images are generally taken at 10 second intervals. Time of division is estimated as time of image that first shows apparent completion of membrane pinching.

For embryos subjected to a temperature gradient that were loaded after the first division, the time of division was estimated in the following manner. The fraction of development for each cell that occurred outside of the temperature gradient was estimated using the measured room temperature and the linear model of time of division at that temperature. One minus this fraction, or the fraction of development remaining, and the time the cell was in the gradient before it divided was used to estimate the time the cell would have taken to divide had it been in the gradient from the moment of its initial formation. This was estimated by dividing the time in gradient by the fraction of development spend in the gradient.

Phenotype scoring

After embryos were unloaded from the device for either control or gradient experiments, they were placed on OP50 seeded agar pads with a mouth pipette,

allowed to develop at room temperature and scored for hatching under a dissection scope 24 hours later. For embryos that did not hatch, they were then further inspected under a compound microscope utilizing DIC at 40X and or 100X

Appendix B: Bibliography

Adkins, R. M., Gelke, E. L., Rowe, D., & Honeycutt, R. L. (2001). Molecular phylogeny and divergence time estimates for major rodent groups: evidence from multiple genes. Molecular Biology and Evolution, 18(5), 777–91. Retrieved from http://www.ncbi.nlm.nih.gov/pubmed/11319262

Artus J, Cohen-Tannoudji M (2008) Cell cycle regulation during early mouse embryogenesis. Mol Cell Endocrinol 282(1–2):78–86. doi:10.1016/j.mce.2007.11.008

Bao, Z., Zhao, Z., Boyle, T. J., Murray, J. I., & Waterston, R. H. (2008). Control of cell cycle timing during C. elegans embryogenesis. Developmental Biology, 318(1), 65–72. https://doi.or

Bartolo, D., Degré, G., Nghe, P., & Studer, V. (2008). Microfluidic stickers. Lab Chip, 8(2), 274–279. https://doi.org/10.1039/B712368J

Begasse, M. L., & Hyman, A. A. (2011). Cell Cycle in Development. (J. Z. Kubiak, Ed.) (Vol. 53). Berlin, Heidelberg: Springer Berlin Heidelberg. https://doi.org/10.1007/978-3-642-19065-0

Begasse, M. L., Leaver, M., Vazquez, F., Grill, S. W., & Hyman, A. A. (2015). Temperature Dependence of Cell Division Timing Accounts for a Shift in the Thermal Limits of *C. elegans* and *C. briggsae*. Cell Reports, 10(5), 647–653. http://doi.org/10.1016/j.celrep.2015.01.006

Bembenek, J. N., Richie, C. T., Squirrell, J. M., Campbell, J. M., Eliceiri, K. W., Poteryaev, D., … White, J. G. (2007). Cortical granule exocytosis in C. elegans is regulated by cell cycle components including separase. Development, 134(21), 3837–3848. https://doi.org/10.1242/dev.011361

Ben-David, E., Burga, A., & Kruglyak, L. (2017). A maternal-effect selfish genetic element in *Caenorhabditis elegans*. Science, 356(6342), 1051–1055. http://doi.org/10.1126/science.aan0621

Bergeland, T., Widerberg, J., Bakke, O., & Nordeng, T. W. (2001). Mitotic partitioning of endosomes and lysosomes. Current Biology, 11(9), 644–651. https://doi.org/10.1016/S0960-9822(01)00177-4

Bianconi, E., Piovesan, A., Facchin, F., Beraudi, A., Casadei, R., Frabetti, F., … Canaider, S. (2013). An estimation of the number of cells in the human body. Annals of Human Biology, 40(6), 463–471. http://doi.org/10.3109/03014460.2013.807878

Birnby, D. A., Link, E. M., Vowels, J. J., Tian, H., Colacurcio, P. L., & Thomas, J. H. (2000). A transmembrane guanylyl cyclase (DAF-11) and Hsp90 (DAF-21) regulate a common set of chemosensory behaviors in *caenorhabditis elegans*.

Genetics, 155(1), 85–104. Retrieved from http://www.ncbi.nlm.nih.gov/pubmed/10790386

Boggs, J.H. and Sibbitt, W.L. (1955) Thermal Conductivity Measurements of Viscous Liquids. Industrial and Engineering Chemistry, 1955. 47(2): p. 289-293.

Bolet, G. (1986). Timing and Extent of Embryonic Mortality in Pigs Sheep and Goats: Genetic Variability. In Embryonic Mortality in Farm Animals (pp. 12–43). Dordrecht: Springer Netherlands. http://doi.org/10.1007/978-94-009-5038-2_2

Bolker, B. F. T., & Sidles, P. H. (1977). Thin-film platinum resistance thermometers: Fabrication and use. Journal of Vacuum Science and Technology, 14(1), 205–209. https://doi.org/10.1116/1.569123

Bong, K. W., Xu, J., Kim, J.-H., Chapin, S. C., Strano, M. S., Gleason, K. K., & Doyle, P. S. (2012). Non-polydimethylsiloxane devices for oxygen-free flow lithography. Nature Communications, 3, 805. https://doi.org/10.1038/ncomms1800

Borkovich, K. A., Farrelly, F. W., Finkelstein, D. B., Taulien, J., & Lindquist, S. (1989). hsp82 is an essential protein that is required in higher concentrations for growth of cells at higher temperatures. Molecular and Cellular Biology, 9(9), 3919–30. https://doi.org/10.1128/MCB.9.9.3919

Brauchle, M., Baumer, K., & Gönczy, P. (2003). Differential activation of the DNA replication checkpoint contributes to asynchrony of cell division in C. elegans embryos. Current Biology : CB, 13(10), 819–27. https://doi.org/10.1016/S

Brenner, S. (1974). The genetics of *Caenorhabditis elegans*. Genetics, 77(1), 71–94.

Budirahardja, Y., & Gonczy, P. (2008). PLK-1 asymmetry contributes to asynchronous cell division of C. elegans embryos. Development, 135(7), 1303–1313. https://doi.org/10.1242/dev.019075

Byerly, L., Cassada, R. C., & Russell, R. L. (1976). The life cycle of the nematode *Caenorhabditis elegans*. Developmental Biology, 51(1), 23–33. https://doi.org/10.1016/0012-1606(76)90119-6

Clute P, Masui Y (1997) Microtubule dependence of chromosome cycles in Xenopus laevis blastomeres under the influence of a DNA synthesis inhibitor, aphidicolin. Dev Biol 185(1):1–13. doi:10.1006/dbio.1997.8540

Cooke, J., & Zeeman, E. C. (1976). A clock and wavefront model for control of the number of repeated structures during animal morphogenesis. Journal of Theoretical Biology, 58(2), 455–76. Retrieved from http://www.ncbi.nlm.nih.gov/pubmed/940335

Croce, R.P., et al., A Thermal Model for Pulsed EM Field Exposure Effects in Cells at Nonthermal Levels. Ieee Transactions on Plasma Science, (2010). 38(2): p. 149-155.

Cruz, M., Garrido, N., Herrero, J., Pérez-Cano, I., Muñoz, M., & Meseguer, M. (2012). Timing of cell division in human cleavage-stage embryos is linked with blastocyst formation and quality. Reproductive BioMedicine Online, 25(4), 371–381. https://doi.org/10.1016/j.rbmo.2012.06.017

Csete, M. E. (2002). Reverse Engineering of Biological Complexity. Science, 295(5560), 1664–1669. http://doi.org/10.1126/science.1069981

Cutforth, T., Rubin, G.M. (1994). Mutations in Hsp83 and cdc37 impair signaling by the sevenless receptor tyrosine kinase in *Drosophila*. Cell, 77(7), 1027–1036. https://doi.org/10.1016/0092-8674(94)90442-1

das Neves, R. P., Jones, N. S., Andreu, L., Gupta, R., Enver, T., & Iborra, F. J. (2010). Connecting Variability in Global Transcription Rate to Mitochondrial Variability. PLoS Biology, 8(12), e1000560. https://doi.org/10.1371/journal.pbio.1000560

Deppe, U., Schierenberg, E., Cole, T., Krieg, C., Schmitt, D., Yoder, B., & Ehrenstein, G. Von. (1978). Cell lineages of the embryo of the nematode *Caenorhabditis elegans*. Developmental Biology, 75(1), 376–380.

Devasenathipathy, S., Santiago, J. G., Wereley, S. T., Meinhart, C. D., & Takehara, K. (2003). Particle imaging techniques for microfabricated fluidic systems. Experiments in Fluids, 34(4), 504–514. https://doi.org/10.1007/s00348-003-0588-y

Driever, W., & Nüsslein-Volhard, C. (1988). The bicoid protein determines position in the *Drosophila* embryo in a concentration-dependent manner. Cell, 54(1), 95–104.

Duffy, D.C., McDonald, J.C., Schueller, O.J., and Whitesides, G.M. (1998). Rapid prototyping of microfluidic systems in poly(dimethylsiloxane). Anal. Chem. 70, 4974-4984.

Edgar LG (1995) Blastomere culture and analysis. Methods Cell Biol 48: 303–321.

Edgar, B. A., & O'Farrell, P. H. (1990). The three postblastoderm cell cycles of Drosophila embryogenesis are regulated in G2 by string. Cell, 62(3), 469–80. Retrieved from http://www.ncbi.nlm.nih.gov/pubmed/2199063

Edgar, L. G., & McGhee, J. D. (1986). Embryonic expression of a gut-specific esterase in Caenorhabditis elegans. Developmental Biology, 114(1), 109–118. https://doi.org/10.1016/0012-1606(86)90387-8

Evans, T. C., Crittenden, S. L., Kodoyianni, V., & Kimble, J. (1994). Translational control of maternal glp-1 mRNA establishes an asymmetry in the C. elegans embryo.. Cell, 77, 183-94. doi:10.1016/0092-8674(94)90311-5

Fay, D. S., & Yochem, J. (2007). The SynMuv genes of *Caenorhabditis elegans* in vulval development and beyond. Developmental Biology, 306(1), 1–9. http://doi.org/10.1016/j.ydbio.2007.03.016

Félix, M.-A., & Wagner, A. (2008). Robustness and evolution: concepts, insights and challenges from a developmental model system. Heredity, 100(2), 132–140. http://doi.org/10.1038/sj.hdy.6800915

Ferguson, J & Mau, AWH. (1973). Spontaneous and stimulated emission from dyes. Spectroscopy of the neutral molecules of acridine orange, proflavine, and Rhodamine B. Australian Journal of Chemistry. 26. 1617-1624. 10.1071/CH9731617.

Filippov, S. K., Lezov, A. V., Sergeeva, O. Y., Olifirenko, A. S., Lesnichin, S. B., Domnina, N. S., … Štepanek, P. (2008). Aggregation of dextran hydrophobically modified by sterically-hindered phenols in aqueous solutions: Aggregates vs. single molecules. European Polymer Journal, 44(10), 3361–3369. https://doi.org/10.1016/j.eurpolymj.2008.07.041

Firebaugh, S. L., Jensen, K. F., & Schmidt, M. A. (1998). Investigation of high-temperature degradation of platinum thin films with an in situ resistance measurement apparatus. Journal of Microelectromechanical Systems, 7(1), 128–135. https://doi.org/10.1109/84.661395

Flores, L. E., Hildebrandt, T. B., Kühl, A. A., & Drews, B. (2014). Early detection and staging of spontaneous embryo resorption by ultrasound biomicroscopy in murine pregnancy. Reproductive Biology and Endocrinology : RB&E, 12, 38. http://doi.org/10.1186/1477-7827-12-38

Foe, V. E., Odell, G. M., & Edgar, B. A. (2009). The development of *Drosophila melanogaster*. (M. Bate & A. Martinez Arias, Eds.). Cold Spring Harbor Laboratory

Gervais, T., El-Ali, J., Günther, A., & Jensen, K. F. (2006). Flow-induced deformation of shallow microfluidic channels. Lab on a Chip, 6(4), 500. https://doi.org/10.1039/b513524a

Gibbs, R. A., Weinstock, G. M., Metzker, M. L., Muzny, D. M., Sodergren, E. J., Scherer, S., … Collins, F. (2004). Genome sequence of the Brown Norway rat yields insights into mammalian evolution. Nature, 428(6982), 493–521. https://doi.org/10.1038/nature02426

Glawdel, T., Almutairi, Z., Wang, S., & Ren, C. (2009). Photobleaching absorbed Rhodamine B to improve temperature measurements in PDMS microchannels. Lab on a Chip, 9(1), 171–4. https://doi.org/10.1039/b805172k

Goldbeter, A., Gérard, C., Gonze, D., Leloup, J.-C., & Dupont, G. (2012). Systems biology of cellular rhythms. FEBS Letters, 586(18), 2955–2965. https://doi.org/10.1016/j.febslet.2012.07.041

Grosser, M., & Schmid, U. (2010). The impact of annealing temperature and time on the electrical performance of Ti/Pt thin films. Applied Surface Science, 256(14), 4564–4569. https://doi.org/10.1016/j.apsusc.2010.02.048

Gupta. (2007). Genomics and biology of the nematode Caenorhabditis briggsae. WormBook. https://doi.org/10.1895/wormbook.1.136.1

Gursky, V. V., Surkova, S. Y., & Samsonova, M. G. (2012). Mechanisms of developmental robustness. Biosystems, 109(3), 329–335. https://doi.org/10.1016/j.biosystems.2012.05.013

Hashimshony, T., Wagner, F., Sher, N. & Yanai, I. (2012). CEL-Seq: single-cell RNA-Seq by multiplexed linear amplification. Cell Rep. 2, 666-73 .

Hashimshony, T., Feder, M., Levin, M., Hall, B. K. & Yanai, I.(2014). Spatiotemporal transcriptomics reveals the evolutionary history of the endoderm germ layer. Nature 519, 219-22

Heim, A., Rymarczyk, B., & Mayer, T. U. (2017). Regulation of Cell Division (pp. 83–116). Springer, Cham. https://doi.org/10.1007/978-3-319-46095-6_3

Hermann, G. J., Leung, B. H., & Priess, J. R. (2000). Left-right asymmetry in C. elegans intestine organogenesis involves a LIN-12/Notch signaling pathway.. Development, 127, 3429-40.

Hird, S.N. and White, J.G. (1993), Cortical and cytoplasmic flow polarity in early embryonic cells of Caenorhabditis elegans. J Cell Biol, 1993. 121(6): p. 1343-55.

Houchmandzadeh, B., Wieschaus, E., & Leibler, S. (2002). Establishment of developmental precision and proportions in the early *Drosophila* embryo. Nature, 415(6873), 798–802. https://doi.org/10.1038/415798a

Ikegami R, Rivera-Bennetts AK, Brooker DL, Yager TD (1997) Effect of inhibitors of DNA replication on early zebrafish embryos: evidence for coordinate activation of multiple intrinsic cell- cycle checkpoints at the mid-blastula transition. Zygote 5(2):153–175

Jiang, Y. J., Aerne, B. L., Smithers, L., Haddon, C., Ish-Horowicz, D., & Lewis, J. (2000). Notch signalling and the synchronization of the somite segmentation clock. Nature, 408(6811), 475–9. https://doi.org/10.1038/35044091

Johnston, I. G., Gaal, B., Neves, R. P. das, Enver, T., Iborra, F. J., & Jones, N. S. (2012). Mitochondrial Variability as a Source of Extrinsic Cellular Noise. PLoS Computational Biology, 8(3), e1002416. https://doi.org/10.1371/journal.pcbi.1002416

Johnston, W.L. and J.W. Dennis, (2011) The eggshell in the C. elegans oocyte-to-embryo transition. Genesis.

Junkersdorf, B., & Schierenberg, E. (1992). Embryogenesis in C. elegans after elimination of individual blastomeres or induced alteration of the cell division order. Roux's Archives of Developmental Biology, 202(1), 17–22. https://doi.org/10.1007/BF00364593

Karlstrom, R. O., Talbot, W. S., & Schier, A. F. (1999). Comparative synteny cloning of zebrafish you-too: mutations in the Hedgehog target gli2 affect ventral forebrain patterning. Genes & Development, 13(4), 388–93. Retrieved from http://www.ncbi.nlm.nih.gov/pubmed/10049354

Kim, D., Chesler, N. C., & Beebe, D. J. (2006). A method for dynamic system characterization using hydraulic series resistance. Lab on a Chip, 6(5), 639. https://doi.org/10.1039/b517054k

Kim, H., Vishniakou, S., & Faris, G. W. (2009). Petri dish PCR: laser-heated reactions in nanoliter droplet arrays. Lab on a Chip, 9(9), 1230. https://doi.org/10.1039/b817288a

Kim, M. M., Giry, A., Mastiani, M., Rodrigues, G. O., Reis, A., & Mandin, P. (2015). Microscale thermometry: A review. Microelectronic Engineering, 148, 129–142. https://doi.org/10.1016/j.mee.2015.11.002

Kobayashi, T., Yamaguchi, T., Hamanaka, S., Kato-Itoh, M., Yamazaki, Y., Ibata, M., … Nakauchi, H. (2010). Generation of Rat Pancreas in Mouse by Interspecific Blastocyst Injection of Pluripotent Stem Cells. Cell, 142(5), 787–799. https://doi.org/10.1016/j.cell.2010.07.039

Kosubek, A., Klein-Hitpass, L., Rademacher, K., Horsthemke, B., & Ryffel, G. U. (2010). Aging of *Xenopus tropicalis* Eggs Leads to Deadenylation of a Specific Set of Maternal mRNAs and Loss of Developmental Potential. PLoS ONE, 5(10), e13532. http://doi.org/10.1371/journal.pone.0013532

Kuntz, S. G., Eisen, M. B., Lerat, E., Vieira, C., & Carareto, C. (2014). Drosophila Embryogenesis Scales Uniformly across Temperature in Developmentally Diverse Species. PLoS Genetics, 10(4), e1004293. https://doi.org/10.1371/journal.pgen.1004293

Lucchetta, E. M., Lee, J. H., Fu, L. A., Patel, N. H., & Ismagilov, R. F. (2005). Dynamics of *Drosophila* embryonic patterning network perturbed in space and time using microfluidics. Nature, 434(7037), 1134–1138. https://doi.org/10.1038/nature03509

Macklon, N. S. (2002). Conception to ongoing pregnancy: the “black box” of early pregnancy loss. Human Reproduction Update, 8(4), 333–343. http://doi.org/10.1093/humupd/8.4.333

Maduro, M. F. (2015). Developmental robustness in the *Caenorhabditis elegans* embryo. Molecular Reproduction and Development, 82(12), 918–931. http://doi.org/10.1002/mrd.22582

Mao, H., Yang, T., & Cremer, P. S. (2002). A Microfluidic Device with a Linear Temperature Gradient for Parallel and Combinatorial Measurements. Journal of the American Chemical Society, 124(16), 4432–4435. https://doi.org/10.1021/ja017625x

Maltezos, G., Johnston, M., & Scherer, A. (2005). Thermal management in microfluidics using micro-Peltier junctions. Applied Physics Letters, 87(15), 154105. https://doi.org/10.1063/1.2089174

McDonald, J.C., Duffy, D.C., Anderson, J.R., Chiu, D.T., Wu, H.K., Schueller, O.J., and Whitesides, G.M. (2000). Fabrication of microfluidic systems in poly(dimethylsiloxane). Electrophoresis 21, 27-40.

Miralles, V., Huerre, A., Malloggi, F., & Jullien, M.-C. (2013). A Review of Heating and Temperature Control in Microfluidic Systems: Techniques and Applications. Diagnostics, 3(1), 33–67. https://doi.org/10.3390/diagnostics3010033

Morel, M., Bartolo, D., Galas, J.-C., Dahan, M., & Studer, V. (2009). Microfluidic stickers for cell- and tissue-based assays in microchannels. Lab Chip, 9(7), 1011–1013. https://doi.org/10.1039/B819090A

Morgan, D. O. (1997). CYCLIN-DEPENDENT KINASES: Engines, Clocks, and Microprocessors. Annual Review of Cell and Developmental Biology, 13(1), 261–291. https://doi.org/10.1146/annurev.cellbio.13.1.261

Murakami, M. S. (2004). Morphogenesis during Xenopus gastrulation requires Wee1-mediated inhibition of cell proliferation. Development, 131(3), 571–580. https://doi.org/10.1242/dev.00971

Murray, A. W., & Kirschner, M. W. (1989). Dominoes and clocks: the union of two views of the cell cycle. Science (New York, N.Y.), 246(4930), 614–21. Retrieved from http://www.ncbi.nlm.nih.gov/pubmed/2683077

Nakamura, K., Takayanagi, T., & Sato, S. (1989). A modified arrhenius equation. Chemical Physics Letters, 160(3), 295–298. https://doi.org/10.1016/0009-2614(89)87599-2

Neves, A., Busso, C., & Gönczy, P. (2015). Cellular hallmarks reveal restricted aerobic metabolism at thermal limits. eLife, 4, e04810. https://doi.org/10.7554/eLife.04810

Packard, C. (n.d.). The Measurement of Quantitative Biological Effects of X-RAYS.. The Journal of Cancer Research October 1 1926 (10) (3) 319-339; DOI: . http://doi.org/10.1158/jcr.1926.319

Palmeirim, I., Henrique, D., Ish-Horowicz, D., & Pourquié, O. (1997). Avian hairy Gene Expression Identifies a Molecular Clock Linked to Vertebrate Segmentation and Somitogenesis. Cell, 91(5), 639–648. https://doi.org/10.1016/S0092-8674(00)80451-1

Pourquié, O. (2001). Vertebrate Somitogenesis. Annual Review of Cell and Developmental Biology, 17(1), 311–350. https://doi.org/10.1146/annurev.cellbio.17.1.311

Pourquié, O. (2007). Building the Spine: The Vertebrate Segmentation Clock. Cold Spring Harbor Symposia on Quantitative Biology, 72(1), 445–449. https://doi.org/10.1101/sqb.2007.72.016

Priess, J. R., & Thomson, J. N. (1987). Cellular interactions in early C. elegans embryos. Cell, 48(2), 241–50. Retrieved from http://www.ncbi.nlm.nih.gov/pubmed/3802194

Regos, A., Lengyel, K., Takacs-Vellai, K., & Vellai, T. (2013). Identification of novel cis-regulatory regions from the Notch receptor genes lin-12 and glp-1 of Caenorhabditis elegans.. Gene Expr Patterns, 13, 66-77.

Richards, J. L., Zacharias, A. L., Walton, T., Burdick, J. T., & Murray, J. I. (2013). A quantitative model of normal Caenorhabditis elegans embryogenesis and its disruption after stress. Developmental Biology, 374(1), 12–23. https://doi.org/10.1016/j.ydbio.2012.11.034

Quaglio, M., Canavese, G., Giuri, E., Marasso, S. L., Perrone, D., Cocuzza, M., & Pirri, C. F. (2008). Evaluation of different PDMS interconnection solutions for silicon, Pyrex and COC microfluidic chips. Journal of Micromechanics and Microengineering, 18(5), 55012. https://doi.org/10.1088/0960-1317/18/5/055012

Rivers, D. M., Moreno, S., Abraham, M., & Ahringer, J. (2008). PAR proteins direct asymmetry of the cell cycle regulators Polo-like kinase and Cdc25. The Journal of Cell Biology, 180(5), 877–885. https://doi.org/10.1083/jcb.200710018

Robertson, S., & Lin, R. (2015). The Maternal-to-Zygotic Transition in C. elegans. Current Topics in Developmental Biology, 113, 1–42. https://doi.org/10.1016/bs.ctdb.2015.06.001

Rose, L., & Gonczy, P. (2014). Polarity establishment, asymmetric division and segregation of fate determinants in early C. elegans embryos. WormBook, 1–43. https://doi.org/10.1895/wormbook.1.30.2

Rutherford, S. L., & Lindquist, S. (1998). Hsp90 as a capacitor for morphological evolution. Nature, 396(6709), 336–342. https://doi.org/10.1038/24550

San-Miguel A, Lu H. Microfluidics as a tool for C. elegans research. In: WormBook: The Online Review of C. elegans Biology [Internet]. Pasadena (CA): WormBook; 2005-. Available from: https://www.ncbi.nlm.nih.gov/books/NBK174829/

Schierenberg, E., & Wood, W. B. (1985). Control of cell-cycle timing in early embryos of Caenorhabditis elegans. Developmental Biology, 107(2), 337–54. Retrieved from http://www.ncbi.nlm.nih.gov/pubmed/3972159

Schmid, U., & Seidel, H. (2008). Effect of high temperature annealing on the electrical performance of titanium/platinum thin films. Thin Solid Films, 516(6), 898–906. https://doi.org/10.1016/j.tsf.2007.04.128

Schnabel, R., Hutter, H., Moerman, D., & Schnabel, H. (1997). Assessing normal embryogenesis in Caenorhabditis elegans using a 4D microscope: variability of development and regional specification. Developmental Biology, 184(2), 234–65. https://doi.org/10.1006/dbio.1997.8509

Schneider, C. A.; Rasband, W. S. & Eliceiri, K. W. (2012), "NIH Image to ImageJ: 25 years of image analysis", Nature methods 9(7): 671-675, PMID 22930834

Shima, D. T., Haldar, K., Pepperkok, R., Watson, R., & Warren, G. (1997). Partitioning of the Golgi apparatus during mitosis in living HeLa cells. The Journal of Cell Biology, 137(6), 1211–28. Retrieved from http://www.ncbi.nlm.nih.gov/pubmed/9182657

Shimura T, Toyoshima M, Taga M, Shiraishi K, Uematsu N, Inoue M, Niwa O (2002) The novel surveillance mechanism of the Trp53-dependent s-phase checkpoint ensures chromosome damage repair and preimplantation-stage development of mouse embryos fertilized with x- irradiated sperm. Radiat Res 158(6):735–742

Sia, S. K., & Whitesides, G. M. (2003). Microfluidic devices fabricated in Poly(dimethylsiloxane) for biological studies. ELECTROPHORESIS, 24(21), 3563–3576. https://doi.org/10.1002/elps.200305584

Springer, M. S., Murphy, W. J., Eizirik, E., & O'Brien, S. J. (2003). Placental mammal diversification and the Cretaceous-Tertiary boundary. Proceedings of the National Academy of Sciences, 100(3), 1056–1061. https://doi.org/10.1073/pnas.0334222100

Sreenan, J. M., & Diskin, M. G. (1986). The Extent and Timing of Embryonic Mortality in the Cow. In Embryonic Mortality in Farm Animals (pp. 1–11). Dordrecht: Springer Netherlands. http://doi.org/10.1007/978-94-009-5038-2_1

Stein, L. D., Bao, Z., Blasiar, D., Blumenthal, T., Brent, M. R., Chen, N., … Waterston, R. H. (2003). The Genome Sequence of Caenorhabditis briggsae: A Platform for Comparative Genomics. PLoS Biology, 1(2), e45. https://doi.org/10.1371/journal.pbio.0000045

Stierngale, T. (2006) "Maintenance of C. elegans." Wormbook: 1-11.

Sthoeger, Z. M., Mozes, E., & Tartakovsky, B. (1993). Anti-cardiolipin antibodies induce pregnancy failure by impairing embryonic implantation. Proceedings of the National Academy of Sciences of the United States of America, 90(14), 6464–7. Retrieved from http://www.ncbi.nlm.nih.gov/pubmed/8341656

Sulston, J. E., & Horvitz, H. R. (1977). Post-embryonic cell lineages of the nematode, Caenorhabditis elegans. Developmental Biology, 56(1), 110–156. https://doi.org/10.1016/0012-1606(77)90158-0

Sulston, J. E., Schierenberg, E., White, J. G., & Thomson, J. N. (1983). The embryonic cell lineage of the nematode *Caenorhabditis elegans*. Developmental Biology, 100(1), 64–119. https://doi.org/10.1016/0012-1606(83)90201-4

Sun, D.W.(2007), Computational fluid dynamics in food processing. Contemporary food engineering ,Boca Raton: CRC Press. xviii, 739 p., 16 p. of plates.

Ward, S., & Miwa, J. (1978). Characterization of temperature-sensitive, fertilization-defective mutants of the nematode *Caenorhabditis elegans*. Genetics, 88(2). Retrieved from http://www.genetics.org/content/88/2/285.short

Wei Y, Multi S, Yang CR, Ma J, Zhang QH, Wang ZB, Li M, Wei L, Ge ZJ, Zhang CH, Ouyang YC, Hou Y, Schatten H, Sun QY (2011) Spindle assembly checkpoint regulates mitotic cell cycle progression during preimplantation embryo development. PLoS One 6(6):e21557. doi:10.1371/journal.pone.0021557

White J. (1988). In "The nematode C. elegans" (W. B. Wood ed.) pp81-122. Cold Spring Harbor Laboratory Press, New York.

Wilson, E. B. (1916). The Distribution of the Chondriosomes to the Spermatozoa in Scorpions. Proceedings of the National Academy of Sciences of the United States of America, 2(6), 321–4. Retrieved from http://www.ncbi.nlm.nih.gov/pubmed/16576154

Wilson, E. B. (1931). The distribution of sperm-forming materials in scorpions. Journal of Morphology, 52(2), 429–483. https://doi.org/10.1002/jmor.1050520205

Wood, W. B., Hecht, R., Carr, S., Vanderslice, R., Wolf, N., & Hirsh, D. (1980). Parental effects and phenotypic characterization of mutations that affect early development in *Caenorhabditis elegans*. Developmental Biology, 74(2), 446–469. http://doi.org/10.1016/0012-1606(80)90445-5

Xia, Y.N., and Whitesides, G.M. (1998). Soft lithography. Ann. Rev. Mater. Sci. 28, 153-184.

Yamaguchi, T., Sato, H., Kato-Itoh, M., Goto, T., Hara, H., Sanbo, M., … Nakauchi, H. (2017). Interspecies organogenesis generates autologous functional islets. Nature, 542(7640), 191–196. https://doi.org/10.1038/nature21070

Yeyati, P. L., Bancewicz, R. M., Maule, J., van Heyningen, V., & Baines, A. (2007). Hsp90 Selectively Modulates Phenotype in Vertebrate Development. PLoS Genetics, 3(3), e43. https://doi.org/10.1371/journal.pgen.0030043

Zhang, Y., Foster, J. M., Nelson, L. S., Ma, D., & Carlow, C. K. S. (2005). The chitin synthase genes chs-1 and chs-2 are essential for C. elegans development and responsible for chitin deposition in the eggshell and pharynx, respectively. Developmental Biology, 285(2), 330–339. https://doi.org/10.1016/j.ydbio.2005.06.037

Zhao, Z., Boyle, T. J., Bao, Z., Murray, J. I., Mericle, B., & Waterston, R. H. (2008). Comparative analysis of embryonic cell lineage between Caenorhabditis briggsae and Caenorhabditis elegans. Developmental Biology, 314(1), 93–99. https://doi.org/10.1016/j.ydbio.2007.11.015